Forschungszentrum Jülich
in der Helmholtz-Gemeinschaft

Institut für Chemie und Dynamik der Geosphäre
Institut IV: Agrosphäre

Measurement, Estimation and Modelling of Groundwater Flow Velocity at Krauthausen Test Site

Andreas Englert

Jül-4084

Measurement, Estimation and Modelling of Groundwater Flow Velocity at Krauthausen Test Site

Andreas Englert

Berichte des Forschungszentrums Jülich ; 4084
ISSN 0944-2952
Institut für Chemie und Dynamik der Geosphäre
Institut IV: Agrosphäre Jül-4084
D 82 (Diss., Aachen, RWTH, 2003)

Zu beziehen durch: Forschungszentrum Jülich GmbH · Zentralbibliothek
D-52425 Jülich · Bundesrepublik Deutschland
☎ 02461/61-5220 · Telefax: 02461/61-6103 · e-mail: zb-publikation@fz-juelich.de

Abstract

To enable precise understanding and prediction of transport in porous media, physical, chemical and biological processes and the interaction between these processes have to be considered. This is an interdisciplinary problem. In the scope of this work the focus is on the physically impelling force of the transport, the groundwater flow velocity.

A groundwater flow velocimeter (Fig. 1), using the point dilution technique, has been developed to measure in situ the groundwater flow velocity. The resolution of the groundwater flow velocimeter in the vertical direction is 25 cm. The in situ dilution measurement of the tracer uranin is carried out by laser-induced fluorimetry. The calibration of the groundwater flow velocimeter and subsequent field experiments at Krauthausen test site showed that the groundwater flow velocity inside a borehole can be measured with sufficient accuracy. The accuracy in deriving the Darcy velocity from the measurements inside a borehole is strongly dependent on the accuracy in determining the α-factor, which corrects for the convergence of streamlines towards the borehole. The estimation of the α-factor is difficult due to a general lack of knowledge of the state of the well. Measurements with the groundwater velocimeter showed that, the local Darcy velocity is strongly space and time dependent.

For the strongly anisotropic structure of the hydraulic conductivity at the Krauthausen test site, statistics for a three dimensional heterogeneous flow velocity field have been estimated using stochastic theories and Monte Carlo analysis which is based on numerical calculations. It is shown that correlograms in the mean flow direction, estimated by 1st order approximation, are in agreement with the results from the Monte Carlo analysis. The variances for the Darcy velocity components, estimated by 1st order approximation, are clearly below the results of the Monte Carlo estimation. Estimation of the variance, based on 2nd order approximation, showed accordance only for the longitudinal component of the Darcy velocity, whereas the vertical transversal component is below and the horizontal transversal component is above the results from Monte Carlo analysis. The estimated mean Darcy velocity is similar for 1st and 2nd order approximation as well as for the Monte Carlo analysis.

Estimation of the Darcy velocity statistics, both from numerical modelling and from stochastic theories, show smaller mean by factor 2, smaller variances by factor 4 and longer correlation length in the horizontal direction by factor 7 than the directly measured Darcy velocity using the groundwater flow velocimeter. The high discrepancies in mean, variance and horizontal autocorrelation length are due to the limited knowledge of the α-factor and the time variability of the Darcy velocities. A comparison shows that the relative standard deviation is similar for modelling, 2nd order approximation and direct measurements with the groundwater flow velocimeter.

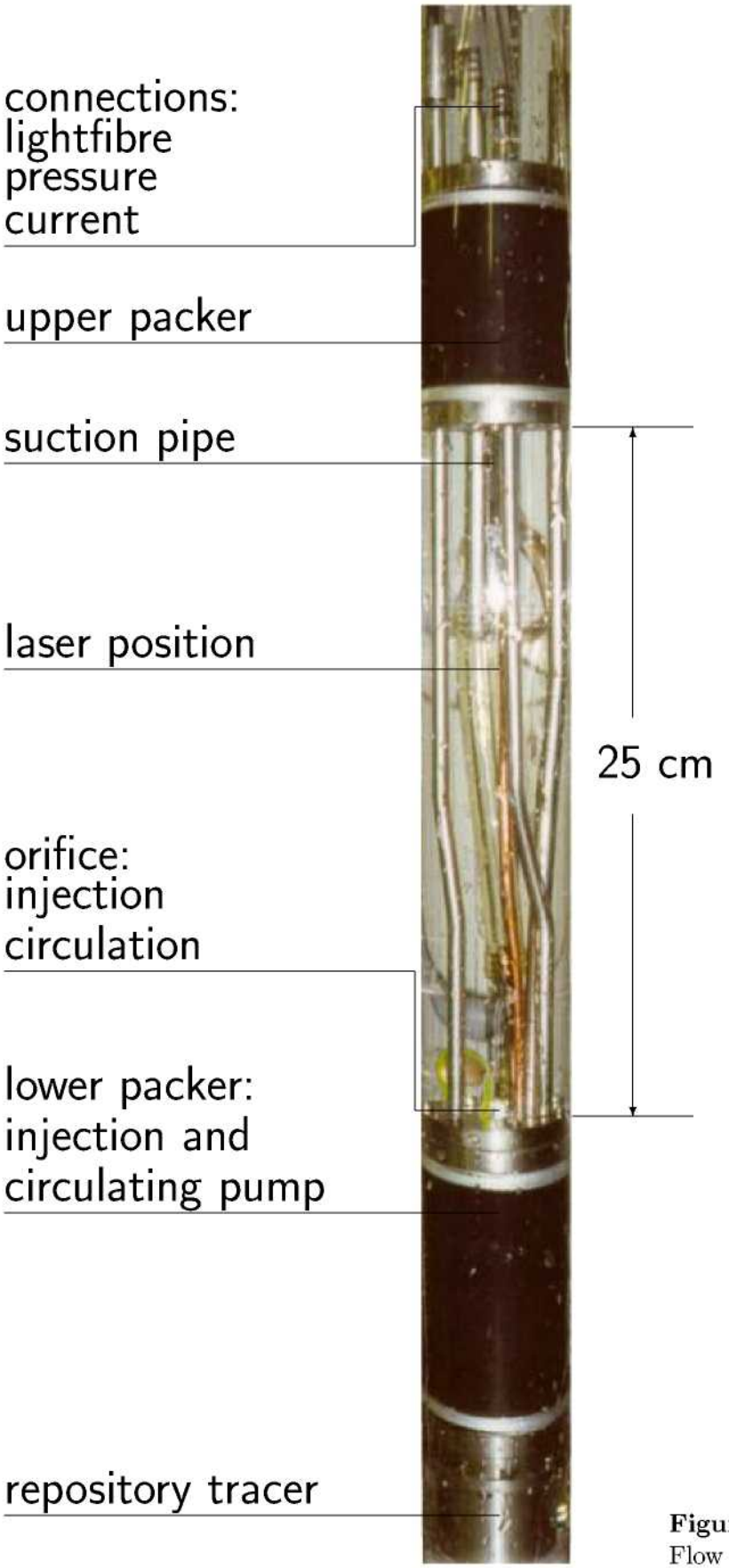

Figure 1: Groundwater Flow Velocimeter.

Kurzfassung

Motivation

In den letzten Jahrzehnten zeigte sich eine weltweite Verknappung der Grundwasserreserven mit Trinkwasserqualität. Die Ursachen hierfür sind der steigende Grundwasserverbrauch, verstärkte Grundwasserverschmutzung und Klimaänderungen, die die Grundwasserneubildung beeinflussen. Die Verknappung der Grundwasserreserven ist stark regionalisiert und sehr unterschiedlich in Ausmaß und Ursache. Zur Verknappung der Grundwasserreserven mit Trinkwasserqualität führt häufig nicht die Abnahme der absoluten Menge an zu Verfügung stehendem Grundwasser, sondern die Verschlechterung der Qualität des Grundwassers. Dies ist überwiegend auf anthropogene Verunreinigungen des Grundwassers zurückzuführen. Hierbei handelt es sich einerseits um großflächigen Eintrag aus der Landwirtschaft, andererseits um lokale Kontaminationsquellen umweltschädlicher Substanzen der Industrie oder undichter Deponien. Um das Risiko einer Grundwasserkontamination abzuschätzen, ist es wichtig, den Grundwasserfluss und den Transport von Stoffen im Grundwasser zu verstehen und vorhersagen zu können. Eine genaue Abschätzung der Risiken einer Gundwasserkontamination kann helfen, die richtigen Strategien und Verfahren für eine Sanierung zu entwickeln.

Transport in porösen Medien ist ein komplexes Wissensgebiet. Für genaue Vorhersagen von Stofftransport im Grundwasser sind physikalische, chemische, biologische Prozesse und deren Wechselwirkungen zu berücksichtigen. Im Rahmen der vorliegenden Arbeit soll die physikalisch entscheidende Größe für den Stofftransport im Grundwasser, die Grundwasserfließgeschwindigkeit, näher untersucht werden.

Die Grundwasserfließgeschwindigkeit bestimmt sowohl die Richtung als auch die maximale Geschwindigkeit des Stofftransports im Grundwasser. Weiterhin hat die Heterogenität der Fließgeschwindigkeit im Zuge des Stofftransports einen großen Einfluss auf die Aufweitung einer Stoffwolke (*Boggs et al.*, 1992; *Englert et al.*, 2000a; *Leblanc et al.*, 1991; *Mackay et al.*, 1986; *Teutsch and Kobus*, 1990; *Vereecken et al.*, 2000). Die Heterogenität der Grundwasserfließgeschwindigkeit resultiert aus der Heterogenität der hydraulischen Durchlässigkeit und der räumlichen und zeitlichen Variabilität des hydraulischen Gradienten im Grundwasserleiter. Im Rahmen der vorliegenden Arbeit werden drei verschiedene Methoden verwendet, um die Heterogenität der Grundwasserfließgeschwindigkeit, genauer der Darcy Geschwindigkeit, in einem Porengrundwasserleiter abzuschätzen: direkte Messung, numerische Modellierung und stochastische Abschätzung (Fig. 2). Die verschiedenen Methoden werden auf den Grundwasserleiter des Testfeldes Krauthausen (*Döring*, 1997; *Englert et al.*, 2000a; *Vereecken et al.*, 2000) angewandt. Ziel der Arbeit ist die Charakterisierung und Vorhersage der zeitlichen und räumlichen Variabilität der Grundwasserfließgeschwindigkeit, um somit das Verständnis für den Stofftransport in porösen heterogenen Medien und dessen Vorhersage zu verbessern.

Grundlagen

In den letzten dreißig Jahren wurden verschiedenste Methoden zur direkten Messung der Grundwasserfließgeschwindigkeit entwickelt: Thermische Flowmeter (*Ballard*, 1996; *Kerfoot and Massard*, 1985; *Alden and Munster*, 1997; *Paillet et al.*, 1996), Laser Doppler Velocimeter (*Momii et al.*, 1993), Colloidal Borescope (*Kearl and Case*, 1992; *Schöttler*, 1997) und die Einbohrlochmessmethode (*Drost et al.*, 1968; *Barczewski and Marshall*,

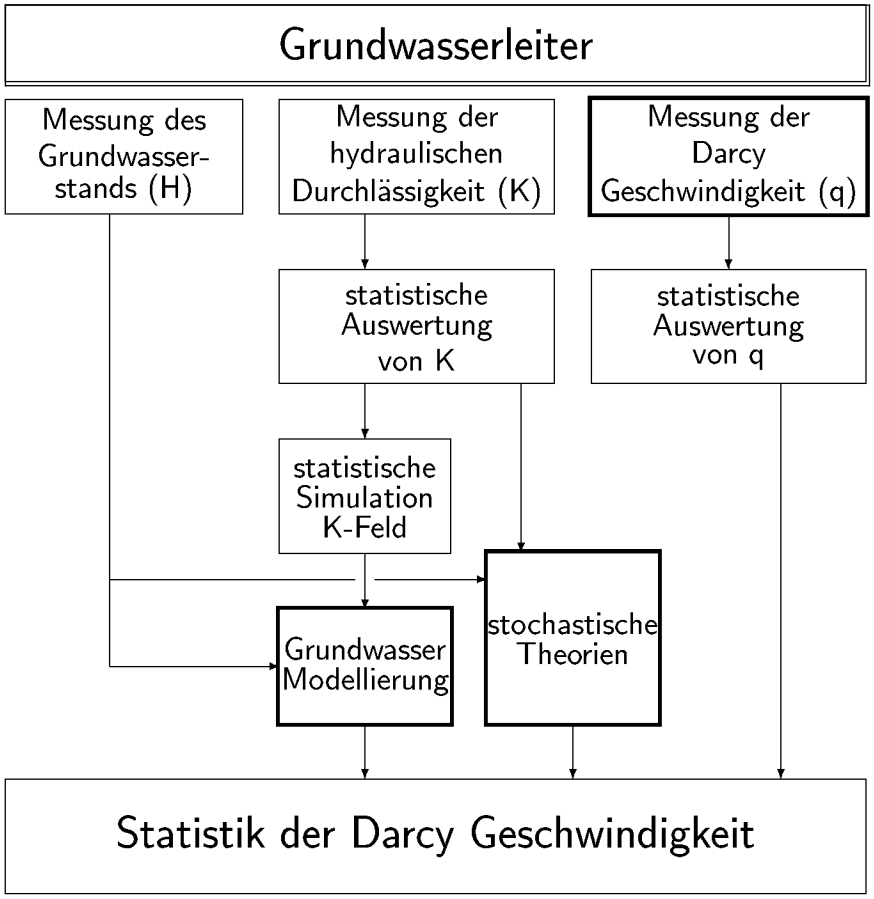

Figure 2: Flussdiagramm der Arbeitsschritte, die in dieser Arbeit genutzt wurden, um die Heterogenität von Grundwasserfließgeschwindigkeitsfeldern zu charakterisieren. Die entscheidenden Verfahren sind durch fett gehaltene Linien hervorgehoben.

1992; *Englert et al.*, 2001). Dabei wurde nur wenig über hochauflösende Grundwasserfließgeschwindigkeitsmessungen im Feldmaßstab veröffentlicht (*Vereecken et al.*, 2000; *Chandra et al.*, 1980).

Ein weit verbreiteter Weg, um die Heterogenität der Grundwasserfließgeschwindigkeit vorherzusagen, ist die numerische Modellierung. In einem ersten Schritt werden hydraulischer Gradient und hydraulische Durchlässigkeiten im Feld gemessen. Zur Messung Letzterer stehen eine ganze Reihe bewährter Methoden zur Verfügung. Messergebnisse zum Testfeld Krauthausen wurden in *Döring* (1997), *Englert et al.* (2000a) und *Vereecken et al.* (2000) veröffentlicht. Die Bestimmung des hydraulischen Gradienten erfolgt über Grundwasserstandsmessungen.

In einem zweiten Schritt werden die Informationen aus den Feldmessungen genutzt, um den Wasserfluss durch die Lösung der Richards' Gleichung (*Richards*, 1931) zu berechnen. Die Methoden hierzu sind zahlreich und vielfältig, sowohl bezüglich der Dimensionierung, als auch der numerischen Methoden (*Bear*, 1972; *Busch et al.*, 1993; *Verruijt*, 1982; *Delleur*, 1999; *Yeh*, 1981). Im Rahmen dieser Arbeit wird ein heterogenes dreidimensionales stationäres Modell unter der Nutzung des TRACE/PARTRACE Computerprogramms (*Neuendorf*, 1996; *Seidemann*, 1996) numerisch berechnet.

In den letzten 20 Jahren wurde intensiv daran geforscht, physikalische Zusammenhänge, die das Grundwasserfließen beschreiben, mit stochastischen Theorien zu kombinieren (*Dagan*, 1989; *Gelhar*, 1993). Ziel dieser Forschung ist es, die Effekte der räumlichen Heterogenität der hydraulischen Durchlässigkeit (K) auf die Statistik der Darcy Geschwindigkeit ($\vec{q}$) und den Grundwasserstand (H) zu beschreiben. Hierzu werden störungstheoretische Ansätze auf die Darcy Gleichung (*Darcy*, 1856) und die Kontinuitätsgleichung angewandt, um die Heterogenität von $\vec{q}$ auf der Basis der Heterogenität von K zu schätzen. Die Lösungen der gestörten Darcy- und Kontinuitätsgleichung sind Funktionen, die überwiegend erster Ordnung (*Bellin et al.*, 1992; *Dagan*, 1986, 1989; *Di Federico and Neuman*, 1998; *Gelhar and Axness*, 1983; *Gelhar*, 1993; *Russo*, 1995), seltener zweiter Ordnung (*Deng and Cushman*, 1995; *Hsu and Neuman*, 1997) gelöst wurden.

Um die Heterogenität der Darcy Geschwindigkeit, der hydraulischen Durchlässigkeit und des hydraulischen Gradienten quantitativ zu erfassen, haben sich geostatistische Methoden bewährt (*Akin and Siemes*, 1988; *Deutsch and Journel*, 1998; *Journel and Huijbregts*, 1989; *Schafmeister*, 1999; *Chilès and Delfiner*, 1999).

Entwicklung eines Messgeräts zur in situ Bestimmung der Grundwasserfließgeschwindigkeit

Um Grundwasserfließgeschwindigkeiten messen zu können, wurde ein Grundwasserfließgeschwindigkeitsmessgerät (Fig. 1) nach dem Prinzip der Verdünnungsmethode entwickelt. Das Messgerät besitzt eine vertikale Auflösung von 25 cm. Die in situ Messung der Verdünnung des verwendeten Markierungsstoffes Uranin erfolgte mit der Laser induzierten Fluoreszenzspektroskopie. Eine Kalibration des Messgeräts zeigte für Geschwindigkeiten zwischen 0,2 m/d und 1.1 m/d relative Fehler von 50%. Messung von Geschwindigkeiten zwischen 1.1 m/d und 14.7 m/d zeigten einen relativen Fehler von 10%. Die Ableitung der Fließgeschwindigkeit im Grundwasserleiter, auf der Basis der Fließgeschwindigkeiten innerhalb eines Bohrlochs, ist stark vom so genannten α-Faktor, welcher die Konvergenz der Stromlinien in Richtung des Bohrlochs korrigiert, abhängig. Der α-Faktor kann aufgrund der Unkenntnis des Zustandes des Ausbaus einer Grundwassermessstelle häufig nur abgeschätzt werden.

Messung der Grundwasserfließgeschwindigkeit am Testfeld Krauthausen

Am Testfeld Krauthausen wurden 361 Grundwasserfließgeschwindigkeitsmessungen mit dem eben vorgestellten Grundwasserfließgeschwindigkeitsmessgerät durchgeführt. Die Messungen zeigten eine hohe Variabilität des Betrages der Darcy Geschwindigkeit zwischen 0,1 m/d und 17,8 m/d. Der geometrische Mittelwert des Betrages der Darcy Geschwindigkeit betrug 1,0 m/d, bei einer Varianz von 1,3 der log-transformierten Werte. Unter Anwendung eines exponentiellen Modells konnte in horizontaler Richtung eine Autokorrelationslänge von $2,5 \pm 1,8$ m und in vertikaler Richtung von $0,2 \pm 0,03$ m ermittelt werden. Das experimentelle Variogramm in vertikaler Richtung zeigte zusätzlich einen Trend der Darcy Geschwindigkeit in vertikaler Richtung und eine Schichtung des Grundwasserleiters am Testfeld Krauthausen.

Ein direkter Vergleich der gemessenen Darcy Geschwindigkeiten mit früheren Messungen der hydraulischen Durchlässigkeit (*Döring*, 1997; *Englert et al.*, 2000a; *Vereecken et al.*, 2000) und Darcy Geschwindigkeiten (*Drost*, 1996; *Englert et al.*, 2000b; *Vereecken et al.*, 2000) zeigte hohe Diskrepanzen. Diese können auf die Zeitabhängigkeit lokaler

Darcy Geschwindigkeiten zurückgeführt werden, was durch Wiederholungsmessungen von Darcy Geschwindigkeiten belegt werden konnte. Dies ist in Übereinstimmung mit zeitaufgelösten Messungen mit dem Colloiadal Borescope (*Kearl and Case*, 1992; *Schöttler*, 1997).

Die Darcy Geschwindigkeitsmessungen, gemittelt auf einen halben Meter in vertikaler Richtung zeigen für das Testfeld Krauthausen einen generellen Anstieg sowohl des geometrischen Mittelwertes als auch der Varianz mit der Höhenposition. Dies ist in Übereinstimmung mit den gemessenen hydraulischen Durchlässigkeiten und der mittleren Abstandsgeschwindigkeit, ermittelt aus Tracerversuchen (*Döring*, 1997; *Englert*, 1998; *Vereecken et al.*, 2000). Zusätzlich konnte die schon in Feldbeobachtungen, Korngrößenanalysen und hydraulischen Durchlässigkeiten abgeleitete Schichtung des Grundwasserleiters des Testfeldes Krauthausen anhand der gemessenen Darcy Geschwindigkeiten wiedergefunden werden.

Die horizontale Korrelationslänge der gemessenen Darcy Geschwindigkeiten ist um den Faktor 2 kleiner als die der Darcy Geschwindigkeiten, die über die $^{82}Br^-$ Verdünnungsmethode bestimmt wurden, und um den Faktor 3 kleiner als die der hydraulischen Durchlässigkeiten. Dies kann auf die Zeitabhängigkeit der Darcy Geschwindigkeiten zurückgeführt werden. Die Autokorrelationslänge in vertikaler Richtung ist für die gemessenen Darcy Geschwindigkeiten und die hydraulischen Durchlässigkeiten ähnlich. Die gemessenen Darcy Geschwindigkeiten sind wie auch die hydraulischen Durchlässigkeiten besser mit einer Lognormal- als mit einer Normalverteilung zu beschreiben.

Wegen der höheren Beprobungsdichte in der Tiefe zwischen 90 m und 92 m über normal Null auf dem Testfeld Krauthausen wurde in der Arbeit diese „Referenzschicht“ für eine intensivere Untersuchung ausgewählt; alle nun folgenden Ergebnisse beziehen sich auf diese Schicht. Aus 91 Messungen mit dem Grundwasserfließgeschwindigkeitsmessgerät wurde ein geometrischer Mittelwert des Betrags der Darcy Geschwindigkeiten von 0,71 m/d bei einer Varianz der log-transformierten Werte von 0,98 ermittelt. Sowohl in vertikaler als auch horizontaler Richtung konnte keine deutliche autokorrelative Struktur beobachtet werden. Dies kann auf eine zu kleine Stichprobe oder die zeitliche Variabilität der Darcy Geschwindigkeiten zurückgeführt werden.

Ein Vergleich der geometrischen Mittelwerte der Darcy Geschwindigkeiten, einerseits aus Messungen mit dem Grundwasserfließgeschwindigkeitsmessgerät, andererseits aus Messungen mit der $^{82}Br^-$ Verdünnungsmethode, zeigt einen Unterschied von Faktor 2. Wendet man die Darcy Gleichung auf den geometrischen Mittelwert der hydraulischen Durchlässigkeiten und den mittleren Gradienten des Testfeldes Krauthausen an, kann eine Darcy Geschwindigkeit von 0,33 m/d berechnet werden, was ein um Faktor 2 kleinerer Wert ist, als der, mit dem Grundwasserfließgeschwindigkeitsmessgerät ermittelte. Die Varianz der log-transformierten Darcy Geschwindigkeiten, gemessen mit dem Grundwasserfließgeschwindigkeitsmessgerät, ist um den Faktor 2 kleiner als die mit der $^{82}Br^-$ Verdünnungsmethode gemessene. Diese Diskrepanzen sind auf unterschiedliche Messzeitpunkte und Messorte, das unterschiedliche Mittelungsvolumen der Verfahren und die Ungenauigkeit bei der Bestimmung des α-Faktors zurückzuführen.

Modellierung und Schätzung der Grundwasserfließgeschwindigkeit

Um aus den Eingangsdaten vom Testfeld Krauthausen ein dreidimensionales heterogenes Grundwasserfließfeld zu berechnen, wurde das TRACE Computerprogramm auf dem CRAY-T3E Parallelcomputer genutzt. Zwei Fälle, die sich allein in den Randbedingungen unterscheiden, wurden modelliert. Im ersten Fall wurde aus dem Grundwassergleichenplan ein mittlerer hydraulischer Gradient abgeleitet und für die Grundwassermodellierung verwendet. Im zweiten Fall wurden die Grundwasserstände an den Rändern des Grundwassergleichenplans als Randbedingungen verwendet. Ein Vergleich der beiden modellierten Fälle zeigte wenig Unterschiede in der resultierenden Statistik der Darcy Geschwindigkeiten. Einzig die Varianzen der x-Komponente der Darcy Geschwindigkeiten unterschieden sich um eine Größenordnung.

Es wurde eine Monte Carlo Analyse der Grundwassermodellierung (erster Fall) auf der Basis von 10 Realisierungen des dreidimensionalen heterogenen K-Feldes durchgeführt. Hierbei konnte gezeigt werden, dass die Ensembleparameter der Monte Carlo Analyse statistisch stabil sind, was für einen sinnvollen Vergleich mit den stochastischen Theorien notwendig ist.

Um die effektive hydraulische Durchlässigkeit unter Verwendung stochastischer Theorien abzuschätzen, wurden für die Lösung erster Ordnung die Formeln von *Dagan* (1989), für die Lösung zweiter Ordnung die Formeln von *Deng and Cushman* (1995) und *Hsu and Neuman* (1997) verwendet. Die Schätzung der Varianz und der Kovarianz wurden für die Annäherung erster Ordnung mit den Formeln von *Russo* (1995) und *Hsu and Neuman* (1997) berechnet. Für Berechnungen der Annäherung zweiter Ordnung wurden Abbildungen aus *Hsu and Neuman* (1997) und Formeln aus *Deng and Cushman* (1995) genutzt.

Vergleich der Ergebnisse

Ein Vergleich der Statistiken aus stochastischen Abschätzungen und numerischen Modellierungen, beide unter Verwendung derselben Informationen aus der Referenzschicht des Testfeldes Krauthausen sei im Folgenden zusammengefasst. Hierbei bezeichnet y die longitudinale Richtung, x die horizontal transversale und z die vertikal transversale Richtung. Dieser Definition folgend sind auch die Komponenten der Darcy Geschwindigkeit bezeichnet.

Die Schätzung zweiter Ordnung der Varianz der y-Komponente der Darcy Geschwindigkeit stimmt sehr gut mit der entsprechenden aus den numerischen Modellierungen abgeleiteten Ensemblevarianz überein. Die Schätzung erster Ordnung liegt dagegen deutlich unter dieser Ensemblevarianz. Die Schätzung sowohl erster als auch zweiter Ordnung der Varianz der x-Komponente der Darcy Geschwindigkeit ist in etwa eine Größenordnung kleiner als die entsprechende aus den numerischen Modellierungen abgeleitete Ensemblevarianz. Die erster Ordnung geschätzte Varianz der z-Komponente der Darcy Geschwindigkeit ist kleiner, wohingegen die zweiter Ordnung geschätzte Varianz größer ist als die entsprechende Ensemblevarianz der numerischen Modellierungen.

Kovarianzen für die x-, y- und z-Komponente der Darcy Geschwindigkeit in y-Richtung aus Schätzungen erster Ordnung unterscheiden sich deutlich von den entsprechenden Ensemblekovarianzen aus den numerischen Modellierungen. Unter Anwendung von Schätzungen zweiter Ordnung stimmt allein die Kovarianz der y-Komponente in y-Richtung mit der entsprechenden Ensemblekovarianz aus den nu-

merischen Modellierungen überein. Für die x-Komponente in y-Richtung liegen die Kovarianzen bis zu einem Abstand von 25 m unterhalb der entsprechenden Ensemblekovarianz aus den numerischen Modellierungen, für größere Abstände liegen sie darüber. Die Ensemblekovarianzen der z-Komponente in y-Richtung aus den numerischen Modellierungen liegen zwischen den erster und zweiter Ordnung abgeschätzten Kovarianzen. Die Korrelogramme in y-Richtung, zeigen für die x- und z-Komponente gute Übereinstimmung, für die y-Komponente sehr gute Übereinstimmung zwischen Abschätzungen erster Ordnung und numerischen Modellierungen.

Während im vorstehenden Vergleich die Komponenten der Darcy Geschwindigkeit betrachtet wurden, beziehen sich die nun folgenden Vergleiche ausschließlich auf die Beträge der Darcy Geschwindigkeit. Die Schätzung der Statistik der Darcy Geschwindigkeit, sowohl aus stochastischen Abschätzungen als auch aus numerischen Modellierungen zeigen einen um Faktor 2 (2) kleineren Mittelwert, eine um Faktor 4 (20) kleinere Varianz und eine um Faktor 7 (4) längere Autokorrelationslänge in horizontaler Richtung als die direkten Messungen mit dem Grundwasserfließgeschwindigkeitsmessgerät (der $^{82}Br^-$ Verdünnungsmethode). Die Autokorrelationslängen der Beträge der Darcy Geschwindigkeiten in vertikaler Richtung aus Modellierung und direkter Messung mit dem Grundwasserfließgeschwindigkeitsmessgerät sind ähnlich. Die großen Unterschiede in den Mittelwerten, den Varianzen und den horizontalen Autokorrelationslängen sind auf die Probleme bei der Bestimmung des α-Faktors und die Zeitabhängigkeit der Darcy Geschwindigkeiten zurückzuführen. Um die Effekte des α-Faktors auf Mittelwert und Varianz auszuschließen, wurde die relative Standardabweichung zu Vergleichszwecken herangezogen. Ein Vergleich der relativen Standardabweichungen zeigt, dass diese für die Messungen mit dem Grundwasserfließgeschwindigkeitsmessgerät, die numerischen Modellierungen und die stochastischen Abschätzungen zweiter Ordnung übereinstimmen, aber um Faktor 2 kleiner sind als die relative Standardabweichung, abgeleitet aus den Messungen mit der $^{82}Br^-$ Verdünnungsmethode.

Schlussfolgerungen

Es zeigte sich für das Beispiel des Testfeldes Krauthausen, dass die stochastischen Theorien erster Ordnung (*Bellin et al.*, 1992; *Dagan*, 1986, 1989; *Di Federico and Neuman*, 1998; *Gelhar and Axness*, 1983; *Gelhar*, 1993; *Russo*, 1995) in guter Übereinstimmung mit numerischen Modellierungen die räumliche Struktur im Sinne des Korrelogramms vorhersagen können. Die Varianz der Darcy Geschwindigkeit wird aber deutlich geringer geschätzt, als von der numerischen Modellierung vorhergesagt. Stochastische Theorien zweiter Ordnung (*Deng and Cushman*, 1995; *Hsu and Neuman*, 1997) stimmen in ihrer Vorhersage der Varianz der Darcy Geschwindigkeitskomponente in Hauptfließrichtung mit der numerischen Modellierung überein, nicht aber in transversaler Richtung. Dies wirft Probleme bei der Abschätzung der Makrodispersion auf, da diese sowohl von der räumlichen Struktur als auch der Varianz der Darcy Geschwindigkeit abhängt.

Messungen auf dem Testfeld Krauthausen zeigten, dass die Darcy Geschwindigkeit nicht nur räumlich, sondern auch zeitlich variiert, was in Übereinstimmung mit zeitaufgelösten Messungen der Darcy Geschwindigkeit, durchgeführt von *Kearl and Case* (1992) und *Schöttler* (1997), ist. Dies kann eine Verkürzung der Autokorrelationslänge und eine Erhöhung der Varianz der Darcy Geschwindigkeiten nach sich ziehen. Schließlich wirft die zeitliche Variabilität der lokalen Darcy Geschwindigkeit Fragen nach

den Konsequenzen für den Stofftransport und insbesondere für Dispersions- und Mischungsprozesse auf.

Weiterführende Arbeiten können durch die Berücksichtigung von zeitlich variierenden Randbedingungen sowohl in numerischen Modellierungen, als auch stochastischen Theorien die zeitliche und räumliche Variabilität der Darcy Geschwindigkeit und ihren Einfluss auf Transportprozesse genauer untersuchen. Ferner sollte schließlich die Vorhersagbarkeit der Heterogenität der Darcy Geschwindigkeit und damit die Vorhersagbarkeit von Transportprozessen jenseits der speziellen Situation auf dem Testfeld Krauthausen überprüft werden.

Danksagung

An dieser Stelle möchte ich allen Personen meinen Dank aussprechen, die zum Erfolg dieser Arbeit beigetragen haben.

Herrn Prof. Dr. H. Vereecken, Leiter des Instituts für Agrosphäre (ICG-IV), danke ich für die Möglichkeit meine Promotion an der Forschungszentrum Jülich GmbH anfertigen zu können, vor allem aber für eine erstklassige Betreuung. Desweiteren bedanke ich mich bei Herrn Prof. Dr. H.-R. Langguth (ehemaliger Leiter des Instituts für Hydrogeologie der RWTH Aachen) für die Übernahme des Koreferats und sein wissenschaftliches Interesse an den Inhalten dieser Arbeit. Bedanken möchte ich mich auch bei Herrn Prof. Dr. S. Peiffer (Leiter des Instituts für Hydrogeologie der RWTH Aachen) für die spontane Übernahme des Koreferats.

Ich danke meinem Abteilungsleiter Dr. J. Vanderborght und meinem ehemaligen Kollegen Dr. O. Nitzsche, die allzeit bereit waren mir mit ihrem großen Wissen um den Transport in porösen Medien zur Seite zu stehen.

Meinen Mitarbeitern der ehemaligen Arbeitsgruppe Verhalten von Schadstoffen in geologischen Systemen (ICG-4) und der heutigen Arbeitsgruppe Stofftransport in Böden und Grundwasser (ICG-IV), namentlich M. Ciocanaru, O. Esser, H. Hardelauf, R. Harms, U. Hashagen, J. Heidbüchel, Dr. M. Herbst, J. Höltkemeier, F. Höpner, R. Jahn Dr. U. Jaekel, Dr. R. Kasteel, Dr. A. Kemna, F. Lamertz, A. Langen, G. Mennicken, K. Müller, M. Münch, D. Niehoff, H. Philipp, Dr. H. Schwarze, H. Sittardt, Dr. O.F. Smidts, Dr. N. Suciu, Dr. A. Tillmann, Dr. P. Ustohal, A. Verweerd und S. de Waal, danke ich für die intensive Unterstützung.

Uneingeschränkt danken möchte ich allen Mitarbeitern des Institut Agrosphäre (ICG-IV) für gute Zusammenarbeit.

Ich danke den Mitarbeitern des ZAT, allen voran H.-G. Bays, F.-J. Bongartz, U. Engels, Dr. H. Glückler, W. Hellebrandt, H. Kämmerling, C. Meixner, W. Renftle, E. Sigismund, Dr. H. Stelzer für ausgezeichnete Zusammenarbeit bei der Entwicklung des Grundwasserfließgeschwindigkeitsmessgeräts. Ohne ihre Leistung wäre die Entwicklung nicht möglich gewesen.

Desweiteren danke ich den Mitarbeitern des ZAM für die hervorragende Unterstützung bei Hard- und Software Problemen.

Bedanken möchte ich mich bei Dr. M. Schöttler (Leiter der Firma PHREALOG) für die vielen Diskussionen um das Messen von Grundwasserfließgeschwindigkeiten.

Abschließend bedanke ich mich bei P. Wilding für die intensive Durchsicht des Manuskripts.

Contents

List of Figures

List of Tables

Abbreviations

Institutes and Organizations

EU	European Union
FZJ	Forschungszentrum Jülich GmbH (Research Centre Jülich)
ZAT	Zentralabteilung Technologie (Central Department of Technology of the FZJ)
ZAM	Zentralinstitut für Angewandte Mathematik (Central Institute for Applied Mathematics of the FZJ)

Physical Symbols

$\vec{q}$	[L/T]	Darcy velocity, specific discharge
K	[L/T]	hydraulic conductivity
H	[L]	total head
h	[L]	pressure head
$\vec{r}$	[-]	position vector
t	[T]	time
S	[1/L]	specific storage coefficient
S_0	[-]	storage coefficient
Q	[1/T]	source sink term
z_0	[L]	elevation head
ρ_f	[M/L^3]	density of a fluid
η_f	[M/LT]	dynamic viscosity of a fluid
$\vec{v}$	[L/T]	path velocity
l	[L]	length
N_R	[-]	Reynolds number
Γ		boundary
Γ_D	[L/T]	Dirichlet boundary condition
Γ_N	[L]	Neumann boundary condition
Γ_C	[L]	Cauchy boundary condition
Θ	[-]	moisture content
Θ_r	[-]	residual water content
Θ_s	[-]	saturated water content
n, m, α_1	[-,-,-]	v. Genuchten parameters
τ	[-]	tortuosity
n_0	[-]	effective porosity
$\vec{q}_n$	[L/T]	mean pore velocity

q_m	[L/T]	measured flow velocity
V	[L^3]	dilution volume
A	[L^2]	area of approaching flow
c	[M/L^3]	concentration
c_0	[M/L^3]	initial concentration
Q	[L^3/T]	flow

Indexes for q, Q, V, A
in the scope of point dilution method:

$_{ha}$	due to horizontal advection
$_{d}$	due to density driven advection
$_{k}$	due to molecular diffusion
$_{c}$	due to mixing device driven advection
$_{va}$	due to vertical advection
$\hat{}$	sum of $_{d}$, $_{k}$, $_{c}$ and $_{va}$

K_0	[L/T]	hydraulic conductivity inside the borehole
K_1	[L/T]	hydraulic conductivity of borehole screen
K_2	[L/T]	hydraulic conductivity of filter pack
K_3	[L/T]	hydraulic conductivity of aquifer
r_1	[L]	inner radius of borehole screen
r_2	[L]	outer radius of borehole screen
r_3	[L]	outer radius of filter pack
r_s	[L]	outer radius of skin region
α	[-]	horizontal convergence factor
γ	[-]	vertical convergence factor
l_p	[L]	length of a packer
s	[-]	skin factor

Statistical Symbols

m	arithmetic mean of a sample
n	number of samples
s^2	variance of a sample
μ	mean of a population
σ^2	variance of a population
σ	standard deviation of a population
μ_g	geometric mean of a population
E	mathematical expectation
P	probability
f	function
C	covariance
γ	semivariance
$\vec{\xi}$	separation vector
ξ_i	separation distance in direction i
ρ	correlogram
z	regionalized variable

Z	probability distribution of z
C_0	sill value
λ	correlation length
W	test value of the Shapiro Wilk test
D	test value of the Kolmogorov Smirnov test
q_i	Darcy velocity component i
$\vec{\xi}'$	$\vec{\xi}/\lambda_h$
Y	$\ln(K)$
J	mean hydraulic gradient
K_g	geometric mean of K
K_{ef}	effective hydraulic conductivity
σ_Y^2	variance of $\ln(K)$
e	λ_v/λ_h
λ_v	correlation length of Y, vertical
λ_h	correlation length of Y, horizontal
ReV	regionalized variable
RV	random variable
RF	random function
cdf	cumulative distribution function

Space Indices

$\underset{1}{y}$	longitudinal direction, mean flow direction
$\underset{2}{x}$	horizontal transversal direction
$\underset{3}{z}$	vertical transversal direction

Instruments

LIF	Laser-Induced Fluorimetry
MLS	Multi-Level-Samplers

Chapter 1

Introduction

The last decades showed that worldwide groundwater resources with drinking quality are running short. This is due to increasing water consumption, increasing contamination and climate changes affecting the recharge of groundwater. The shortage of groundwater with drinking quality is strongly regionally dependent and may differ enormously in intensity and causes. Often, groundwater quantity is not the limiting factor for drinking water supply, but its low quality. This is mainly due to anthropogenic contamination of the groundwater. This is caused, on the one hand, by the local input of hazardous substances from industrial activities and leaky waste disposal sites and, on the other hand, through the diffuse input of hazardous substances, mainly from agricultural activities. To predict the risk of groundwater contamination, waterflow and solute transport in the subsurface have to be understood and predictable. This enables the application of appropriate methods and strategies for the remediation of contaminated sites.

Transport in groundwater is known to be complex. For precise understanding and prediction, physical, chemical and biological processes and the interaction between these processes have to be considered. This is an interdisciplinary problem. In the scope of this work the focus is on the physically impelling force of the transport, the groundwater flow velocity.

Initially, groundwater flow velocity governs the direction and the maximal transport velocity. Furthermore, the heterogeneity of groundwater flow velocity has a large impact on the spreading of the concentration plume during the transport in the aquifer (*Boggs et al.*, 1992; *Englert et al.*, 2000a; *Leblanc et al.*, 1991; *Mackay et al.*, 1986; *Teutsch and Kobus*, 1990; *Vereecken et al.*, 2000). Groundwater flow velocity is known to be heterogeneous due to the heterogeneity of hydraulic conductivity and time dependent variability of the hydraulic gradient in the aquifer. In this work the focus is on three different ways estimating the heterogeneity of groundwater flow velocity, i.e. the Darcy velocity using direct measurement, numerical modelling and stochastic estimation (Fig. 1.1). The different approaches have been applied to the aquifer at Krauthausen test site (*Döring*, 1997; *Englert et al.*, 2000a; *Vereecken et al.*, 2000).

Within the last thirty years, several methods of direct measurement of groundwater flow velocity have been developed, thermal flowmeters (*Ballard*, 1996; *Kerfoot and Massard*, 1985; *Alden and Munster*, 1997; *Paillet et al.*, 1996), laser Doppler velocimeter system (*Momii et al.*, 1993), colloidal borescope (*Kearl and Case*, 1992; *Schöttler*, 1997) and the point dilution method (*Drost et al.*, 1968; *Barczewski and Marshall*, 1992;

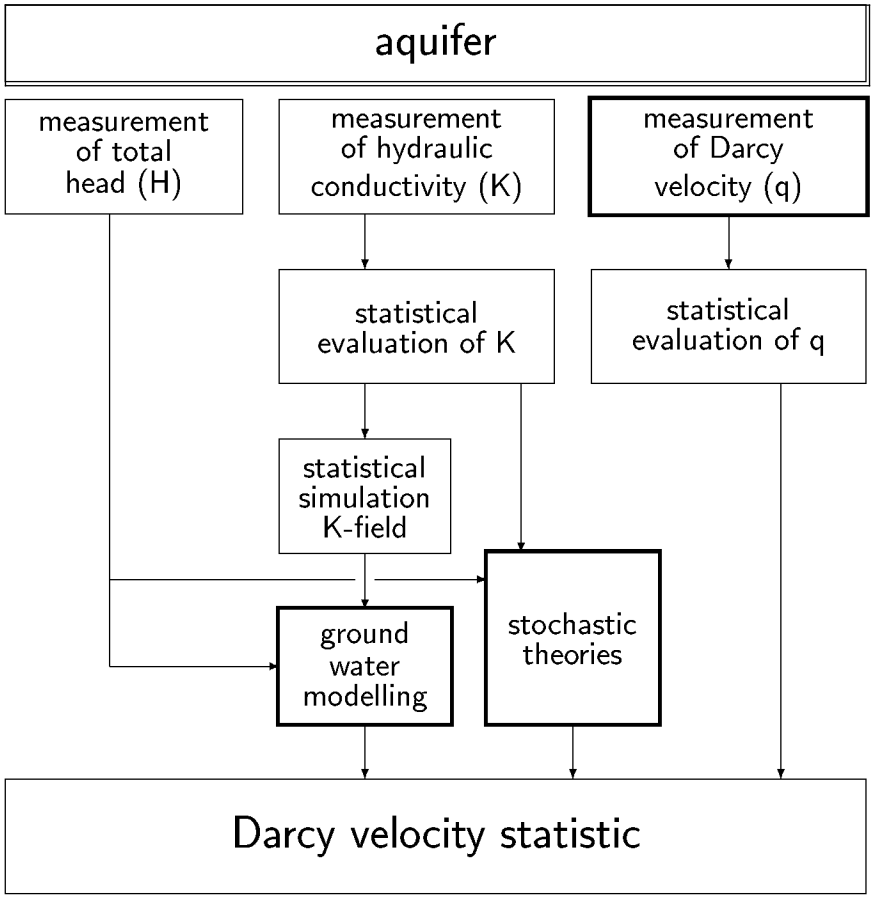

Figure 1.1: Flowchart of the measurements and procedures used in this work for estimating the heterogeneity of a groundwater flow velocity field. The main objectives in the scope of determining the Darcy velocity statistic are indicated by bold lines.

Englert et al., 2001). However, little is published on high-resolution Darcy velocity field measurements, which include a large number of samples (*Vereecken et al.*, 2000; *Chandra et al.*, 1980).

The most popular way to estimate the heterogeneity of groundwater flow velocity is modelling. The first step is to measure the heterogeneity of the hydraulic conductivity and hydraulic gradient. Hydraulic conductivity measurements are well established and a large range of methods are available. In the case of Krauthausen test site, this was shown by *Döring* (1997), *Englert et al.* (2000a) and *Vereecken et al.* (2000). Hydraulic gradient measurements are derived from piezometric head measurements. This information is then used to predict water flow velocity solving the Richards' equation (*Richards*, 1931). The approaches are manifold in dimension and numerical methods (*Bear*, 1972; *Busch et al.*, 1993; *Verruijt*, 1982; *Delleur*, 1999; *Yeh*, 1981). In this work, a heterogeneous three dimensional stationary model was computed using the TRACE/PARTRACE computer program (*Neuendorf*, 1996; *Seidemann*, 1996).

Over the last twenty years, extensive research has been carried out on combining physical equations, which describe groundwater flow, with stochastic processes (*Dagan*, 1989; *Gelhar*, 1993). This research aimed to estimate the effect of spatial heterogeneity

of the hydraulic conductivity (K) on the Darcy velocities ($\vec{q}$) and total heads (H). Perturbation theory is applied to Darcy's law and continuity equation in order to find functions deriving the heterogeneity of $\vec{q}$ from the heterogeneity of K. These functions are solutions of the perturbated Darcy's law and continuity equation. Extensive work has been carried out on 1st order solutions (*Bellin et al.*, 1992; *Dagan*, 1986, 1989; *Di Federico and Neuman*, 1998; *Gelhar and Axness*, 1983; *Gelhar*, 1993; *Russo*, 1995), but only a little on 2nd order solutions of the perturbated equations (*Deng and Cushman*, 1995; *Hsu and Neuman*, 1997).

Statistical and geostatistical methods are an appropriate tool to quantify the heterogeneity of groundwater flow velocity, hydraulic conductivity and hydraulic gradient (*Akin and Siemes*, 1988; *Deutsch and Journel*, 1998; *Journel and Huijbregts*, 1989; *Schafmeister*, 1999; *Chilès and Delfiner*, 1999).

The aim of this work is to compare the different approaches for estimating groundwater flow velocity focusing on the example of the Krauthausen aquifer to advance the comprehension of groundwater flow processes. In detail, the aims of this work are:

- to develop a groundwater flow velocimeter that is able to determine with high resolution the magnitude of the Darcy velocity in situ
- to determine the spatial heterogeneity of the Krauthausen flow velocity field
- to compare the groundwater flow velocimeter measurements with other measurements at Krauthausen test site
- to compare results, concerning the Darcy velocity statistics, from Monte Carlo simulations with those from stochastic theories
- to compare the measured statistics of the magnitude of the Darcy velocity with results from stochastic theories and numerical modelling

Chapter 2

Theory of Groundwater Flow

In this chapter the basic principles describing water flow in heterogeneous aquifers are presented. It focuses on methods for describing the spatial variability of hydraulic conductivity and Darcy velocity. This includes a presentation of the basic equations describing groundwater flow, the stochastic characterization of spatial heterogeneity of an aquifer, and numerical approaches to solving the groundwater flow equations.

2.1 Basic Equations

Theory of water flow through porous media is well established. Detailed information on fundamental principals of water flow through porous media is presented, for instance, in *Bear* (1972), *Busch et al.* (1993), *Verruijt* (1982) or *Delleur* (1999).

In this chapter three dimensional water flow through porous media is described using a combination of Darcy's law (Eq. 2.1) and the continuity equation (Eq. 2.2). Darcy's law was established by *Darcy* (1856). It postulates, that volumetric water flux is proportional to the hydraulic gradient ∇H. The proportionality factor is known as the hydraulic conductivity K and the volumetric water flux is called Darcy velocity $\vec{q}$. Independent of Darcy's findings, *Buckingham* (1907) studied water flow through unsaturated porous media. He found, that the pressure head h is a function of the soil moisture Θ, and consequently K depends on h.

$$\vec{q}_{(\vec{r},t)} = -K_{(\vec{r},h)} \nabla H_{(\vec{r},t)} \tag{2.1}$$

The validity of Darcy's law is limited to laminar flow processes. The upper limit of the validity is given by Reynolds number $N_R = \frac{\rho_f \vec{v} l}{\eta_f} = 1$, where ρ_f is the density of the fluid, $\vec{v}$ is the path velocity along the way l and η_f is the dynamic viscosity of the fluid. Higher Reynolds numbers indicate turbulent flow. The lower limit of validity of Darcy's law is at pore diameters of approximately 3 - 8 μm, which depends on the content of clay minerals (*Langguth and Voigt*, 1980). For smaller pore diameters, the interaction between water molecules and clay minerals is no longer negligible. Therefore volumetric water flux tends to zero due to adhesive forces.

The continuity equation (Eq. 2.2) expresses the principle of mass conservation. This means that no mass can be gained or lost.

$$\left(\frac{\partial \Theta}{\partial h_{(\vec{r},t)}} + S_{(h)} \right) \frac{\partial h_{(\vec{r},t)}}{\partial t} = -\nabla \vec{q}_{(\vec{r},t)} \tag{2.2}$$

The continuity equation describes the interaction between perturbations in Θ and h and their effects on the volumetric fluxes $\vec{q}_{(\vec{r},t)}$ in the flow domain for saturated and unsaturated water flow. $S_{(h)}$ is the specific storage coefficient.

Combining Equations 2.1 and 2.2 results in the generalized Richards' equation:

$$\left(\frac{\partial\Theta}{\partial h_{(\vec{r},t)}} + S_{(h)}\right)\frac{\partial h_{(\vec{r},t)}}{\partial t} = \nabla(K_{(\vec{r},h)}\nabla H_{(\vec{r},t)}) + Q_{(\vec{r},t)} \tag{2.3}$$

where $h_{(\vec{r},t)}$ is the pressure head, $\vec{r}$ is the position vector in a three dimensional space, t is time, $K_{(\vec{r},h)}$ is the hydraulic conductivity, $H_{(\vec{r},t)}$ is the total head, $Q_{(\vec{r},t)}$ is the source/sink term, Θ is the moisture content and $S_{(h)}$ is the specific storage coefficient where

$$H_{(\vec{r},t)} = h_{(\vec{r},t)} + z_{0(\vec{r})} \tag{2.4}$$

and $z_{0(\vec{r})}$ is the elevation head. In this universal form, Richards' equation describes isothermal water flow through saturated and unsaturated porous media depending on time t, pressure head h and space $\vec{r}$. The left-hand side of the Richards' equation $\left(\frac{\partial\Theta}{\partial h_{(\vec{r},t)}} + S_{(h)}\right)\frac{\partial h_{(\vec{r},t)}}{\partial t}$ describes the reaction in the flow domain due to perturbations in h. On the right-hand side, $\nabla(K_{(\vec{r},h)}\nabla H_{(\vec{r},t)})$ describes the flow through the observed flow domain and $Q_{(\vec{r},t)}$ specifies sources and sinks within the observed flow domain.

For unsaturated flow, a relationship between the moisture content Θ, pressure head h and hydraulic conductivity K need to be specified. A frequently used approach to describe $\Theta(h)$ and $K(\Theta)$ was developed by *van Genuchten* (1980) (Eq. 2.5) and *Mualem* (1977) (Eq. 2.6):

$$S = \frac{\Theta - \Theta_r}{\Theta_s - \Theta_r} = (1 + (\alpha_1 \cdot h)^n)^{-m} \tag{2.5}$$

where Θ_r is the residual water content, Θ_s is the saturated water content and n, m, α_1 are the v. Genuchten parameters,

$$K(S) = K_{sat} \cdot S^{\tau} \cdot (1 - [1 - S^{\frac{1}{m}}]^m)^2 \tag{2.6}$$

where $m = 1 - 1/n$ and τ is the tortuosity.

With regard to stationary groundwater flow, the hydraulic conductivity no longer depends on the pressure head. Additionally, all time dependencies in the Richards' equation become inapplicable and the left-hand side of Richards' equation becomes zero:

$$0 = \nabla(K_{(\vec{r})}\nabla H_{(\vec{r})}) + Q \tag{2.7}$$

2.2 Steady State Flow in a Borehole

Due to differing hydraulic conductivities inside the well, in the well screen, in the filter pack and in the aquifer, the flow in a borehole is characterized by the convergence of the streamlines towards the borehole, where hydraulic conductivity is infinite. A schematic description for a flow situation without a vertical component and an isotropic aquifer is given in Figure 2.1. Whenever vertical components of flow direction occur, the

image of the flow field is no longer symmetrical, which leads to the following approaches quantifying the convergence effect becoming invalid.

Within direct methods of flow velocity measurement (point dilution method, colloidal borescope, thermal flowmeters and laser Doppler velocimeter system), the convergence of the flow towards the borehole has to be quantified to calculate the Darcy velocity in the aquifer.

In literature, several approaches quantifying the convergence can be found. *Drost et al.* (1968) found a theoretical equation calculating the convergence factor α, which describes the relation between the inflow width and the diameter of the borehole (Fig. 2.1). This means that the flow velocity measured in a borehole is higher than in the aquifer sediment by factor α. Factor α depends on the construction of the borehole schematically shown in Figure 2.2.

With r_i being the radius of the element of the well construction and K_i being the appropriate hydraulic conductivity, α can be calculated by:

$$\alpha = \frac{8}{(1+\frac{K_3}{K_2})(1+(\frac{r_1}{r_2})^2+(\frac{K_2}{K_1}(1-(\frac{r_1}{r_2})^2))+(1-\frac{K_3}{K_2})((\frac{r_1}{r_3})^2+(\frac{r_2}{r_3})^2+\frac{K_2}{K_1}((\frac{r_1}{r_3})^2-(\frac{r_2}{r_3})^2))} \tag{2.8}$$

If the borehole construction is without a filter pack or the filter pack equals the aquifer ($r_3 = r_2$ and $K_3 = K_2$), the Equation 2.8 simplifies to:

$$\alpha = \frac{4}{1+(\frac{r_1}{r_2})^2+(\frac{K_3}{K_1})(1-(\frac{r_1}{r_2})^2)} \tag{2.9}$$

If the borehole construction consists only of a borehole ($r_3 = r_2 = r_1$ and $K_3 = K_2 = K_1$), the Equation 2.8 simplifies to:

$$\alpha = 2 \tag{2.10}$$

In *Kearl* (1997), Equation 2.10 coincides with the analogous heat conduction problem from *Carslaw and Jaeger* (1959) and the with the circle theorem (*Milne-Thompson*, 1968) for permeable cylinders in a uniform flow field. Equation 2.9 was already established by *Ogilvi* (1958) (*Drost et al.*, 1968). Equation 2.8 leads to α values ranging between -0.5 and 4.

Sano (1983) theoretically derived an equation relating the velocity inside a borehole to that in the aquifer by applying Stokes' equation to the flow inside a borehole and the generalized Darcy equation to the flow in the porous media. *Momii et al.* (1993) assumed that in general the diameter of a borehole is about 5 to 25 cm and the order of the permeability of the porous medium is less then 1 cm/s, therefore the solution of *Sano* (1983) is approximated by:

$$\alpha = 3 \tag{2.11}$$

Momii et al. (1993) verified this in laboratory experiments using a laser Doppler velocimeter system.

Previous approaches to quantifying the convergence of the streamlines in a borehole assume the perfect development of the groundwater observation well. In practice, the drilling and development of boreholes is associated not only with perturbations due to the

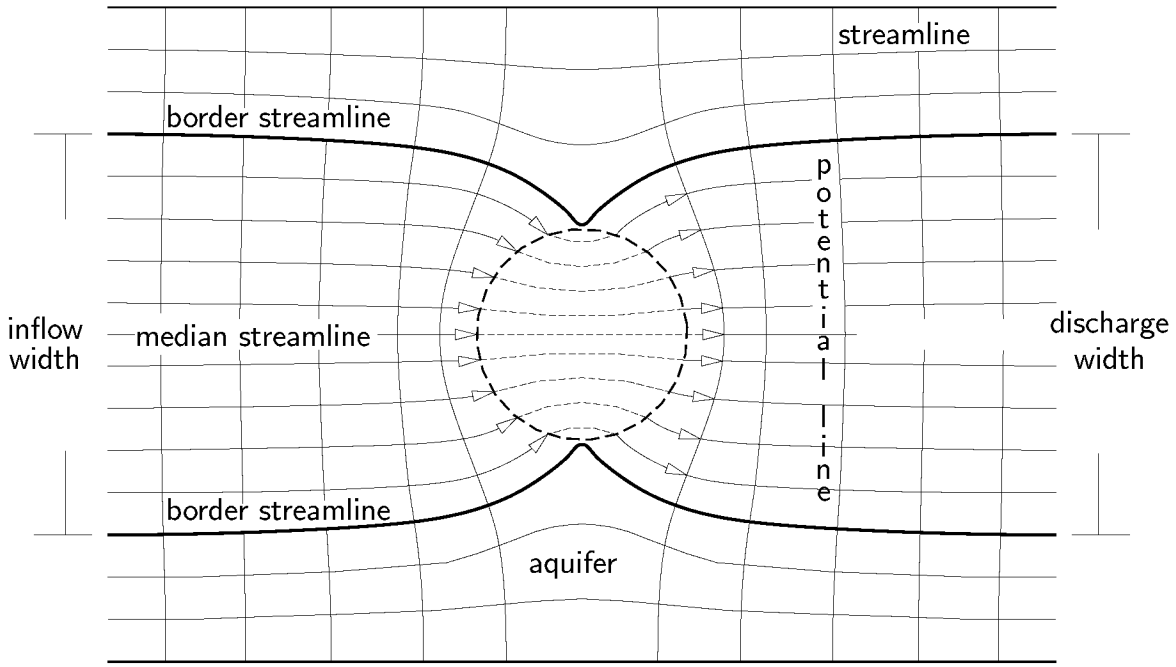

Figure 2.1: Schematic flow pattern inside and surrounding a well (*Drost et al.*, 1968).

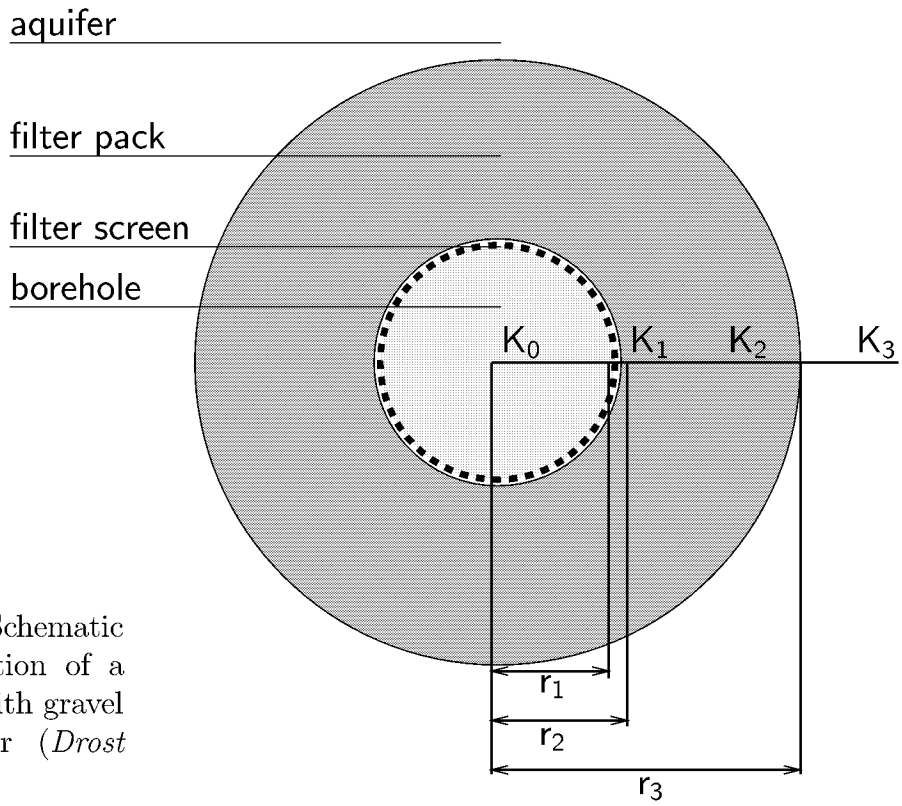

Figure 2.2: Schematic horizontal cross-section of a screened borehole with gravel pack in an aquifer (*Drost et al.*, 1968).

artificial materials (well screen and filter pack), but also of the natural aquifer material. Additional time dependent changes of the groundwater observation well occur due to particle transport and chemical processes.

The skin factor s has been defined by several authors (e.g. *Earlougher* (1977) or *Bidaux and Tsang* (1991)) to quantify the damage (positive skin factor) or the development (negative skin factor) of a borehole. In the conventional theory of *Earlougher* (1977) or *Novakowski* (1989), the skin region r_s (region damaged or developed around the borehole) is defined as homogeneous in K. In contrast, *Bidaux and Tsang* (1991) developed a complex theory with K depending on the distance to the borehole. In figure 12 of *Bidaux and Tsang* (1991) the dependency of the convergence factor on the thickness of the skin region and the skin factor is given for both the conventional and the complex skin theory. Within a variation of skin effect ranging between -4 to 10 and a dimensionless skin thickness ($\frac{r_s}{r_2} - 1$) ranging between 10^{-2} to 10^3, the convection factor varies between 0.1 and 4 for the conventional theory and between 0.1 and 11 for the complex theory.

Due to packers used in direct methods, the Darcy velocity measured in the borehole is, apart from the horizontal convergence effects, influenced by vertical convergence. This leads to an even higher velocity being measured in the borehole than is outside the borehole. For packer lengths between 0 mm and 500 mm, *Klotz* (1977) found a correction factor γ as a function of the packer lengths l_p

$$\gamma = 1 + 0.7 \cdot 10^{-3} l_p \tag{2.12}$$

quantifying the vertical convergence effect.

2.3 Heterogeneity of Hydraulic Parameters

Hydraulic properties of soils and aquifers, such as porosity and hydraulic conductivity and consequently the state variables such as Darcy velocities, are known to vary in space (*Boggs et al.*, 1992; *Englert et al.*, 2000a; *Leblanc et al.*, 1991; *Mackay et al.*, 1986; *Teutsch and Kobus*, 1990; *Vereecken et al.*, 2000). To enable the study of the spatial heterogeneity by means of geostatistical methods, hydraulic parameters and state variables are considered as **re**gionalized **v**ariables (ReV). These methods are well known and can be studied in detail e.g. in *Akin and Siemes* (1988), *Deutsch and Journel* (1998), *Journel and Huijbregts* (1989), *Schafmeister* (1999) and *Chilès and Delfiner* (1999).

2.3.1 Univariate Statistics

Within a flow domain, the univariate statistics of a ReV z are described by applying moment analysis to measured z data sets. Also referred to as arithmetic mean $m(z)$ and empirical variance $s^2(z)$, the first and second moment of a data set are:

$$m(z) = \frac{\sum_{i=1}^{n} z_i}{n} \tag{2.13}$$

$$s^2(z) = \frac{\sum_{i=1}^{n} (z_i - m(z))^2}{n-1} \tag{2.14}$$

As well as these descriptive statistical parameters, histograms are used for visualization of data sets (for example see Fig. 5.1).

Most often, populations have the form of a Gaussian normal probability density function:

$$f_{(z)} = \frac{1}{\sigma\sqrt{2\pi}} e^{-\frac{1}{2}\left(\frac{z-\mu}{\sigma}\right)^2} \tag{2.15}$$

with the mean of the population:

$$\mu(z) = \frac{\sum_{i=1}^{n} z_i}{n} \tag{2.16}$$

and the variance of the population:

$$\sigma^2(z) = \frac{\sum_{i=1}^{n} (z_i - \mu)^2}{n} \tag{2.17}$$

In hydrogeology, another probability density function often occurs, which is the log-normal probability density function:

$$f_{(z)} = \frac{1}{\sigma z\sqrt{2\pi}} e^{-\frac{1}{2}\left(\frac{\ln z-\mu}{\sigma}\right)^2} \tag{2.18}$$

where μ and σ^2 refer to the log-transformed log-normal probability density function, which is a Gaussian normal probability density function. Thus, Equations 2.16 and 2.17 are applied accordingly. The mean of a log-normal probability density function is often expressed by the geometric mean:

$$\mu_g(z) = e^{\frac{\sum_{i=1}^{n} \ln z_i}{n}} \tag{2.19}$$

where the variance is expressed by σ^2 of log-transformed data.

Whenever a data set is described by the appropriate probability density function, statistical tests are performed to prove the conformance between the data sample and the predicted probability density function. Data sets with $n < 2000$ are tested by the Shapiro Wilk test (W-test) (*Shapiro and Wilk*, 1965), data sets with $n > 2000$ are tested with the Kolmogorov Smirnov test (D-test). Within both tests, data sets are non parametrically tested on normality. Both calculate a test parameter (W or D), which is presented together with a probability of finding samples with a worse match with a normal distribution than the studied data set. This probability gives the significance level at which the normality of the data set is acceptable from a statistical point of view. Both tests compare the data set with a normal distribution by means of plotting together their cumulative form, both scaled to a total cumulative sum of 1. The W value denotes a correlation between a normal distribution and the data set. This leads to values close to 1 for good matches. The D value denotes the greatest difference between a normal distribution and the data set. For good matches, the D value is small.

2.3.2 Spatial Heterogeneity

Spatial heterogeneity is not completely random but usually exhibits some form of structure in an average sense, which reflects the fact that points close in space tend to assume

close values. *Matheron* (1965) coined the term regionalized variable (ReV) to designate a numerical function $z_{(\vec{r})}$ depending on a continuous space index $\vec{r}$, and combining high irregularity of detail with spatial correlation. Geostatistics can then be defined as "the application of probalistic methods to ReVs" (*Chilès and Delfiner*, 1999). Thus, the ReV is treated as a random variable RV. In other words, geostatistics characterize any unsampled (unknown) value z as a RV Z, the probability distribution of which describes the uncertainty about z, including the RV model Z, and more specifically its probability distribution being location dependent (*Deutsch and Journel*, 1998). The cumulative distribution function (cdf) of a continuous RV $Z(\vec{r})$ is denoted, where P is the probability:

$$f(\vec{r};z) = P\{Z(\vec{r}) \leq z\} \tag{2.20}$$

Just as an RV $Z(\vec{r})$ is characterized by its cdf (Eq. 2.20), a random function (RF) $Z(\vec{r})$ for the entire studied space can be characterized by the set of all its Ω-variate cdfs for any number of Ω and any choice of the Ω locations $\vec{r}_\omega$, $\omega = 1,...,\Omega$:

$$f(\vec{r}_1...\vec{r}_\omega; z_1...z_\Omega) = P\{Z(\vec{r}_1) \leq z_1, ..., Z(\vec{r}_\Omega) \leq z_\Omega\} \tag{2.21}$$

The amount of data generally available is insufficient to conclude the entire spatial law $f(\vec{r}_1...\vec{r}_\omega; z_1...z_\Omega)$. In geostatistics (more precisely, linear geostatistics), only the first two moments of the RF are used; in other words, no distinction is made between two RF's $Z_{\vec{r}_1}$ and $Z_{\vec{r}_2}$, which have the same first- and second-order moments and both functions are considered to be comprising of the same model (*Journel and Huijbregts*, 1989). The first order moment is given by the mean μ:

$$E\{Z(\vec{r})\} = \mu(Z(\vec{r})) \tag{2.22}$$

The second order moments variance σ^2, covariance C and variogram γ are given by:

$$\sigma^2\{Z(\vec{r})\} = E\{[Z(\vec{r}) - \mu(Z(\vec{r}))]^2\} \tag{2.23}$$
$$C(\vec{r}_1,\vec{r}_2) = E\{[Z(\vec{r}_1) - \mu(Z(\vec{r}_1))][Z(\vec{r}_2) - \mu(Z(\vec{r}_2))]\} \tag{2.24}$$
$$2\gamma(\vec{r}_1,\vec{r}_2) = \sigma^2\{Z(\vec{r}_1) - Z(\vec{r}_2)\} = 2(C(0) - C(\vec{r}_1,\vec{r}_2)) \tag{2.25}$$

The above mentioned moments are only valid if the requirement of stationarity is given. For the covariance function, stationarity of 2nd order is required. This means, on the one hand, that $E\{Z(\vec{r})\}$ exists and does not depend on $\vec{r}$:

$$E\{Z(\vec{r})\} = \mu(Z), \forall\vec{r} \tag{2.26}$$

and, on the other hand, that for each pair of RV's $\{Z(\vec{r}+\vec{\xi}), Z(\vec{r})\}$ the covariance exists and depends on the separation distance $\vec{\xi}$:

$$C(\vec{\xi}) = E\{Z(\vec{r}+\vec{\xi}) \cdot Z(\vec{r})\} - (\mu(Z))^2, \forall\vec{r} \tag{2.27}$$

Stationarity of 2nd order requires the existence of the covariance and consequently the existence of a finite variance. This is not always the case, whereas the variogram always exists (*Akin and Siemes*, 1988). Thus the intrinsic hypothesis, a somewhat milder type

of stationarity is required for the variogram. This means, on the one hand, that $E\{Z(\vec{r})\}$ exists and does not depend on $\vec{r}$:

$$E\{Z(\vec{r})\} = \mu(Z), \forall \vec{r} \tag{2.28}$$

and, on the other hand, that for all vectors $\vec{\xi}$ the increment $[Z(\vec{r}+\vec{\xi}) - Z(\vec{r})]$ has a finite variance which does not depend on $\vec{r}$:

$$\sigma^2\{Z(\vec{r}+\vec{\xi}) - Z(\vec{r})\} = E\{[Z(\vec{r}+\vec{\xi}) - Z(\vec{r})]^2\} = 2\gamma(\vec{\xi}), \forall \vec{r} \tag{2.29}$$

The lesser demand on the RF model by the intrinsic hypothesis has been recently shown to be of no consequence for most practical situations (*Deutsch and Journel*, 1998). However, in accordance with standard practice, the variogram is used for the evaluation of experimental data sets in the following chapters. For studies concerning stochastic processes, the covariance and the correlogram ρ is used:

$$\rho(\vec{\xi}) = \frac{C(\vec{\xi})}{C(0)} = 1 - \frac{\gamma(\vec{\xi})}{C(0)} \tag{2.30}$$

For the estimation of the variogram, the experimental variogram $\gamma_{(\vec{\xi})}$ is used:

$$\gamma_{(\vec{\xi})} = \frac{1}{2N_{(\vec{\xi})}} \sum_{i=1}^{N} (z_{(\vec{r}_i)} - z_{(\vec{r}_i+\vec{\xi})})^2 \tag{2.31}$$

Two models are used to fit the experimental variograms, covariances and correlograms within the method of least squares:
a) Exponential Model:

$$\gamma_{(\vec{\xi})} = C_0 \cdot [1 - \exp(-|\vec{\xi}/\lambda|)] \tag{2.32}$$
$$C(\vec{\xi}) = C_0 \cdot [\exp(-|\vec{\xi}/\lambda|)] \tag{2.33}$$
$$\rho(\vec{\xi}) = \exp(-|\vec{\xi}/\lambda|) \tag{2.34}$$

b)Gaussian Model:

$$\gamma_{(\vec{\xi})} = C_0 \cdot [1 - \exp(-|\vec{\xi}^2/\lambda^2|)] \tag{2.35}$$
$$C(\vec{\xi}) = C_0 \cdot [\exp(-|\vec{\xi}^2/\lambda^2|)] \tag{2.36}$$
$$\rho(\vec{\xi}) = \exp(-|\vec{\xi}^2/\lambda^2|) \tag{2.37}$$

where C_0 is the sill and λ is the correlation length.

Within the geostatistical estimation of a hydraulic parameter, its spatial heterogeneity is described by the mean, the variance and the correlation length with regard to a specific model. These parameters are used to compare different aquifer situations quantitatively. However, these parameters are also used to generate synthetic aquifer situations, which are given the same parameters as a natural aquifer. This procedure is called stochastic simulation. Stochastic simulation is the process of drawing alternative, equally probable, joint realizations of the component RVs from an RF model (*Deutsch and Journel*, 1998).

2.4 Stochastic Theories

During the last twenty years extensive research has been carried out on the combining of physical equations describing groundwater flow with stochastic processes. The aim of this field of research is to characterize the effect of the spatial heterogeneity of K on Darcy velocities and total heads. Detailed information on stochastic theories on groundwater flow can be found, for example, in *Dagan* (1989) and *Gelhar* (1993).

In stochastic theories on groundwater flow, K is considered a stochastic field of 2nd order stationarity (Section 2.3.2). The mean hydraulic gradient (J) is assumed to be parallel to the mean flow direction and is constant over the entire flow domain, i.e. there is no trend in K, there are no sources and sinks and the domain is of infinite extend. The flow velocity field is assumed to be divergence free and the porosity is constant over the entire flow domain. Following this, the continuity equation (Eq. 2.2) can be rewritten as

$$\nabla \vec{q} \;=\; 0 \tag{2.38}$$

Defining $Y = \ln(K)$ and inserting the Darcy's law (Eq. 2.1), the continuity equation becomes

$$\nabla^2 H + \nabla Y \cdot \nabla H \;=\; 0 \tag{2.39}$$

Perturbation theory is applied to the continuity equation and Darcy's law in order to find functional relations between the heterogeneity of $\vec{q}$ and the heterogeneity of K, which is shown in the following.

Expressing the variables in the Darcy and the continuity equation by means of a sum of the ensemble mean and fluctuation, denoted by $'$ around this mean,

$$Y = \mu(Y) + Y';\; \vec{q} = \mu(\vec{q}) + \vec{q}';\; H = \mu(H) + H'$$

and the mean fluctuation is zero,

$$\mu(Y') = 0;\; \mu(\vec{q}') = 0;\; \mu(H') = 0$$

the continuity equation (Eq. 2.39) becomes

$$\nabla^2(\mu(H) + H') + \nabla(\mu(Y) + Y') \cdot \nabla(\mu(H) + H') \;=\; 0 \tag{2.40}$$

Formally, the total head can be described as an asymptotic sequence including 0th, 1st, 2nd or higher order terms:

$$H = \mu(H) + H' = H^{[0]} + H^{[1]} + H^{[2]}....$$

which leads to the following formulation of Equation 2.40:

$$\nabla^2(H^{[0]} + H^{[1]} + H^{[2]}....) + \nabla(\mu(Y) + Y') \cdot \nabla(H^{[0]} + H^{[1]} + H^{[2]}....) \;=\; 0 \tag{2.41}$$

Equation 2.41 gives the 0th, 1st, 2nd or higher order terms. Those can be rewritten, considering no trend in Y ($\nabla\mu(Y) = 0$):

$$\begin{aligned}
\nabla^2 H^{[0]} + \nabla\mu(Y)\cdot\nabla H^{[0]} &= 0 \Leftrightarrow \nabla^2 H^{[0]} = 0 && (2.42)\\
\nabla^2 H^{[1]} + \nabla\mu(Y)\cdot\nabla H^{[1]} + \nabla Y'\cdot\nabla H^{[0]} &= 0 \Leftrightarrow \nabla^2 H^{[1]} + \nabla Y'\cdot\nabla H^{[0]} = 0 && (2.43)\\
\nabla^2 H^{[2]} + \nabla\mu(Y)\cdot\nabla H^{[2]} + \nabla Y'\cdot\nabla H^{[1]} &= 0 \Leftrightarrow \nabla^2 H^{[2]} + \nabla Y'\cdot\nabla H^{[1]} = 0 && (2.44)
\end{aligned}$$

For the estimation of the flow, a similar expansion for the Darcy equation is introduced:

$$\begin{aligned}
\vec{q} &= -K\nabla H\\
\mu(\vec{q}) + \vec{q}' &= -e^{(\mu(Y)+Y')}\cdot\nabla(\mu(H)+H')\\
\mu(\vec{q}) + \vec{q}' &= -K_g\cdot(1+Y'+\frac{Y'^2}{2}+\frac{Y'^3}{6}...)\cdot(\nabla H^{[0]}+\nabla H^{[1]}+\nabla H^{[2]}....) && (2.45)
\end{aligned}$$

where $K_g = e^{\mu(Y)}$ is the geometric mean of K.
Formally, the Darcy velocity can be described as an asymptotic sequence,

$$\vec{q} = \mu(\vec{q}) + \vec{q}' = \vec{q}^{[0]} + \vec{q}^{[1]} + \vec{q}^{[2]}....$$

which, introduced in the perturbated Darcy equation (Eq. 2.45), gives 0th, 1st, 2nd or higher order terms:

$$\begin{aligned}
\vec{q}^{[0]} &= -K_g\cdot\nabla H^{[0]} && (2.46)\\
\vec{q}^{[1]} &= -K_g\cdot(\nabla H^{[1]} + \nabla H^{[0]}Y') && (2.47)\\
\vec{q}^{[2]} &= -K_g\cdot\left(\nabla H^{[2]} + Y'\nabla H^{[1]} + \nabla H^{[0]}\frac{Y'^2}{2}\right) && (2.48)
\end{aligned}$$

Inserting these perturbated terms of $\vec{q}$ into the definitions of the corresponding quantities, one gets equations estimating the variance and the covariance of Darcy velocity components on the basis of statistical parameters of hydraulic conductivities and hydraulic gradient. Considering 0th and 1st terms of the perturbated Darcy's law, results are called 1st order approximation, denoted as $^{(1)}$. Considering also the 2nd order terms, results are called 2nd order approximation, denoted as $^{(2)}$:

$$\begin{aligned}
C_q^{(1)}(0) &= \sigma^2(\vec{q}^{[0]} + \vec{q}^{[1]}) && (2.49)\\
C_q^{(2)}(0) &= \sigma^2(\vec{q}^{[0]} + \vec{q}^{[1]} + \vec{q}^{[2]}) && (2.50)\\
C_q^{(1)}(\xi) &= C(\vec{q}^{[0]} + \vec{q}^{[1]}) && (2.51)\\
C_q^{(2)}(\xi) &= C(\vec{q}^{[0]} + \vec{q}^{[1]} + \vec{q}^{[2]}) && (2.52)
\end{aligned}$$

Additionally, the effective hydraulic conductivity ($K_{ef} \equiv \frac{\mu(\vec{q})}{\mu(\nabla H)}$) can be estimated.

$$\begin{aligned}
K_{ef}^{(1)} &= \frac{\mu(\vec{q}^{[0]} + \vec{q}^{[1]})}{\mu(\nabla H^{[0]} + \nabla H^{[1]})} && (2.53)\\
K_{ef}^{(2)} &= \frac{\mu(\vec{q}^{[0]} + \vec{q}^{[1]} + \vec{q}^{[2]})}{\mu(\nabla H^{[0]} + \nabla H^{[1]} + \nabla H^{[2]})} && (2.54)
\end{aligned}$$

In *Gelhar and Axness* (1983), the theoretical validity of these equations is given for small values σ_Y^2. *Schwarze et al.* (2001) found very good agreement between 1st order approximation and simulation results for $\sigma_Y^2 = 0.1$. The validity for higher σ_Y^2 remains unclear.

In the following, solutions of the Equations 2.49 - 2.54 are given for 2D and 3D. It is assumed that the correlation length in the two horizontal directions are equal, although differing from the vertical correlation length. $C_{q_k}^{(j)}(\xi_l')$ denotes the j-th order covariance approximation of Darcy velocity component k in direction l.

Two Dimensional Groundwater Flow

Considering 1st order approximation and an isotropic case, the variances of the Darcy velocity components $C_{q_1}^{(1)}(0)$ and $C_{q_2}^{(1)}(0)$ are given for an exponential and for a Gaussian covariance model of Y by *Dagan* (1989):

$$C_{q_1}^{(1)}(0) = \frac{3}{8}(K_g J)^2 \sigma_Y^2 \tag{2.55}$$

$$C_{q_2}^{(1)}(0) = \frac{1}{8}(K_g J)^2 \sigma_Y^2 \tag{2.56}$$

Considering 2nd order approximation, the variances of the Darcy velocity components $C_{q_1}^{(2)}(0)$ and $C_{q_2}^{(2)}(0)$ are given:

a) for an exponential covariance model of Y with $\sigma_Y^2 = 1$ by *Hsu et al.* (1996):

$$C_{q_1}^{(2)}(0) = 1.08 \cdot C_{q_1}^{(1)}(0) \tag{2.57}$$

$$C_{q_2}^{(2)}(0) = 1.34 \cdot C_{q_2}^{(1)}(0) \tag{2.58}$$

b) for a Gaussian covariance model of $\ln K$ with $\sigma_Y^2 = 1$ by *Hsu and Neuman* (1997):

$$C_{q_1}^{(2)}(0) = 1.01 \cdot C_{q_1}^{(1)}(0) \tag{2.59}$$

$$C_{q_2}^{(2)}(0) = 1.19 \cdot C_{q_2}^{(1)}(0) \tag{2.60}$$

The effective hydraulic conductivity is for both 1st and 2nd order the geometric mean of the hydraulic conductivity (*Dagan*, 1989; *Gelhar*, 1993). This applies for exponential and Gaussian models.

$$K_{ef}^{(1)} = K_{ef}^{(2)} = K_g \tag{2.61}$$

Three Dimensional Groundwater Flow

Considering 1st order approximation, the variances and covariances of Darcy velocity components $C_{q_1}^{(1)}(\vec{\xi_1'})$, $C_{q_2}^{(1)}(\vec{\xi_1'})$ and $C_{q_3}^{(1)}(\vec{\xi_1'})$ are given for an exponential and Gaussian covariance model of $\ln K$ by *Russo* (1995) and *Hsu and Neuman* (1997). In the following, the covariances concern the mean flow direction, whereupon $e = \frac{\lambda_v}{\lambda_h}$, λ_v is the correlation length in vertical, λ_h is the correlation length in the horizontal direction and ξ_i' denotes $\frac{\xi_i}{\lambda_h}$ in the i-th direction:

$$\frac{C_{q_1}^{(1)}(0)}{\sigma_Y^2(K_gJ)^2} = 1 + \frac{19e^3 - 10e^5}{16e(-1+e^2)^2} - \frac{e(13-4e^2)\arcsin[(1-e^2)^{\frac{1}{2}}]}{16(1-e^2)^{\frac{1}{2}}(-1+e^2)^2} \tag{2.62}$$

$$\frac{C_{q_2}^{(1)}(0)}{\sigma_Y^2(K_gJ)^2} = \frac{e\{e(1-e^2)^{\frac{1}{2}} + 2e^3(1-e^2)^{\frac{1}{2}} + \arcsin[(1-e^2)^{\frac{1}{2}}] - 4e^2\arcsin[(1-e^2)^{\frac{1}{2}}]\}}{16(1-e^2)^{\frac{1}{2}}(-1+e^2)^2} \tag{2.63}$$

$$\frac{C_{q_3}^{(1)}(0)}{\sigma_Y^2(K_gJ)^2} = \frac{-3e^2}{4(-1+e^2)} + \frac{e(1+2e^2)\arcsin[(1-e^2)^{\frac{1}{2}}]}{4(-1+e^2)^{\frac{1}{2}}(-1+e^2)^2} \tag{2.64}$$

$$\frac{C_{q_1}^{(1)}(\xi_1')}{\sigma_Y^2(K_gJ)^2} = \int_{-1}^{+1}\left(\frac{1}{2} - \frac{r^2e[4-5r^2+r^4+(3r^2-r^4)e^2]}{4[(1-r^2)+(r^2e^2)]^{\frac{3}{2}}}\right)\cdot(1-|r\xi_1'|)\exp(-|r\xi_1'|)dr \tag{2.65}$$

$$\frac{C_{q_2}^{(1)}(\xi_1')}{\sigma_Y^2(K_gJ)^2} = \int_{-1}^{+1}\frac{r^2e(1-r^2)(1-|r\xi_1'|)\exp(-|r\xi_1'|)dr}{4[(1-r^2)+r^2e^2]^{\frac{1}{2}}} \tag{2.66}$$

$$\frac{C_{q_3}^{(1)}(\xi_1')}{\sigma_Y^2(K_gJ)^2} = \int_{-1}^{+1}\frac{r^2e(1-r^2)(1-|r\xi_1'|)\exp(-|r\xi_1'|)dr}{4[(1-r^2)+r^2e^2]^{\frac{3}{2}}} \tag{2.67}$$

Both for exponential and Gaussian correlation model, the effective hydraulic conductivity in the horizontal direction can be estimated by 1st order approximation as follows (*Dagan*, 1989):

$$K_{ef}^{(1)} = K_g\cdot\left(1+\sigma_Y^2\left(\frac{1}{2} - \frac{\frac{e^2}{1-e^2}\left(\frac{1}{e\sqrt{1-e^2}}\arctan\sqrt{\frac{1}{e^2}-1}-1\right)}{2}\right)\right) \tag{2.68}$$

In order to estimate second order approximations, correction factors, given in *Hsu and Neuman* (1997) and *Deng and Cushman* (1995), can be used. The correction factors depend on e and σ_Y^2. In the following, the correction factors are not universal, but valid for the special situation at the Krauthausen test site (see Tab. 5.4).

The corrections for 2nd order approximation are given for a Gaussian correlation model for Y in figure 5 of *Hsu and Neuman* (1997). Here the correction for $e = 0.01$ and $\sigma_Y^2 = 1$ is presented:

$$C_{q_1}^{(2)}(0) = 2.4\cdot C_{q_1}^{(1)}(0) \tag{2.69}$$

For $C_{q_2}^{(2)}(0)$ and $C_{q_3}^{(2)}(0)$, the correction factor cannot be accurately identified, due to the small scale of figure 5 in *Hsu and Neuman* (1997).

The correction factor for the effective hydraulic conductivity is given in figure 7 of *Hsu and Neuman* (1997):

$$K_{ef}^{(2)} = 1.6\cdot K_g \tag{2.70}$$

The corrections for 2nd order approximation for a exponential correlation model for Y are given in figure 2 of *Deng and Cushman* (1995). Here, the correction for $e = 0.017$ and $\sigma_Y^2 = 1$ is presented for the y-component:

$$C_{q_1}^{(2)}(0) = 2.4\cdot C_{q_1}^{(1)}(0) \tag{2.71}$$

For $C_{q_2}^{(3)}(0)$ and $C_{q_3}^{(3)}(0)$, the correction factor is independent from e and identical for the x- and z-component (*Deng and Cushman*, 1995).

$$C_{q_2}^{(2)}(0) = C_{q_2}^{(1)}(0)(1+\sigma_Y^2) \tag{2.72}$$

$$C_{q_3}^{(2)}(0) = C_{q_3}^{(1)}(0)(1+\sigma_Y^2) \tag{2.73}$$

The horizontal component of the effective hydraulic conductivity can be estimated as follows (*Deng and Cushman*, 1995):

$$K_{ef}^{(2)} = K_g\left(1+\left(\frac{1}{2}+\beta\right)\sigma_Y^2+\frac{1}{2}\left(\frac{1}{2}+\beta\right)^2\left(\sigma_Y^2\right)^2\right) \tag{2.74}$$

with

$$\beta = \frac{1}{2\cdot\frac{|1-e^2|}{e^2}}\left(1-\frac{arctan\sqrt{\frac{|1-e^2|}{e^2}}}{e^2\sqrt{\frac{|1-e^2|}{e^2}}}\right)$$

for $e < 1$.

2.5 Numerical Solutions

In order to compute water flow, Richards' equation (Eq. 2.3) has to be solved. Due to the fact that the strongly non-linear Richards' equation cannot be solved analytically in most cases, numerical methods have to be applied. Detailed information on the fundamentals of numerical solutions for water flow is presented for instance in *Bear* (1972), *Busch et al.* (1993), *Verruijt* (1982), *Delleur* (1999) or *Yeh* (1981).

The common techniques for solving the Richards' equation are the methods of finite elements (FE) and finite differences (FD). Both methods require a grid of the flow domain, for which the water flow is needed. Additionally, initial conditions for each grid node and boundary conditions along the complete boundary of the flow domain have to be defined.

Two major types of boundary conditions are usually considered:

- specification of total head, called Dirichlet boundary condition $H_{D(\vec{r})}$
- specification of the flux, called Neumann $\vec{q}_{N(\vec{r})}$ or Cauchy $\vec{q}_{C(\vec{r})}$ boundary condition

The key assumption for the Dirichlet boundary condition is that, regardless of the groundwater flow within the flow domain and at the boundary, this will have no influence on the potential of the outside water body, in such a way that this potential remains fixed as determined by the boundary condition (*Delleur*, 1999). The mathematical expression of the Dirichlet boundary condition, for stationary groundwater modelling, is shown in the following equation:

$$H_{\Gamma(\vec{r})} = H_{D(\vec{r})} \qquad \forall \qquad \vec{r} \in \Gamma_D \tag{2.75}$$

A flux boundary condition (Neumann or Cauchy) implies that, regardless of the state and flow of the groundwater inside the flow domain and at the boundary, the normal

flux is fixed by external conditions and remains as determined by the boundary condition (*Delleur*, 1999). Neumann boundary conditions (Eq. 2.76) take into account the pressure head $h_{(\vec{r})}$, where the Cauchy boundary conditions (Eq. 2.77) consider the total head $H_{(\vec{r})}$.The mathematical expressions are:

$$K\nabla h_{\Gamma(\vec{r})} = \vec{q}_{N(\vec{r})} \quad \forall \quad \vec{r} \in \Gamma_N \tag{2.76}$$

$$K\nabla H_{\Gamma(\vec{r})} = \vec{q}_{C(\vec{r})} \quad \forall \quad \vec{r} \in \Gamma_C \tag{2.77}$$

The choice of the type of boundary condition depends on the hydrogeological problem, which is to be solved by groundwater modelling. A typical example for Cauchy boundary conditions is a stationary flux into the flow domain. Neumann and Cauchy boundary conditions are typically used for the definition of no flux boundaries, such as water divides or aquifer aquitard interfaces. More complex boundary situations can also be defined by combinations of the previously mentioned types of boundary conditions. For instationary problems $H_{D(\vec{r})}, \vec{q}_{N(\vec{r})}, \vec{q}_{C(\vec{r})}$ depends on time.

Chapter 3

Development of a New Groundwater Flow Velocimeter

3.1 Measurement of Groundwater Flow Velocity

3.1.1 Indirect Methods

The estimation of mean groundwater flow velocities on the basis of **Darcy's law** (Eq. 2.1) is carried out by measuring pressure head and hydraulic conductivities in groundwater observation wells. Pressure head measurements are used to estimate the mean hydraulic gradient by interpolating. This method is still the major procedure used in hydrogeology to estimate the Darcy velocities. The mean Darcy velocity magnitude and direction can be evaluated.

Another classical method for estimating the Darcy velocities is the **multi-well tracer test**. One groundwater observation well (injection well) is used to inject a tracer, whereas all other available groundwater observation wells are used to monitor tracer concentrations. The tracer is transported by the natural groundwater flow. The time dependent tracer concentration is measured at observation wells resulting in breakthrough curves (BTCs). The interpretation of BTCs allows the estimation of the mean pore velocity magnitude $|\vec{q}_n|$. With $|\vec{q}| = \frac{|\vec{q}_n|}{n_0}$, Darcy velocity magnitude $|\vec{q}|$ directly relates to $|\vec{q}_n|$ and the effective porosity n_0. Additionally, the mean direction of the flow velocity can be estimated by calculating the longitudinal axis of the tracer plume. Thus, the mean Darcy velocity magnitude and direction can be evaluated.

Leap and Kaplan (1988) derived an equation for determining regional groundwater velocity from the results of a **single-well drift-and-pumpback tracer test**, which accounts for regional advection during back-pumping, by employing the following steps:

- A pulse of conservative tracer is injected into a well and allowed to drift with the regional gradient for an arbitrary length of time. The actual direction of flow will be along the regional gradient, assuming isotropy and homogeneity are given.

- The pulse is then pumped back into the well at a constant rate and sampled for concentration at different times resulting in a breakthrough curve.

- The rate of pumpback, drift time, pumpback time, effective porosity, and the aquifer thickness are then used to compute the regional groundwater velocity.

A similar technique is published by *Bachmat et al.* (1988). *Hall et al.* (1991) describes experiments carried out using this method. In the scope of single-well drift-and-pumpback tracer tests, mean Darcy velocity magnitude can be evaluated.

3.1.2 Direct Methods

The basic operating principle of **thermal flowmeters** is to bury a thin, cylindrical heater at the point where the groundwater flow velocity is to be measured. If the heat flux out of the cylinder is uniform over the surface of the cylinder, then the temperature distribution on the surface of the cylinder will vary according to the direction and magnitude of the groundwater flow velocity passing the cylinder. In general, relatively warm temperatures are observed on the downstream side of the probe and relatively cool temperatures are on the upstream side because the heat introduced into the formation by the heater is advected around the instrument by fluid flow passing the tool (*Ballard*, 1996). This measurement allows 3-dimensional flow direction measurement. For flow velocities between $8.64 \cdot 10^{-3}$ m/d and $2.2 \cdot 10^{-2}$ m/d, uncertainties of $\pm 25\%$ in magnitude and $\pm 15°$ in azimuth are obtainable. At higher flow, velocities measurement uncertainties in the magnitude and direction of the flow velocity are only a few percent and a few degrees (*Ballard*, 1996). Similar thermal flowmeters are described in *Kerfoot and Massard* (1985), *Alden and Munster* (1997) and *Paillet et al.* (1996).

Momii et al. (1993) developed a **laser Doppler velocimeter system** for horizontal groundwater measurements in a borehole. At the crossing point of two laser beams, an interference fringe with a known spacing is formed. The crossing point of the two beams is the measurement point. When a particle crosses the lighter parts in the fringe pattern of the measurement point, the intensity of light, scattered from the particle increases. When it crosses the darker parts, the intensity decreases. The temporal change in the intensity of scattered light caused by the particle crossing the fringe pattern can be detected by a photosensor. The peak frequency, the so called Doppler frequency of the detected signals varies proportional to the velocity of the particle. Thus, the velocity can be simply obtained by the product of the spacing of the interference fringe and the Doppler frequency. Rotation of the fringe pattern additionally allows flow direction measurement. Results obtained in laboratory experiments show that the laser Doppler velocimeter system can measure both the magnitude and the direction of groundwater velocity with sufficient accuracy down to $8.64 \cdot 10^{-2}$ m/d in a borehole (*Momii et al.*, 1993).

Kearl and Case (1992) and *Schöttler* (1997) independently developed a method to measure groundwater velocities based on the observation of particle movement in a monitoring well using the **colloidal borescope**. The colloidal borescope consists of a set of lenses and miniature video cameras capable of observing natural particles in monitoring wells. The borescope focuses on a plane between 1 to 2 mm^2 and observes the movement of colloids in a time range of 1 to 15 s. This enables a almost continuous monitoring of groundwater velocity and direction (*Kearl*, 1997; *Schöttler*, 2001). A typical field

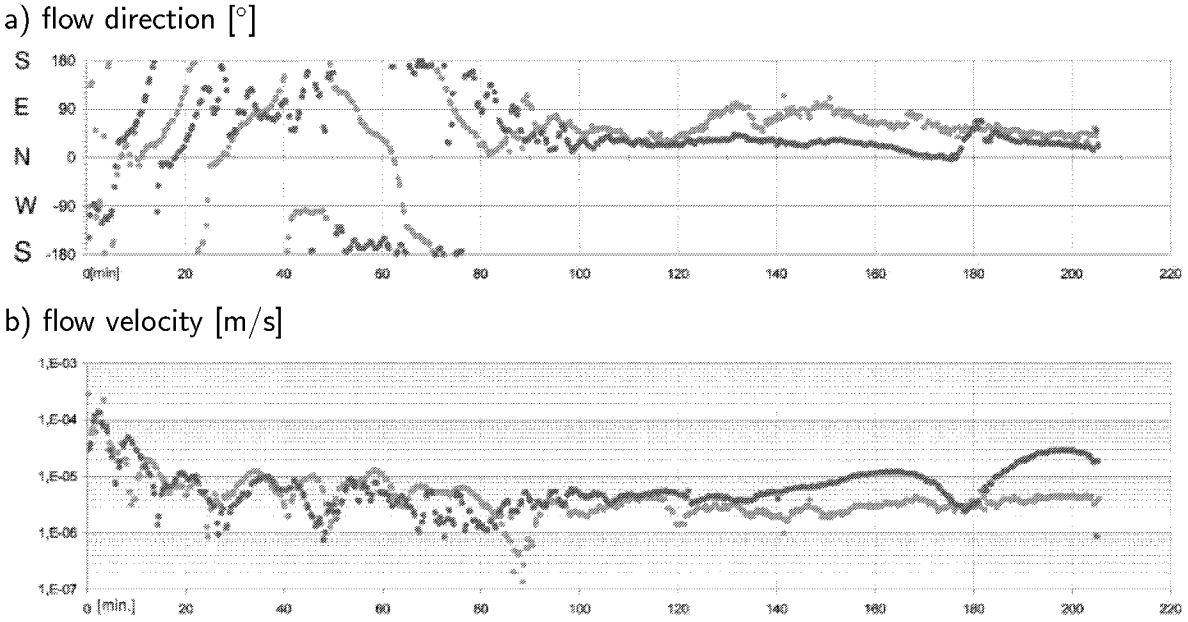

Figure 3.1: Typical field observation with the colloidal borescope (*Schöttler*, 2001). In a), the evolution of flow direction with time is shown. In b), the corresponding evolution of flow velocity with time is shown. Two evolution curves, bright and dark grey are given, syncron measured at two different vertical positions (1 m distant).

observation is shown in Figure 3.1. Thus, the colloidal borscope permits measurement of groundwater flow velocities in magnitude and direction with high resolution in time and space.

Since the 1960s, extensive work on **point dilution method**, for measuring the flow rate of ground water, has been carried out by various groups (*Drost et al.*, 1968). The point dilution method aims to relate the observed dilution of a tracer, introduced into a borehole, to groundwater flow. If there is steady flow and the tracer is homogeneously distributed throughout the dilution volume at all times, an apparent flow velocity can be calculated (Fig. 3.2 and Eq. 3.1).

The measured flow velocity q_m is a sum of different phenomena expressed in the following equation:

$$q_m = q_{ha} + q_k + q_d + q_c + q_{va} \tag{3.2}$$

with q_{ha} being the horizontal advection , q_k the density driven convection, q_d the molecular diffusion, q_c the apparent flow rate caused by the mixing device and q_{va} the vertical advection. If the contributing velocities are known, the measured velocity can be used to evaluate the horizontal advection q_{ha}, which is proportional to the magnitude of the horizontal flow velocity averaged over the area of approaching flow A.

Drost and Neumaier (1974) use a bypass connecting the area above the upper packer with the one below the lower packer to provide a hydraulic shortcut. This avoids flow passing the gravel pack outside the borehole. Control of the flow passing the bypass gives information on the vertical component of the flow velocity.

The point dilution method is performed using different tracers, e.g. the radioac-

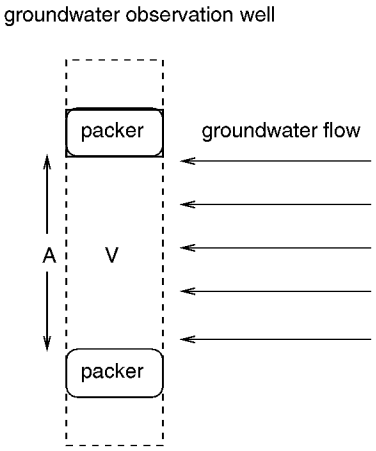

$$q_m = -\frac{V}{At} \cdot \ln \frac{c}{c_0} \tag{3.1}$$

q_m = measured flow velocity
V = dilution volume
A = area of approaching flow
t = time after beginning of dilution
c = concentration at t
c_0 = initial concentration

Figure 3.2: Principal set up and equation of a point dilution test.

tive tracer $^{82}Br^-$ (*Drost et al.*, 1968), salt tracers or the fluorescence tracer uranin ($C_{20}H_{20}Na_2O_5$) (*Barczewski and Marshall*, 1992; *Englert et al.*, 2001). *Drost et al.* (1968) additionally obtained the flow direction by rotating a collimator probe sensitive to incident radiation.

3.2 Dilution Measurement with Laser-Induced Fluorimetry

The single-well point dilution method requires the in situ determination of the tracer concentration in the groundwater observation well. In situ dilution can be measured by the use of fibre optic in combination with the laser-induced fluorimetry (LIF). The first reference in literature for in situ uranin measurement in groundwater with fibre optic, in combination with LIF, is *Barczewski* (1985). In the following, the focus is on the equipment used in this work. More detailed information on fluorescence measurements is to be found in *Guilbault* (1973), *Schulmann* (1977) or *Schwedt* (1981).

A nitrogen laser is used to send a laserbeam with a wavelength of 337 nm through a coumarin 102 ($C_{16}H_{17}NO_2$) solution (Fig. 3.3). Here, the coumarin 102 molecules are exited and after a so-called internal conversion (< 0.1 ns), electrons fall back to their primary energy level within nano seconds. Meanwhile, light in the range 454 nm to 506 nm is emitted with a maximum intensity at 470 nm. This light is then routed through a fibre optic cable, 16 m in length and a diameter of 200 μm. At the end of the fibre optic cable, the beam enters the defined volume inside the groundwater observation well. Here the uranin ($C_{20}H_{20}Na_2O_5$) molecules are exited by the light beam. After internal conversion, electrons return to their primary energy level emitting a light including wavelengths from 480 nm to 600 nm with a maximum at 510 nm. The uranin emission light is routed through six fibre optic cables, each 16 m long and 200 μm in diameter to a spectrometer where the arriving bulk beam is separated into different beams of a specific wavelength. Coming from the spectrometer, the split lightbeam is recorded by a CCD camera. Here, the intensity of each wavelength is detected. This information is sent to a computer, where the data is stored (Fig. 3.3). The spectrograms show typical

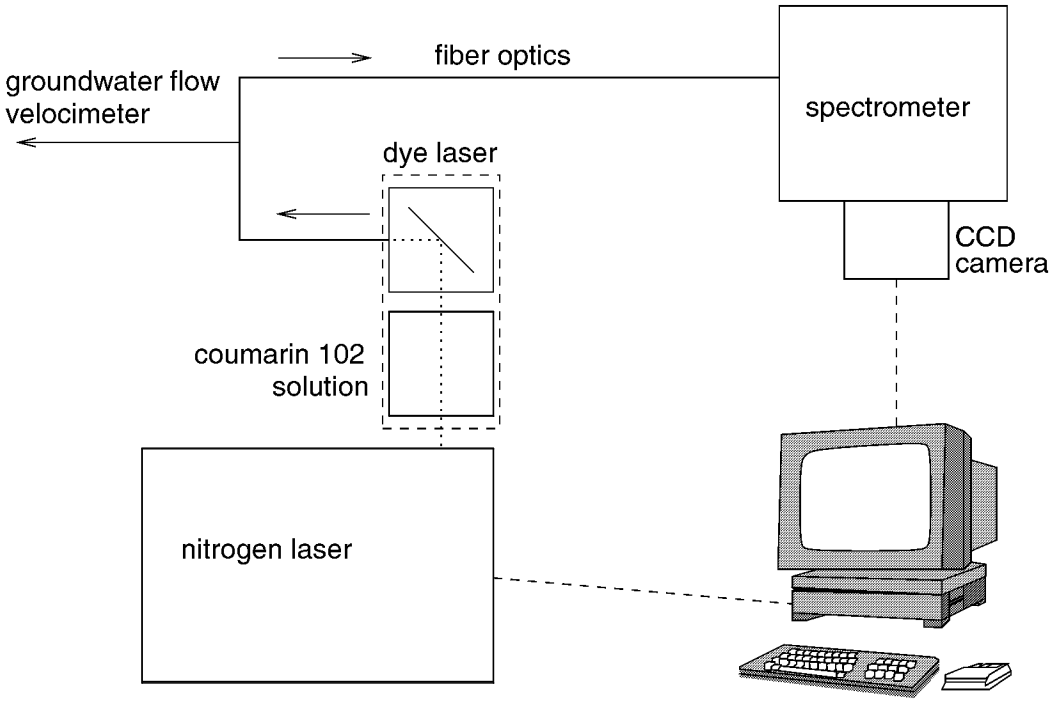

Figure 3.3: Schematic set up of the laser-induced fluorescence spectroscopy: dotted lines represent the laser beam, solid lines represent fibre optics and dashed lines represent electronic connections.

intensity distributions, as in Figure 3.4 (*Englert et al.*, 2001).

The uranin concentration, if below 1 mg/l, and the intensity of uranin fluorescence are directly proportional (*Barczewski and Marshall*, 1992). In order to compute the intensity of uranin fluorescence, the integral below the uranin peak (490 - 600 nm) is computed and corrected with the integral below the background signal from 336 - 446 nm. Due to the maximum uranin concentration of 1 mg/l inside the defined volume of the groundwater flow velocimeter, the uranin concentration dilution is identical to the intensity decrease. This allows direct use of the background corrected uranin intensity peak for computations of the slope of uranin concentration slow-down curves. Replication measurements of uranin concentrations showed an error of 2% at concentrations of 1000 and 750 μg/l, 2.5% at concentrations 500 μg/l and 4% at 250 μg/l. These measurements were taken during daylight in perspex cylinders with metallic bottoms, to simulate the calibration conditions (Section 3.4).

3.3 Functionality

At first, the groundwater flow velocimeter (Fig. 1) is lowered into a screened two-inch groundwater observation well (Fig. 3.5)(*Englert et al.*, 2001). At a specific depth, the probe is fixed by bloating packers. The packers define a volume of 0.54 l and an area of approaching flow of 1.36 dm^2.

After 5 minutes of slow-down phase, ten impulses, each 50 μl of a 1 g/l uranin solution, are injected from a store tank into the defined volume by a small pump. The injected

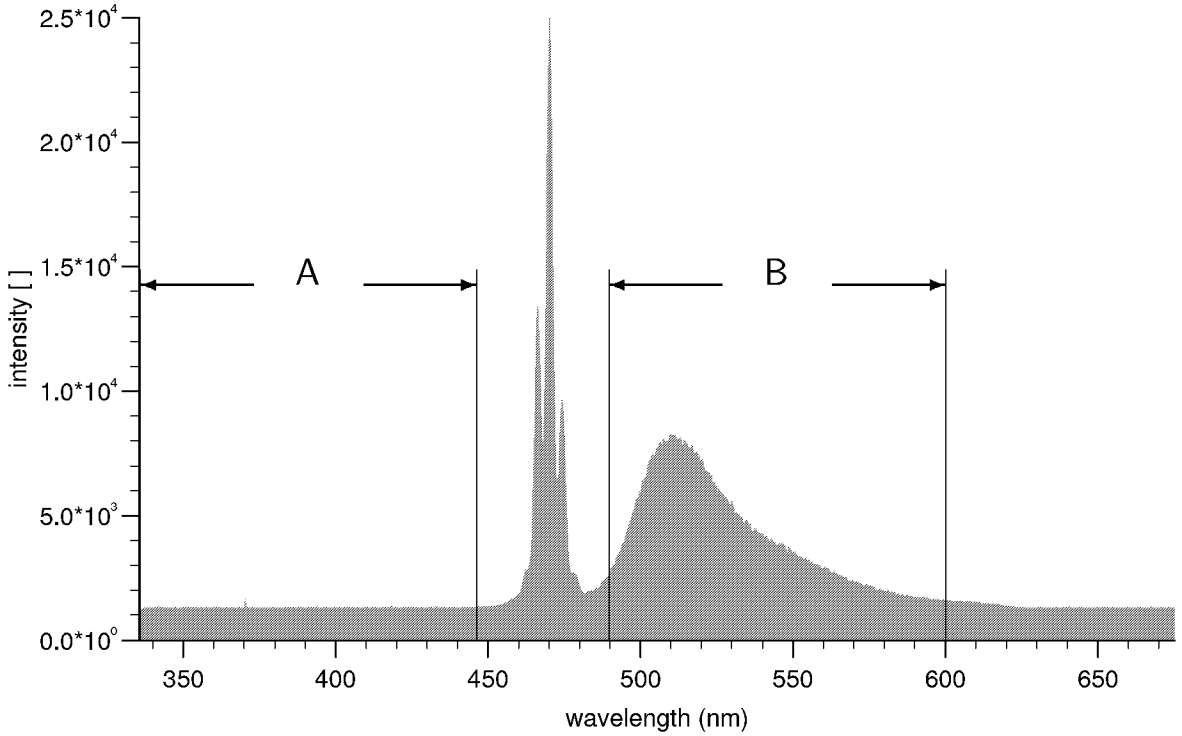

Figure 3.4: Typical fluorescence spectrum: The left peak is the the reflected emission peak of coumarin 102. The right peak is the emission peak of uranin. The integral along A represents the background signal, which is subtracted from the integral along B to extract the uranin peak from the complete spectrum.

uranin solution (500 μl) is continuously homogenized by circulation. Groundwater is sucked into the circulation pump at the top of a 3 mm tube placed in the centre of the defined volume. The circulation pump injects water back into the defined volume through an orifice placed at the bottom of the volume. The pumping rate of the circulation pump amounts to 5 l/h. Both the circulating and the injection pump are installed in the lower packer. The pressure inside the lower packer and the store tank for the tracer is trimmed to the hydraulic pressure outside the packer.

The uranin concentration is diluted due to the groundwater flow. Uranin concentrations are measured every 30 seconds over a period of 10 minutes by LIF. The detected decrease in the LIF signal is proportional to the flow rate passing through the defined volume. Taking into account the area of approaching flow, the flow velocity in the defined volume can be calculated (Fig. 3.2 and Eq. 3.1). A typical curve of LIF signal decrease, in the scope of a single-well dilution test, can be seen in Figure 3.6. For the determination of the dilution D, the slope of the decrease curve of the LIF intensity is fitted by linear regression. This leads to the modification of Equation 3.1 for evaluation of q_m:

$$q_m = \frac{V}{A} \cdot -D \tag{3.3}$$

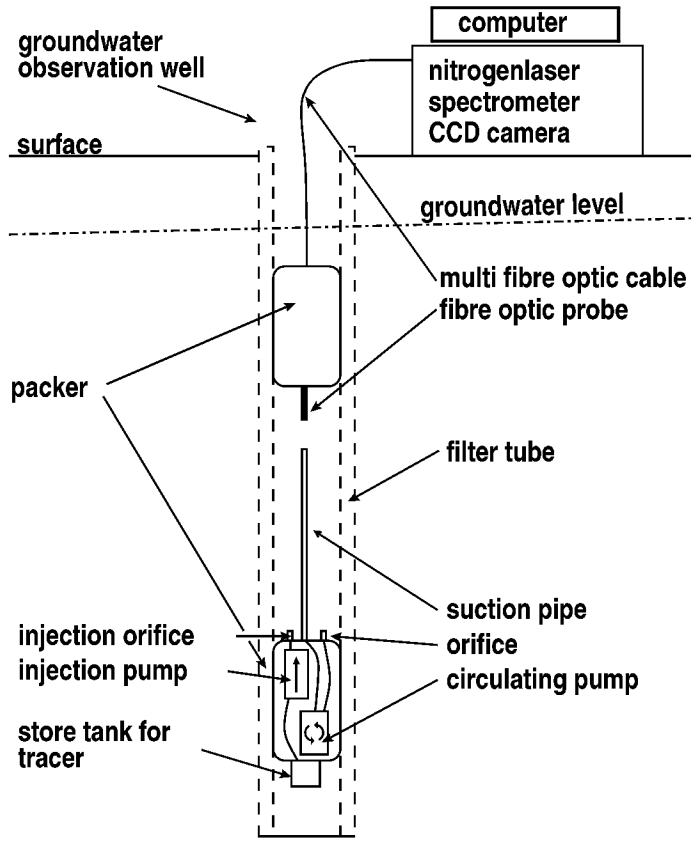

Figure 3.5: Schematic set up of the groundwater flow velocimeter.

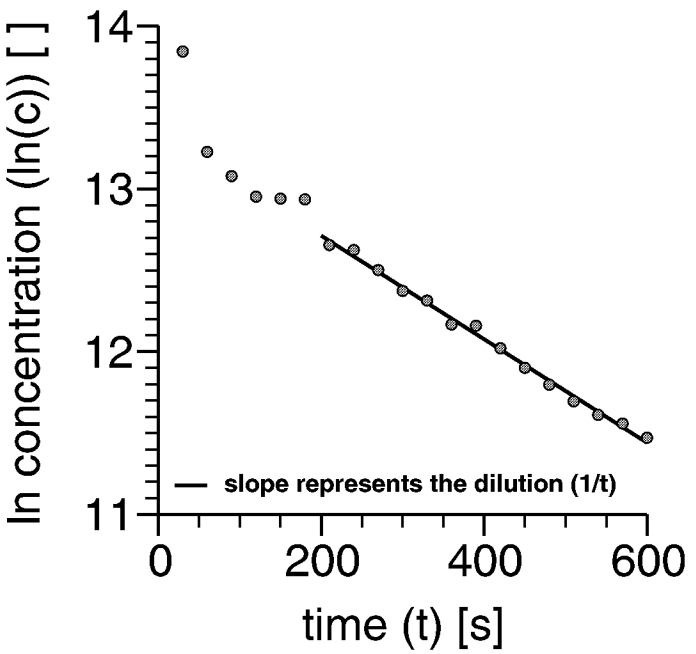

Figure 3.6: Typical uranin dilution curve using LIF.

3.4 Calibration

A perspex experimental set up (Fig. 3.7) is used to calibrate the groundwater flow velocimeter with regard to different flow rates in order to study accuracy of the groundwater flow velocimeter with LIF (*Englert et al.*, 2001). Using a steady hydraulic potential, the inflow is controlled by an infinitely variable valve. The outflow is controlled by the height of the flexible tube at the spout of the experimental set up. Both inflow and outflow are monitored by flowmeters of a rotameter type.

A two inch perspex filter tube, constructed the same way as those used at Krauthausen test site (Chapter 4.1.2), is used inside the experimental set up. The filter tube is placed in the middle of the experimental set up in such a way that all flow runs through it. The probe is lowered into this filter tube and the packers are bloated. By sealing the filter tube beneath the lower packer with a perspex tube and assuming the water level stays below the uppermost end of the upper packer, it is ensured that all flow runs through the defined volume of the probe.

The calibration of the groundwater flow velocimeter point to the flow Q adjusted by the variable valve and controlled by flowmeters. Test series included flow which ranged between 0 l/h and 20 l/h (Fig. 3.8).

Regression analysis showed a slope of $\frac{1}{0.58\text{l}}$ with a standard error of 0.01 l. R^2 amounts to 0.99. This shows good reproducibility for measurements before and after field campaign. Detailed study of the residuals of regression analysis showed errors of $\leq$ 50% for 0.3 l/h < Q <1.5 l/h and $\leq$ 10% for 1.5 l/h < Q <20 l/h for Q measurements using the groundwater flow velocimeter. Due to the impracticability of adjusting values of $Q < 0.3$ l/h within the experimental set up, those Q could not be studied. At $Q > 20$ l/h, the point dilution method showed erratic values due to the pumping rate of the circulation pump. This means the advection through the defined volume of the probe is too high to warrant a homogenization of the tracer within a pumping rate of 5 l/h of the circulation pump.

The slope of the calibration is the experimentally found inverse volume of the probe. The difference between the true volume of the groundwater flow velocimeter (Section 3.3) and the experimentally determined volume amounts to 0.04 l. The dilution in a no-flow situation in the experimental setup equals $1.0\frac{1}{h}$. The difference from 0 of dilution shows the lower limit of velocity measurement using a pumping rate of 5 l/h for the circulation pump. The difference between the true and experimantal volume quantifies the sum of density driven convection, molecular diffusion, apparent flow rate caused by the mixing device and vertical convection. This can be expressed by:

$$Q_{ha} = Q_m - \hat{Q} \tag{3.4}$$

with Q_{ha} being the horizontal advective flow predicted using calibration results, Q_m being the flow predicted by theory (Eq. 3.1) and $\hat{Q}$ being the difference $Q_m - Q_{ha}$. For the evaluation of Q_{ha}, the following equation is used:

$$Q_{ha} = (V_m - \hat{V}) \cdot -D = V_{ha} \cdot -D \tag{3.5}$$

with V_m being the true volume, V_{ha} being the volume experimentally evaluated, D being the dilution experimentally measured and $\hat{V}$ being the difference $V_m - V_{ha}$.

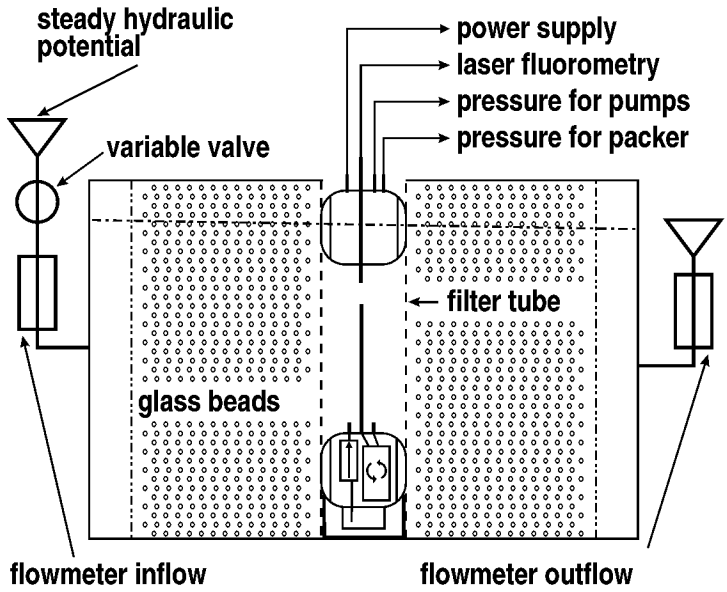

Figure 3.7: Schematic set up of the groundwater flow velocimeter calibration.

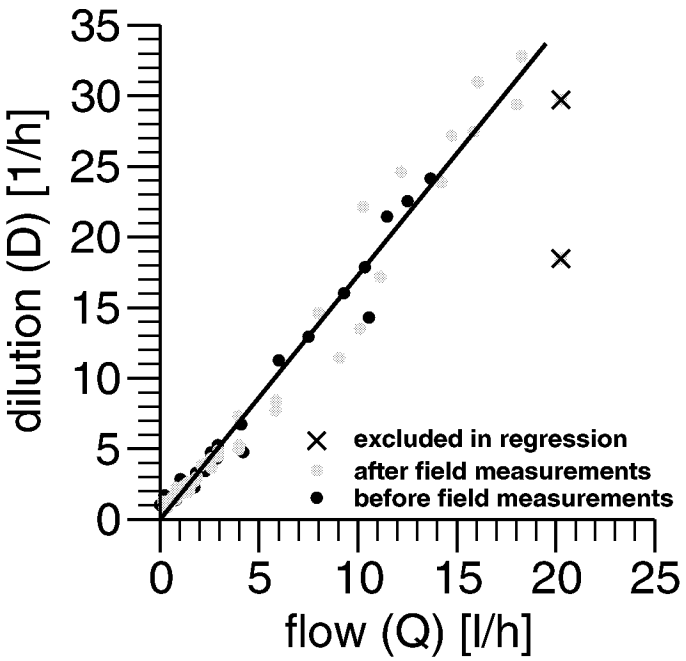

Figure 3.8: Calibration line of the point dilution measurements in the calibration set up.

For field measurements using the groundwater flow velocimeter, horizontal flow velocity inside the borehole q_{ha} can be evaluated using the following equation:

$$q_{ha} = \frac{V_m \cdot -D}{A} - \frac{\hat{V} \cdot -D}{A} = \frac{V_{ha} \cdot -D}{A} \tag{3.6}$$

with A being the area of approaching flow. The horizontal flow velocity q_{ha}, measured in the borehole differs from the Darcy velocity in the aquifer due to convergence effects (Section 2.2). The magnitude of the Darcy velocity ($|q|$) in the aquifer can be calculated using correction factors α and γ:

$$|q| = \frac{q_{ha}}{\alpha\gamma} \tag{3.7}$$

Chapter 4

Darcy Velocity Measurements at Krauthausen Test Site

4.1 Hydrogeological Framework

The Krauthausen test site is located in the southern part of the Lower Rhine Embayment, Germany. It is situated approximately 10 km northwest of the city of Düren, 7 km southeast from the Jülich research centre (FZJ) and has an extension of 200 × 70 m. In the scope of the EU project "Critical parameters governing the mobility and fate of pesticides in soil/aquifer systems: An experimental and modelling study based on coherent interpretation of transport parameters and physico-chemical characteristics measured at multiple scales", the Krauthausen test site was set up in 1993 by the Jülich research centre (*Döring*, 1997; *Englert et al.*, 2000a; *Vereecken et al.*, 2000).

Since Tertiarian age, the Lower Rhine Embayment, which is the tectonic lengthening of the Dutch rift valley, has been an area of subsidence. Since the subsidence started, up to 1200 m Tertiarian and up to 100 m Quaternarian sediments have been deposited on Variscian folded sediments from Devonian and Carboniferous age. The stratigrafic sequence from Tertiarian times shows sequences of terrestrial sediments, transported from the south, and marine sediments, transported from the north. The sediments are mostly sandy gravelly or clayey. In the coastal areas, thick layers of peat have been deposited. These peat deposits can be found today in the up to 100 m thick brown coal layers. The Quaternarian sediments in the southern part of the Lower Rhine Embayment are mostly fluvial deposits from the Rhine/Maas river system. In the northern part of the Lower Rhine Embayment, push moraines and aqueoglacial deposits of the Saale inland ice have been added. In most parts of the Lower Rhine Embayment the above mentioned sediments are covered by aeolian sediments (*Walter*, 1992; *Klostermann*, 1992). The sequences of permeable and impermeable layers lead to a typical multi-layer aquifer system. The major receiving stream is the Rhine river. The Lower Rhine Embayment shows several tectonic compartments, due to northwest-southeast striking faults. These are often hydraulic barriers. The Krauthausen test site is located on a small inserted block between the Rur block and the Erft block.

4.1.1 The Uppermost Aquifer

Studies at Krauthausen test site focus on the uppermost aquifer. With a thickness of approximately 9 m, this aquifer is limited by flood plain deposits at the top and a clay layer at the bottom (Fig. 4.1). The aquifer consists mainly of gravelly and sandy

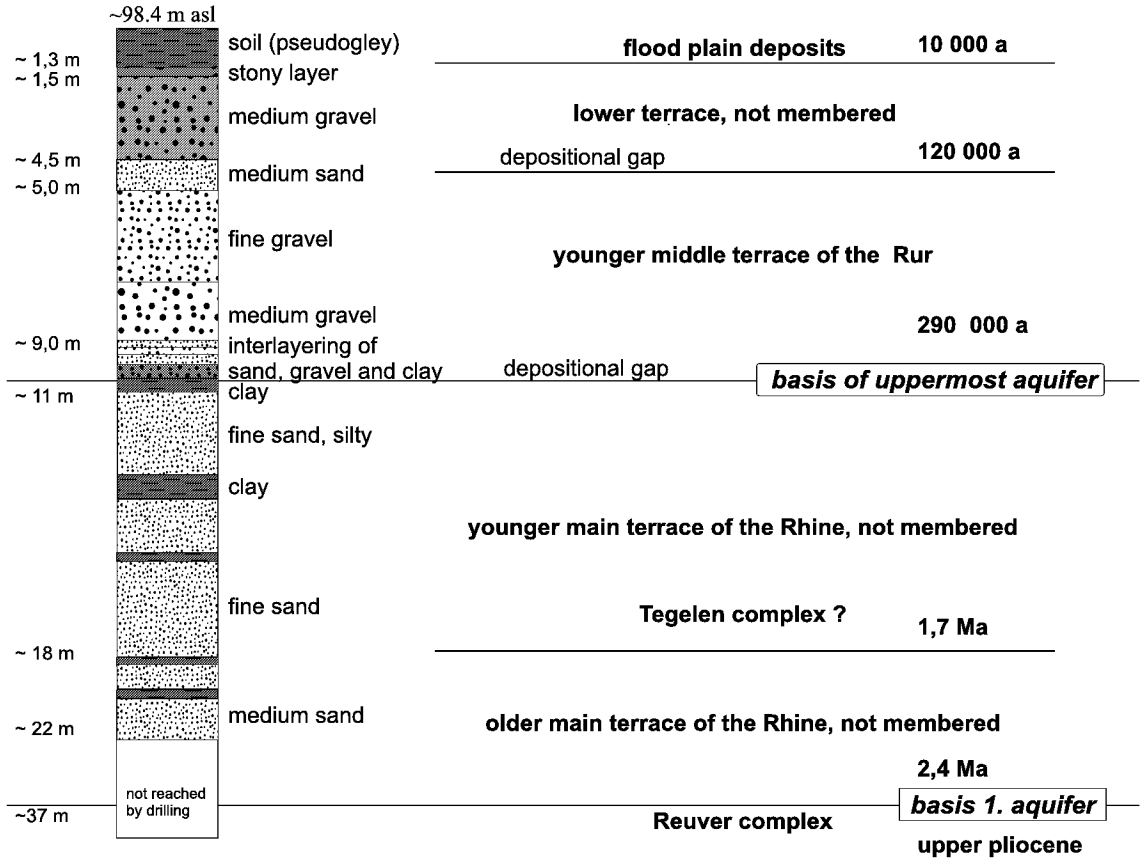

Figure 4.1: Generalized cross-section of the uppermost aquifer, Krauthausen test site, derived from field studies (*Döring*, 1997) and stratified by *Prüfert* (1999).

sediments. These sediments have been deposited by the braided river system of the Rur. The clay and silt content of the aquifer sediments vary between 0.5% and 7.5%, and the mean total porosity is 26% with a standard deviation of 7%. The mean cation exchange capacity of the aquifer sediments is 0.44 meq/100g. The mean specific surface is 0.7 m^2/g.

The groundwater table at Krauthausen test site varies from 1 m to 3 m below surface, showing a mean gradient of 0.2%. Within these variations in the groundwater table, the mean flow direction of the groundwater changes. At low groundwater tables, flow is parallel to the length of the test site in a northwesterly direction. At high groundwater tables, the mean flow direction is parallel to the length of the test site in the middle part of the test site, but rotates in a west-northwesterly direction in the northwest and in a northerly direction in the southeast of the test site. At high groundwater tables (<1.5 m), the aquifer is semi-confined. At lower groundwater tables, the aquifer is semi-unconfined. This variation in the groundwater table causes a time dependent change in

the storage coefficient (S_0) within one magnitude. When the groundwater table is high, S_0 amounts to $7.7 \cdot 10^{-4}$, when it is low, S_0 amounts to $1.0 \cdot 10^{-2}$. The mean hydraulic conductivity, based on the results of pumping tests, amounts to $3.8 \cdot 10^{-3}$ m/s. The average precipitation in the area is about 690 mm/a.

The groundwater is bicarbonate rich and has high concentrations of nitrate (Tab. A.1 (*Schulze*, 1998)) caused by intensive agricultural land use. The pH value is 6.7, and the EH value varies between 250 mV and 300 mV. The content of dissolved oxygen goes up to to 7.7 mg/l. The electric conductivity of the groundwater is 1.1 mS/cm.

4.1.2 Technical Layout

On test site Krauthausen, 74 drillings were deepened using a dry rotary drilling method. One drilling has a diameter of 620 mm. All other drillings have a diameter of 324 mm. The well design of the various boreholes differs (Fig. 4.2). The borehole with a drilling diameter of 620 mm is equipped with a 7 in casing, screened between 1 m and 10 m below surface. The boreholes with a diameter of 324 mm are equipped with 2 in casings, either screened at various depths or not screened at all. Sixty-four wells are equipped with Multi-Level-Samplers (MLS), consisting of a bundle of 24 PE tubes attached to the outside wall of the casing. The diameter of the PE tubes is 0.5 cm.

The well design consists of clay sealings at the top and the bottom of the borehole. Between the sealings, the borehole is is filled with gravel pack. Gravelly sediments from Krauthausen and filter gravel are used for the gravel pack. The filter gravel is made up of gravel between 2 mm and 3 mm in diameter. Using table 7 in *Klotz* (1977), the hydraulic conductivity of filter gravel can be estimated as $2.6 \cdot 10^{-2}$ m/s. The gravelly sediments from Krauthausen test site, used as filter gravel, show a mean hydraulic conductivity of $3.8 \cdot 10^{-3}$ m/s and a variance of log-transformed hydraulic conductivity of 1.3 (Subsection 4.1.3). The screen of the borehole is equipped with 0.5 mm slits. In *Klotz* (1990), table 12 shows a hydraulic conductivity of $3.1 \cdot 10^{-3}$ m/s for this type of screen. The casing tubes have a length of one or two metres and are connected by screw connections. The screw connections have a length of 20 cm and are not screened.

4.1.3 Heterogeneity of Hydraulic Conductivity

On the Krauthausen test site several techniques were employed to determine the hydraulic conductivity of the aquifer. The various approaches differ in technique as well as in the volume used to average the hydraulic conductivity. Pumping tests were used to determine the mean hydraulic conductivity of the complete uppermost aquifer at Krauthausen test site. These pumping tests were performed in the 7 in well, located in the centre of the test site. The rate of production was 70 m^3/h and 80 m^3/h. Both pumping tests showed a mean hydraulic conductivity for the uppermost aquifer of $3.8 \cdot 10^{-3}$ m/s (*Englert et al.*, 2000a; *Vereecken et al.*, 2000).

Using small scale pumping tests, the hydraulic conductivities were determined on a zonal scale. These were performed at a production rate of 2 m^3/h at 24 2 in wells. Evaluation of the pumping tests shows a geometric mean of hydraulic conductivity of $1.5 \cdot 10^{-3}$ m/s and a variance of the log-transformed hydraulic conductivity of 0.11 (*Lamertz*, 2001).

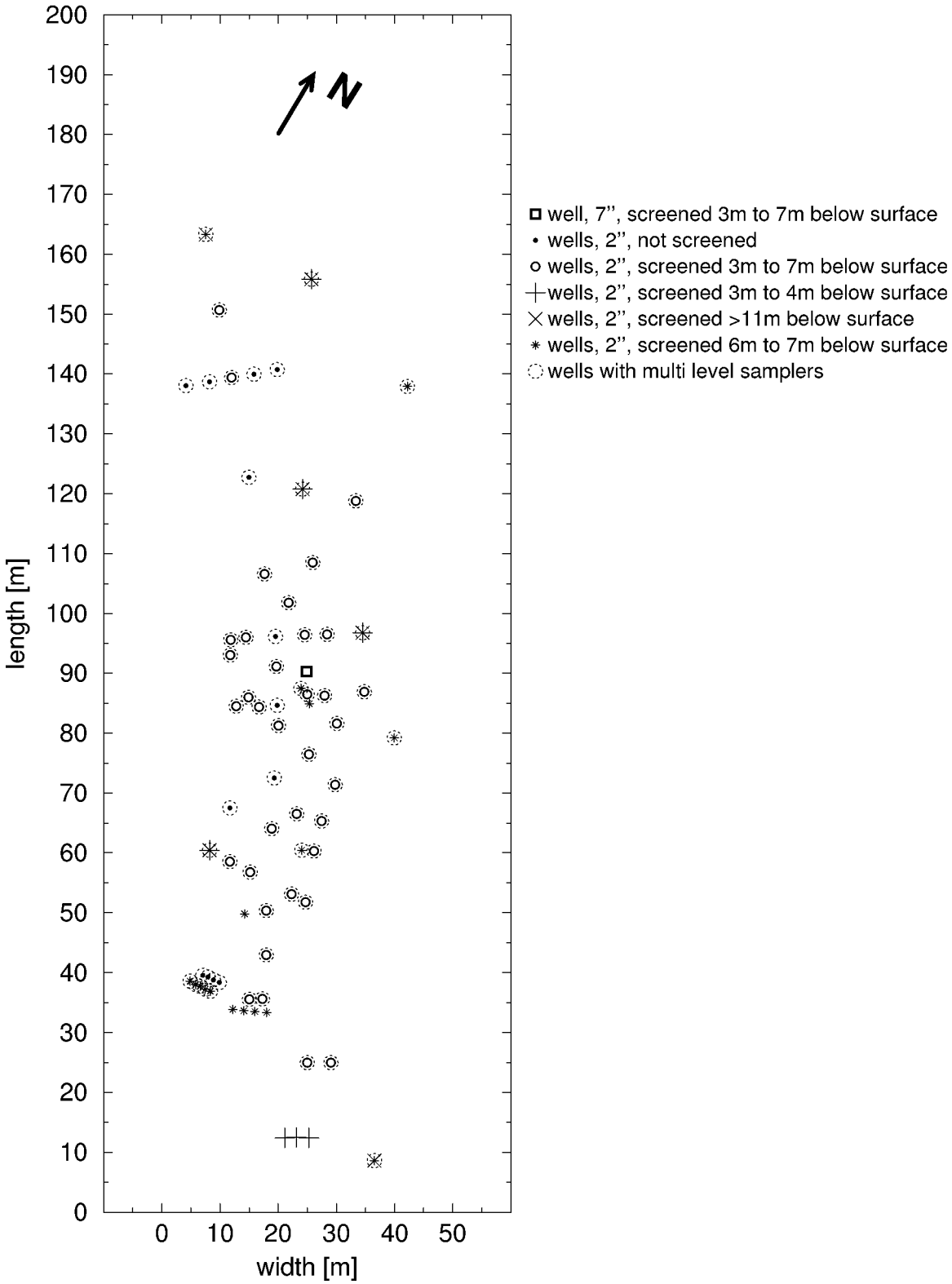

Figure 4.2: Geometrical distribution of observation wells and their equipment at Krauthausen test site.

The inflow to the well by layer can be determined using a borehole flowmeter in the course of a pumping test. This enables a vertical resolution of the hydraulic conductivity of the aquifer (*Molz et al.*, 1989). At Krauthausen test site, these pumping tests were performed at a production rate of 1.5 m^3/h. Borehole flowmeter measurements at twenty-two 2 in wells showed a geometric mean of hydraulic conductivity of $3.8 \cdot 10^{-3}$ m/s and a variance of the log-transformed hydraulic conductivity of 1.3. Using an exponential model, the vertical correlation length amounts 0.37 ± 0.09 m with a nugget of 0.46 ± 0.11 (*Englert et al.*, 2000a; *Vereecken et al.*, 2000).

Apart from the above mentioned hydraulic in situ measurements, grain size analysis was used to determine local hydraulic conductivities. For this, the methods of *Seiler* (1973) *Beyer* (1964) and *Bialas and Kleczkowski* (1970) were used. At Krauthausen test site, 392 sediment samples were collected between the soil surface and 87 m above mean sea level and analyzed for grain size distribution. About 340 of these sediment samples were drawn from the uppermost aquifer. The samples were taken from 34 boreholes, and three of them were sampled from bottom to top with a sampling interval of 10 cm and 20 cm. Thirty-one boreholes were sampled from 90.4 m to 92.2 m above mean sea level with a sampling interval of 20 cm. Taking all samples from the uppermost aquifer into account, the statistical parameters describing the heterogeneity are as shown in Tab. A.2.

A cluster analysis of the grain size distributions of the sediment samples showed a layering of the aquifer (*Englert*, 1998). This layering coincides with the findings of *Vereecken et al.* (2000). As a result, the aquifer can be divided into five layers (layer 0 to layer 4). The uppermost layer (layer 0) belongs to the lower terrace, the others belong to the younger middle terrace of the Rur. The hydraulic conductivities averaged based on half metre intervals, show clear differences in mean and variance between the various layers (Fig. 4.3). The younger middle terrace of the Rur has a geometric mean for the several layers of between $7.2 \cdot 10^{-4}$ m/s and $1.69 \cdot 10^{-3}$ m/s. The major differences between the layers of the younger middle terrace are in the variance. At the base of the younger middle terrace of the Rur (layer 4), the variance is very high, 3.81, due to the interlayering sediments detected at this depth. Between layer 4 and layer 3 the variance decreases by factor 7 to 0.56. Going upwards, the variance increases by factor 2, with a variance of 1.07 for layer 2 and a variance of 2.16 for layer 1. Inside the lower terrace (layer 0), the geometric mean of hydraulic conductivities amounts to $2.80 \cdot 10^{-3}$ m/s and the variance of the log-transformed hydraulic conductivity is 2.98. The values of geometric mean and variance are listed in detail in Table A.9.

Due to the fact that the complete uppermost aquifer was sampled at only three boreholes, reliable statistical estimates for the hydraulic conductivities of the Krauthausen test site is restricted to the layer between 90.4 m to 92.2 m above mean sea level. This layer is sampled at 34 wells and is part of layer 2. In the following, this sampling area is called **reference layer**.

Focusing on the K values derived by the method of *Seiler* (1973), and taking into consideration the effective pore diameter at the 10th percentile, the geometric mean of K within the reference layer is $1,9 \cdot 10^{-3}$ m/s at a variance of $ln(K)$ of 1.00. With respect to the W-test, the 173 K values are well described by the log-normal distribution (W= 0.99, Pr <W=0.89). The range is $\sim$ 12 m for the horizontal and $\sim$ 20 cm for the vertical direction. The geostatistical parameters of hydraulic conductivities for the reference layer are given explicitly in Table A.3. Because of the high errors for the range, both

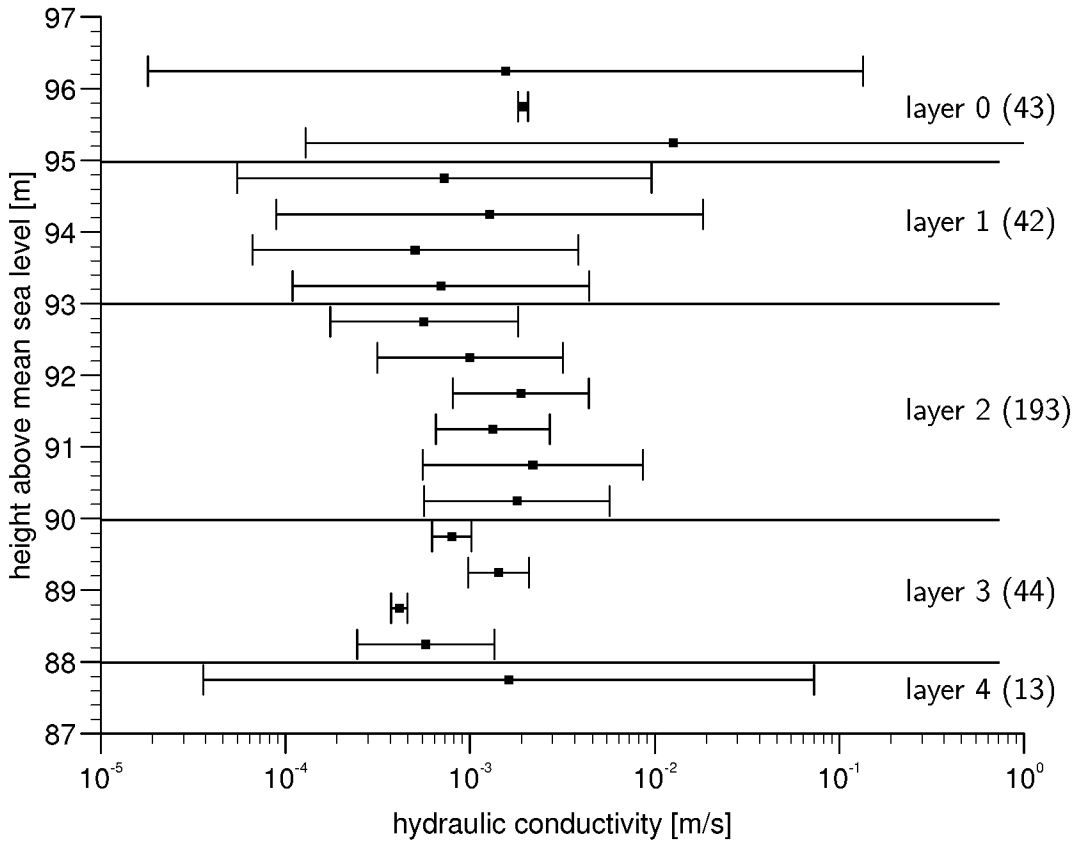

Figure 4.3: Distribution with depth of hydraulic conductivities derived from grain size distribution, Krauthausen test site. The quads denote the geometric mean, the error bars show the standard deviation. The number in brackets behind the layers denote the number of measurements in the layers.

for the Gaussian and the exponential model, it is not possible to single out one of these models.

4.1.4 The α-Factor

The α-factor (Section 2.2, Eq. 2.8 - 2.11) plays an important role in correcting the convergence of the streamlines towards the borehole. In order to evaluate the α-factor, detailed information of the well design is needed at each position of velocity measurements. The α-factor can only be estimated due to the fact that the original well design can change in time in an unknown way, and even the original well design is only vaguely known.

Equations for evaluating the α-factor, taking into account the skin factor, give an impression of to what extent the α-factor can vary. These equations indicate variations in α of 0.1 to 11, depending on the well development or damage of the aquifer and filter pack surrounding the borehole. However, the application of these equations is not feasible, due to the lack of measurability of the skin factor.

The range of the α-factor for the wells at Krauthausen between 0.03 and 3.48 can be estimated using Equation 2.8 and the following assumptions:

- The slits of the well screen originally had a width of 0.5 mm. Due to particle transport and chemical processes they can become clogged. This leads to an assumed range of K_1 from $1.0 \cdot 10^{-4}$ m/s to $3.1 \cdot 10^{-3}$ m/s.
- The hydraulic conductivity of the gravel pack K_2, consisting of filter gravel or Krauthausen sediments, can range between $2.0 \cdot 10^{-4}$ m/s and $4.9 \cdot 10^{-2}$ m/s.
- The hydraulic conductivity of aquifer sediments K_3 can range between $2.0 \cdot 10^{-4}$ m/s and $3.0 \cdot 10^{-2}$ m/s.
- The radii (r_1, r_2, r_3) are given in Subsection 4.1.2.

Assuming that K_1 is still $3.1 \cdot 10^{-3}$ m/s and K_2 has become equal to K_3 ($3.8 \cdot 10^{-3}$ m/s), a mean α-factor of 1.95 can be estimated. This value is used in the following. *Drost* (1996) used an α-factor of 2.6.

4.2 Measurement Campaigns

4.2.1 Application of the New Groundwater Flow Velocimeter

From May 14 2001 to August 2 2001, measurements of groundwater flow velocity were taken using the groundwater flow velocimeter (Chapter 3). The groundwater level declined during the field campaign from 97.06 m to 96.26 m above mean sea level (Fig. 4.4). Beside the general trend, the groundwater level fluctuates by a few centimeters at irregular intervals. The aquifer was semi-confined during the field campaign.

Two contour maps of the water table, at the beginning and at the end of the field campaign, are given in Figure A.1. These contour maps show the variation in time and space of the mean hydraulic gradient. The magnitude of the mean hydraulic gradient

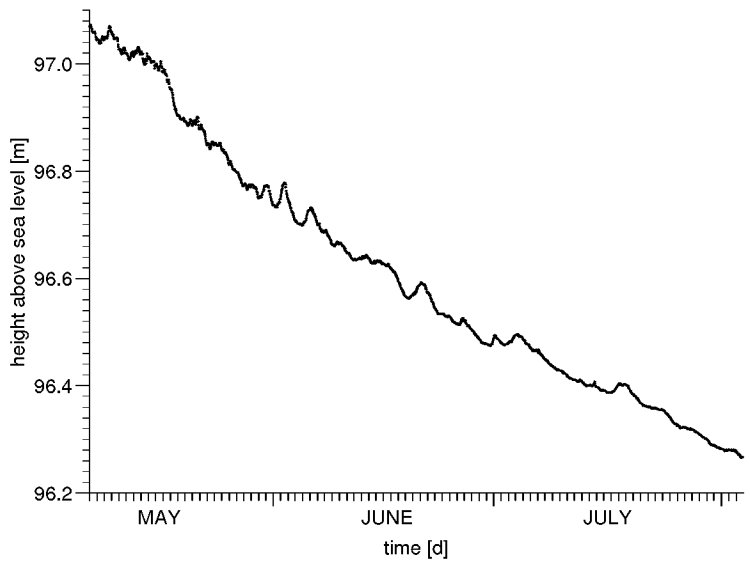

Figure 4.4: Development of the total head during measurements with the groundwater flow velocimeter in 2001, at well number 29

varied between 0.15% and 0.3%. The variation of the direction of the mean hydraulic gradient is between 300° and 0°.

During the field campaign, groundwater velocity measurements were taken at 361 positions in 21 wells (Fig. 4.5 and Tab. A.4). Due to the curvature of the screen at

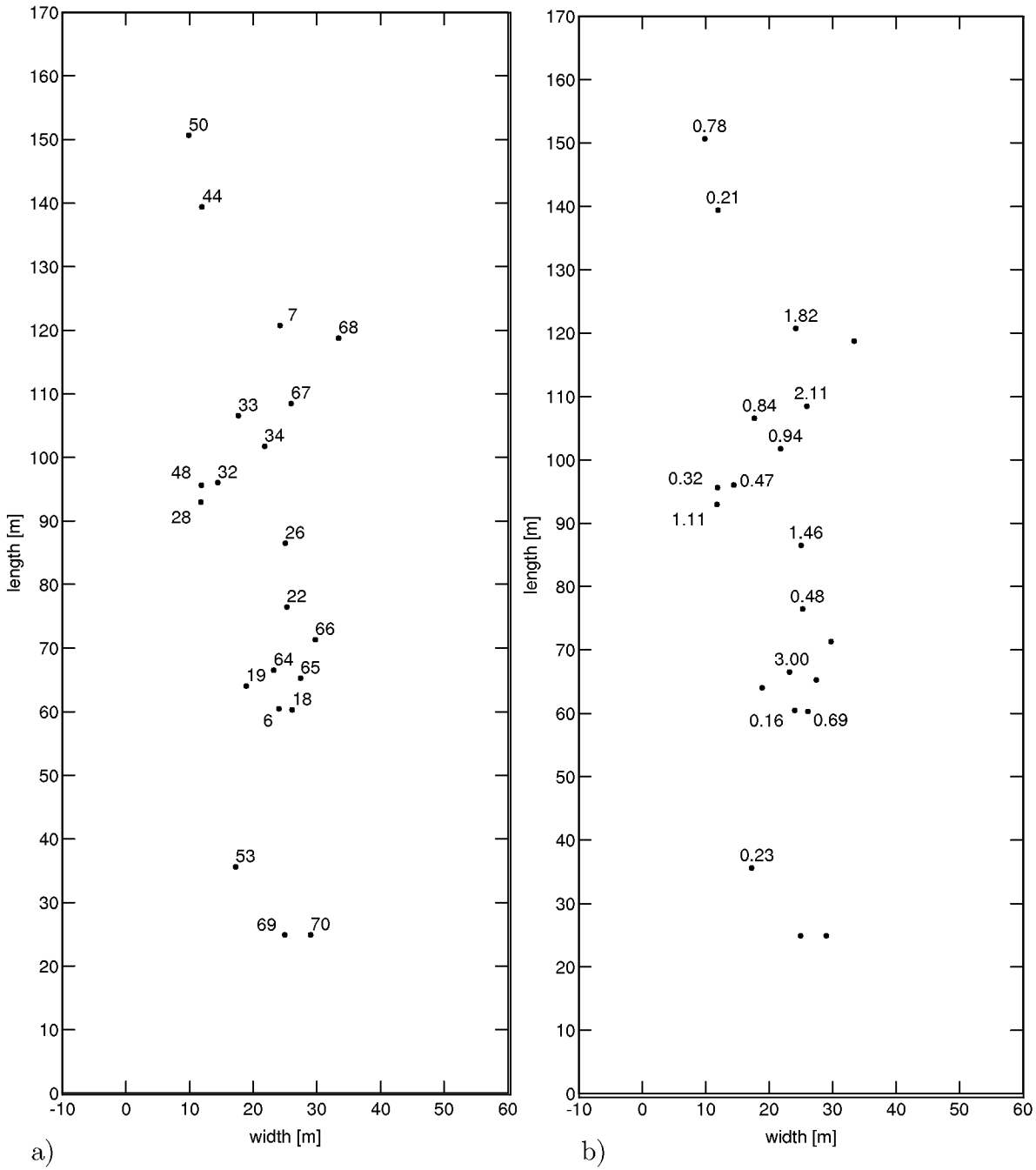

Figure 4.5: Measurements of Darcy velocities with the groundwater flow velocimeter: a) number of the studied well, b) geometric mean of Darcy velocities measured at the well in the depth 90 m to 92 m above mean sea level.

wells 19 and 65, the groundwater flow velocimeter could only be lowered to a depth

of 94.3 m above mean sea level. Thus, only a few measurements could be taken at these locations. Well number 6 was only screened between 92.29 m and 91.29 m above mean sea level, which limits measurements to these depths. All other measurements were taken in fully screened wells so that only time limitations for the field campaign hindered measurements of the complete filter screen. The locations of linkage between screened tubes (Subsection 4.1.2) were detected and excluded from the measurements.

The measurements showed a high level of variability in the magnitude of the Darcy velocity ranging between 0.09 m/d and 17.84 m/d. These measurements resulted in a geometric mean of the magnitude of the Darcy velocities of 1.01 m/d.

The magnitudes of the Darcy velocities in the younger middle terrace of the Rur (layer 4-1) showed a clear evolution in the geometric mean and variance in the several layers (Fig. 4.6). Starting from the bottom, the geometric mean of the Darcy velocities rise from layer to layer by factor ~1.7, with a geometric mean of 0.31 m/d for layer 4 and 1.42 m/d for layer 1. The variances of the log-transformed Darcy velocities increase by factor 1.5-2 from layer to layer going upward in the stratigraphy, with a variance of 0.37 for layer 4 and a variance of 1.40 for layer 1. The lower terrace showed a geometric

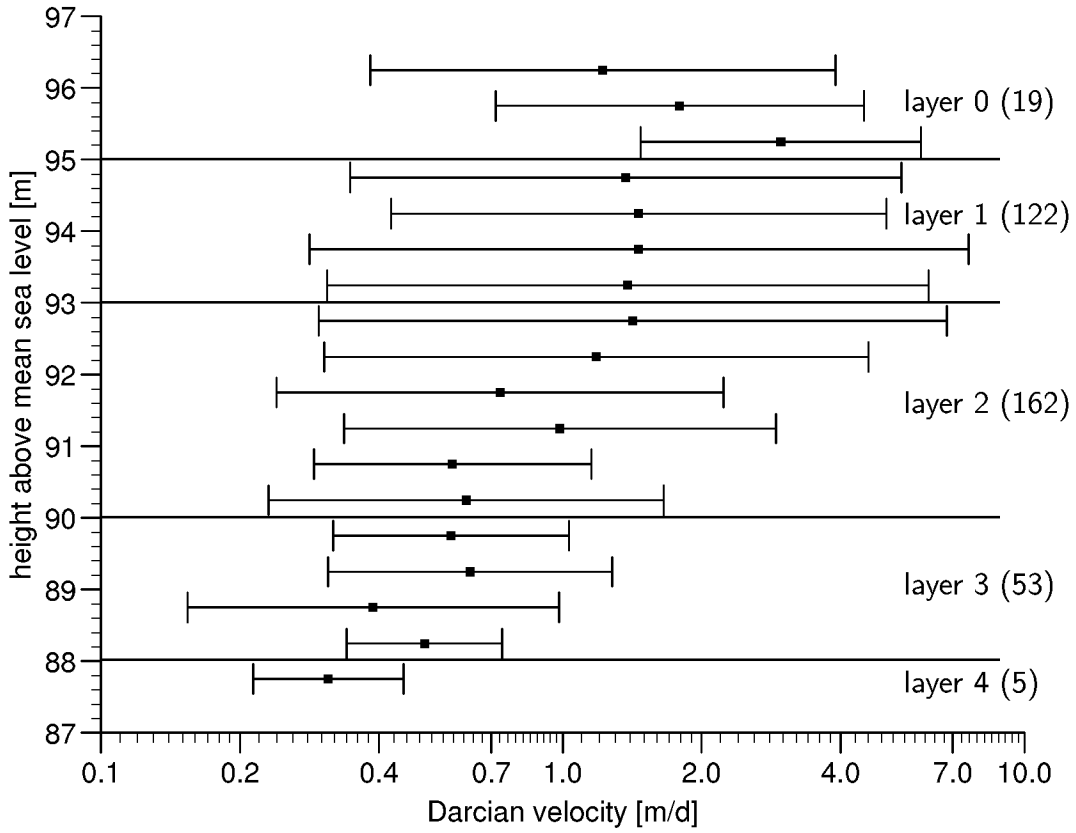

Figure 4.6: Distribution with depth of Darcy velocities measured applying the groundwater flow velocimeter, Krauthausen test site. The quads denote the geometric mean, the error bars show the standard deviation. The number in brackets denote the number of measurements in the layers.

mean for the Darcy velocities of 2.43 m/d and a variance of 0.78. The geometric means and variances for each layer are given in Table A.9.

A detailed study of the well wise geometric mean within the various layers is shown in Figures A.2-A.6 and Table A.5. High heterogeneities for all layers can be deduced from these studies. A clear zonal division of the aquifer in the horizontal direction can not be detected. This is either due to the absence of such zones or because the density of measurement points is not high enough.

Due to the restriction of detailed studies of hydraulic conductivities to the reference layer, Table A.4 and Figure 4.5 focus on the reference layer for comparison purposes. As expected, the reference layer shows, similar values to layer 2 for geometric mean and variance of the magnitude of the Darcy velocities. A statistical evaluation of the measured Darcy velocities for the reference layer as well as for all measurements are given in Section 5.1.

Repetition measurements were taken to prove the time dependency of the groundwater flow velocity. The time gap between the first and the second measurement was approximately one day. The repetition of measurements with the groundwater flow velocimeter showed for measurements < 1.3 m/d that the deviations were within the accuracy of the groundwater flow velocimeter (Tab. A.6). At well 32, at a depth of 91.14 m above mean sea level, the relative deviation between the first and second measurement is 83.84%. This exceeds the measurement errors by far. It therefore indicates a time dependency of the groundwater flow velocity.

4.2.2 Results of Point Dilution Measurements with $^{82}Br^-$

Measurements of the Darcy velocities applying the point dilution method with $^{82}Br^-$ (Subsection 3.1.2) were taken at 29 wells from March 12, 1996 to March 14, 1996 by *Drost* (1996) (Fig. 4.7). Wells 22, 32 and 53 were studied between 88.79 m and 94.80 m above mean sea level. Measurements at all other wells were taken at a depth of 89.79 m to 90.79 m above mean sea level (Tab. A.7). The length of averaging within these measurements was 0.5 m, which is double of the length of averaging of the measurements using the groundwater flow velocimeter. In contrast to the measurements with the groundwater flow velocimeter, the $^{82}Br^-$ dilution measurements included flow direction measurement for the horizontal plane and the measurement of vertical flow inside the wells. The locations of linkage between screened tubes (Subsection 4.1.2) were not observed.

The groundwater table at well 29 was 95.8 m above mean sea level at that time. This shows that the aquifer was, in contrast to the measurements with the groundwater flow velocimeter, semi-unconfined. A contour map of the groundwater table (not shown) showed similar directions and magnitudes of the mean hydraulic gradient as deduced from the time of the groundwater flow velocimeter measurements (Fig. A.1).

Measurements demonstrated that there was no vertical flow inside the wells. The flow direction measurement in the horizontal plane showed high variabilities, including flow directions in the opposite direction of the mean hydraulic gradient. Detailed studies of the flow direction in *Vereecken et al.* (2000) showed variations between 210° and 90°. The mean flow direction was 340°. It was shown that the main flow direction differs between the different layers. In layer 1, the direction of flow was NNE and changed to a

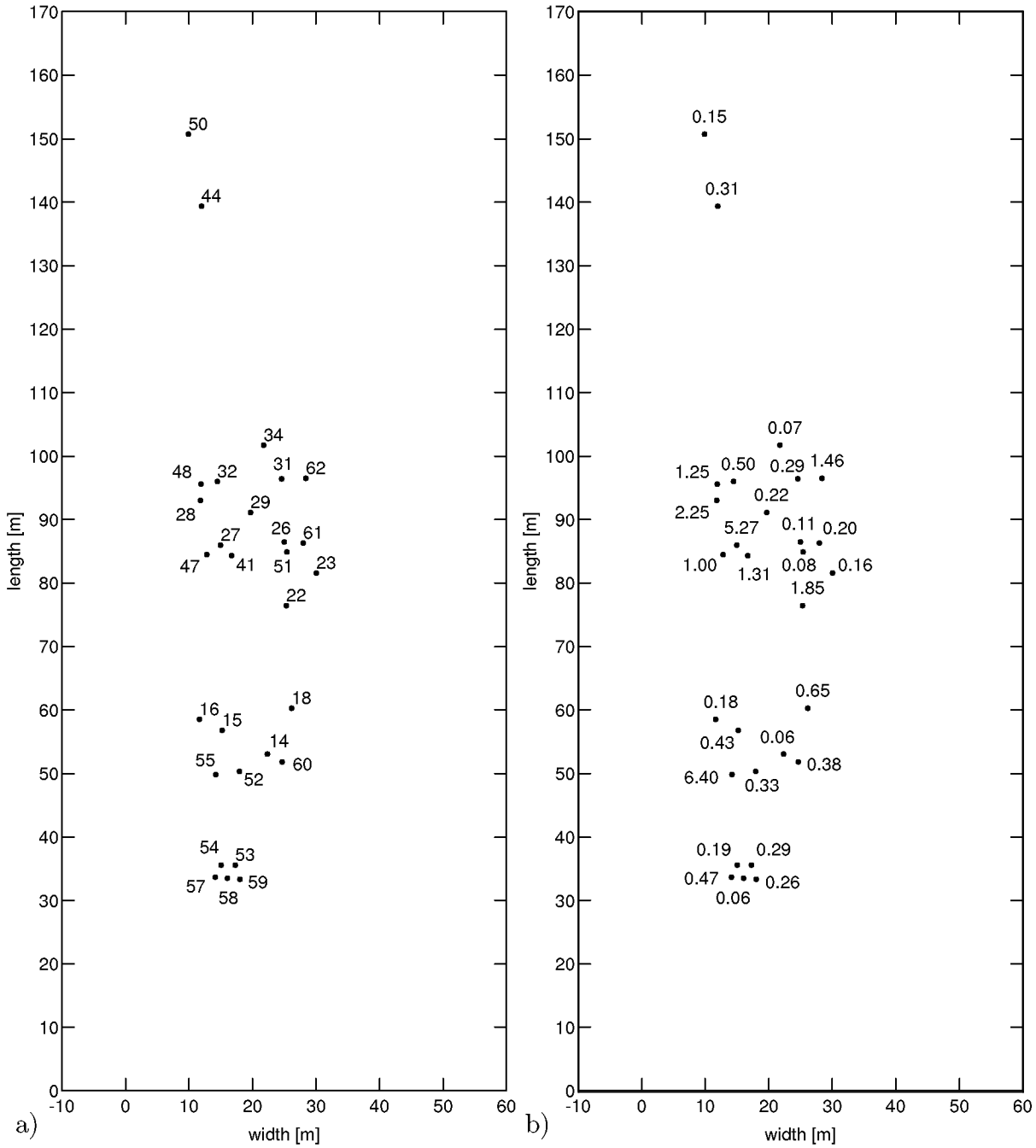

Figure 4.7: Measurements of the Darcy velocities with $^{82}Br^{-}$ dilution: a) number of the studied well, b) geometric mean of Darcy velocities measured at the well at a depth of 90 m to 92 m above mean sea level.

NW direction in layer 2. In layer 3, the flow direction was NNE again.

The measurements showed a high variability in the magnitude of the Darcy velocity, ranging between 0.01 m/d and 12.60 m/d. The measurements resulted in a geometric mean of the magnitude of the Darcy velocities of 0.42 m/d.

The measurements with $^{82}Br^{-}$ included layer 1 - 3, belonging to the younger middle

terrace of the Rur. The evolution with depth of geometric mean and variance of the Darcy velocity, based on half metre intervals, is presented in Fig. 4.8. Layer 3 shows the lowest geometric mean of 0.41 m/d. Moving upward, the geometric mean of the magnitude of the Darcy velocities rises by factor ~1.2 from layer to layer, being 0.64 m/d at layer 1. The variance is 2.21 for layer 3. the variance goes down by factor ~1.4 from layer to layer, being 1.24 for layer 1. Table A.9 shows the geometric mean and the variance by layer in detail.

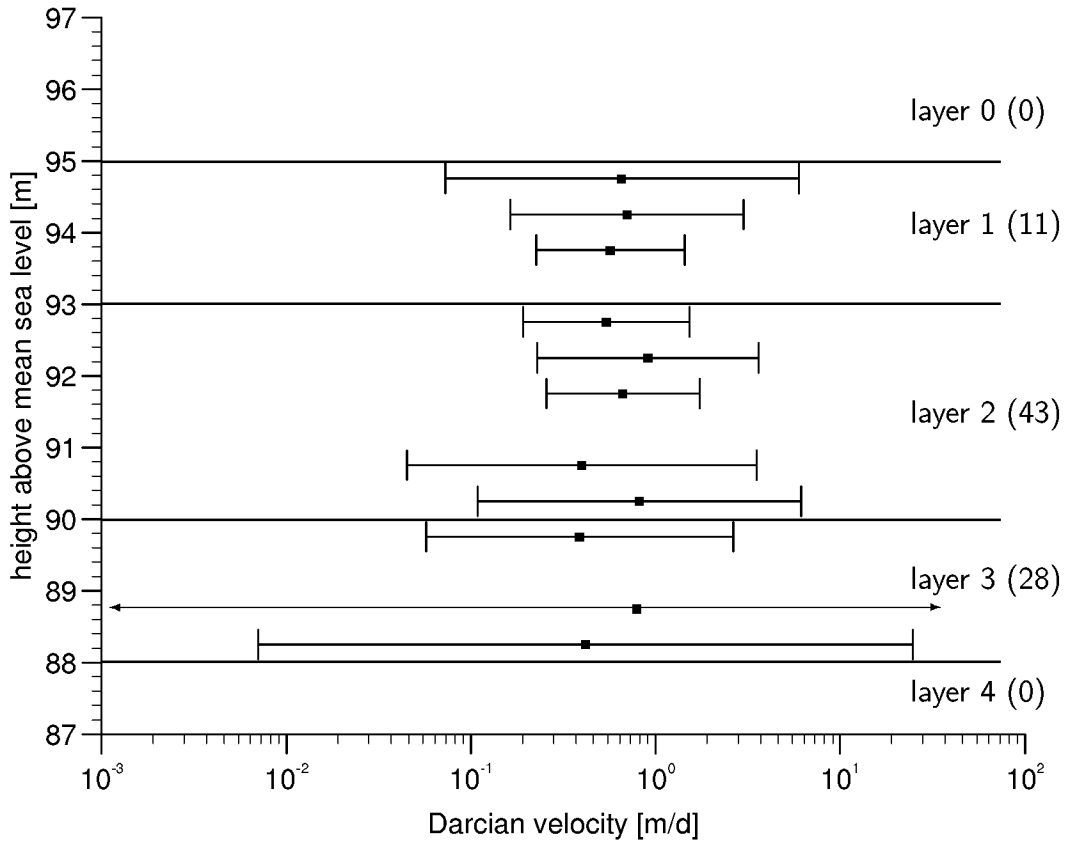

Figure 4.8: Distribution with depth of the Darcy velocities measured applying the point dilution method with $^{82}Br^{-}$, Krauthausen test site. The quads denote the geometric mean, the error bars show the standard deviation. The number in brackets denote the number of measurements in each layer.

Due to the high sampling density in the reference layer, Figure 4.7 is focused on these depths. The corresponding values for the geometric mean and variance by well are given in Table A.7. From this, high heterogeneities can deduced for the reference layer. A clear zonal division of the aquifer in the horizontal direction could not be determined, either due to the low density of measurement points or to the absence of such zones. The geometric mean of the Darcy velocities in the reference layer is 0.41 m/d and the variance is 2.01. Detailed studies for the reference layer, as well as for all data, are presented in Section 5.1.

4.2.3 Comparison

In the following, a direct comparison of the measured hydraulic conductivities and Darcy velocities is given for well 22 and 32, layers 1 - 3 (Fig. 4.9). An initial look at the direct

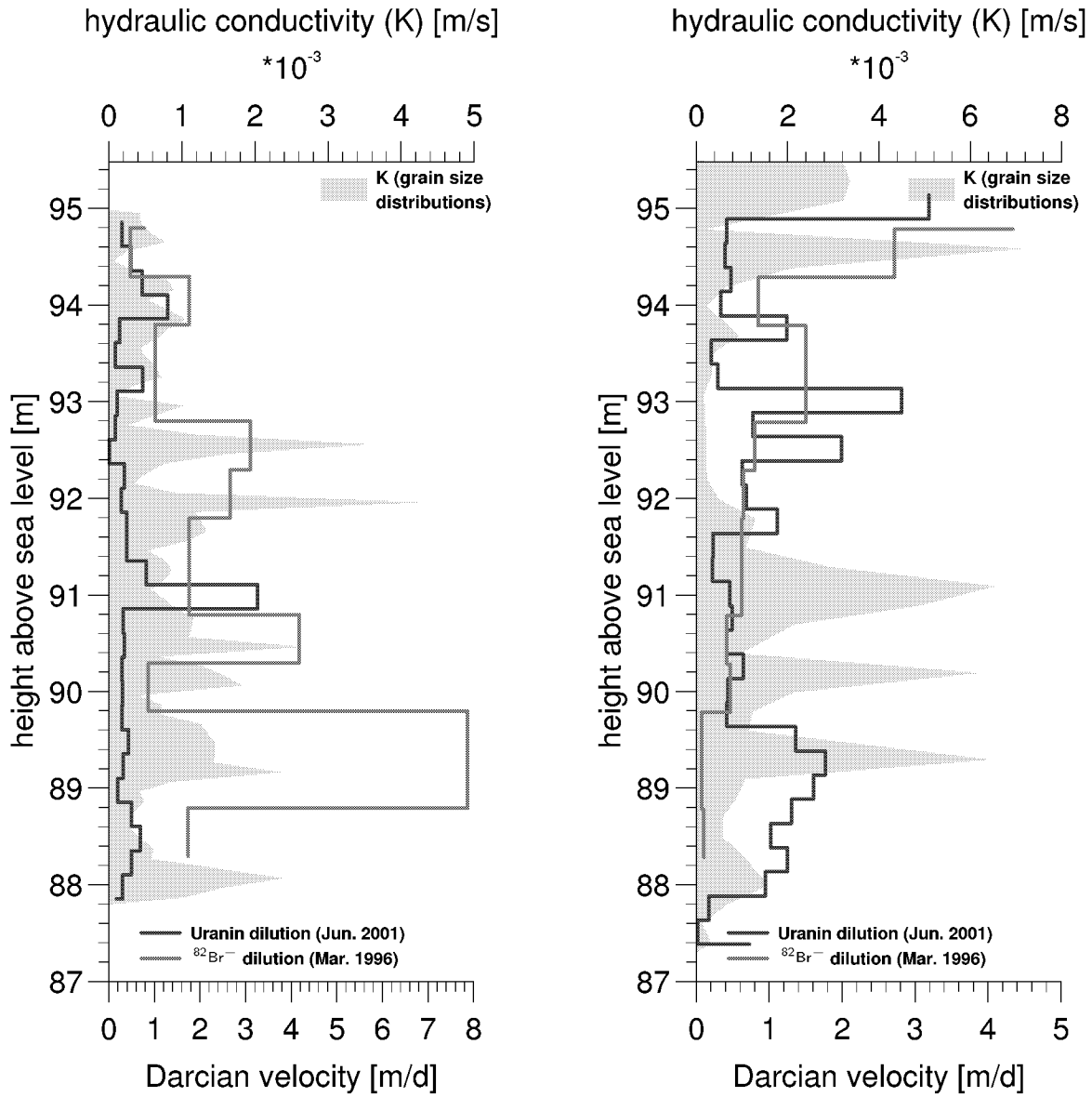

Figure 4.9: Development of the Darcy velocities and hydraulic conductivities with depth, a) well 22 b) well 32.

compared measurements seems to indicate that the measurements are not reliable. The measured Darcy velocities do not coincide with each other, nor do they coincide with the hydraulic conductivities. Once in a while, the measured velocities coincide, e.g. well 32 from 90 m to 95 m above mean sea level. And, once in a while, the hydraulic

conductivities coincide with the Darcy velocities measured with the groundwater flow velocimeter, e.g. 87.5 m to 89.8 m above mean sea level at well 32. In a few instances, the hydraulic conductivities coincide with the Darcy velocities measured with $^{82}Br^{-}$, e.g. 88 m to 95 m above mean sea level at well 22. However, only at well 22 between 93.5 m to 94.5 m above mean sea level, do all the different measurements coincide together. A well-wise comparison of the measurements of Darcy velocities for the reference layer (Tab. 4.1) shows discrepancies in mean and variance.

Table 4.1: Comparison of Statistical Parameters of In Situ Measured Darcy Velocities within the Reference Layer (Test Site Krauthausen), by Well

	$^{82}Br^{-}$			uranin		
well	N	$\mu_g(q)$ [m/d]	$\sigma^2(\ln q)$	N	$\mu_g(q)$ [m/d]	$\sigma^2(\ln q)$
18	2	0.65	0.20	7	0.69	1.16
22	3	1.85	0.62	7	0.48	0.88
26	2	0.11	0.02	6	1.46	0.73
28	2	2.25	3.98	4	1.11	0.02
32	3	0.50	0.04	7	0.47	0.77
34	2	0.07	7.49	7	0.94	0.05
44	2	0.31	1.46	7	0.21	0.10
48	2	1.25	0.79	7	0.32	0.25
50	2	0.15	0.38	6	0.78	0.14
53	3	0.29	0.01	7	0.23	0.00

In the previous comparison, averaging based on different intervals and measurement errors have to be taken into account. However, the discrepancies are too high to be explained by these effects. Therefore, it can be concluded that Darcy velocities vary not only with space but also with time. This coincides with the time resolved measurements taken with the colloidal borescope (Fig. 3.1). The measurements with the colloidal borescope presented here were taken in Rhine terraces close to the city of Düsseldorf, which feature gravelly sediments similar to those of Krauthausen test site. The first 20 minutes of the measurement showed a very high variability in the flow direction and magnitude due to the perturbations from the deepening of the colloidal borescope. Excluding these first 20 minutes, the measurements showed high variations in direction and in magnitude of the Darcy velocity. The magnitude of the measured Darcy velocities range from 0.2 m/d to 1.7 m/d within three hours.

As previously outlined, the measurements of hydraulic conductivities as well as the point dilution measurements with $^{82}Br^{-}$ are focused on the reference layer. In order to get an impression of how reliable the estimation of statistical parameters outside the reference layer are, statistical parameters have to be estimated for the reference layer for two cases, differing in the size of their samples. In case one, measurements inside the reference layer from three wells (22, 32, 7) are taken into account. In case two, all measurements taken in the reference layer are taken into account. The comparison (Tab. A.8) shows relative deviations between the two cases of 10% to 60%. These

deviations indicate that estimations based on only three locations are vague.

Based on half metre intervals, the vertical evolution of the measured hydraulic conductivities and the measured Darcy velocities are shown in Figure 4.10 and Table A.9. The measurement of Darcy velocities, both with the groundwater flow velocimeter and

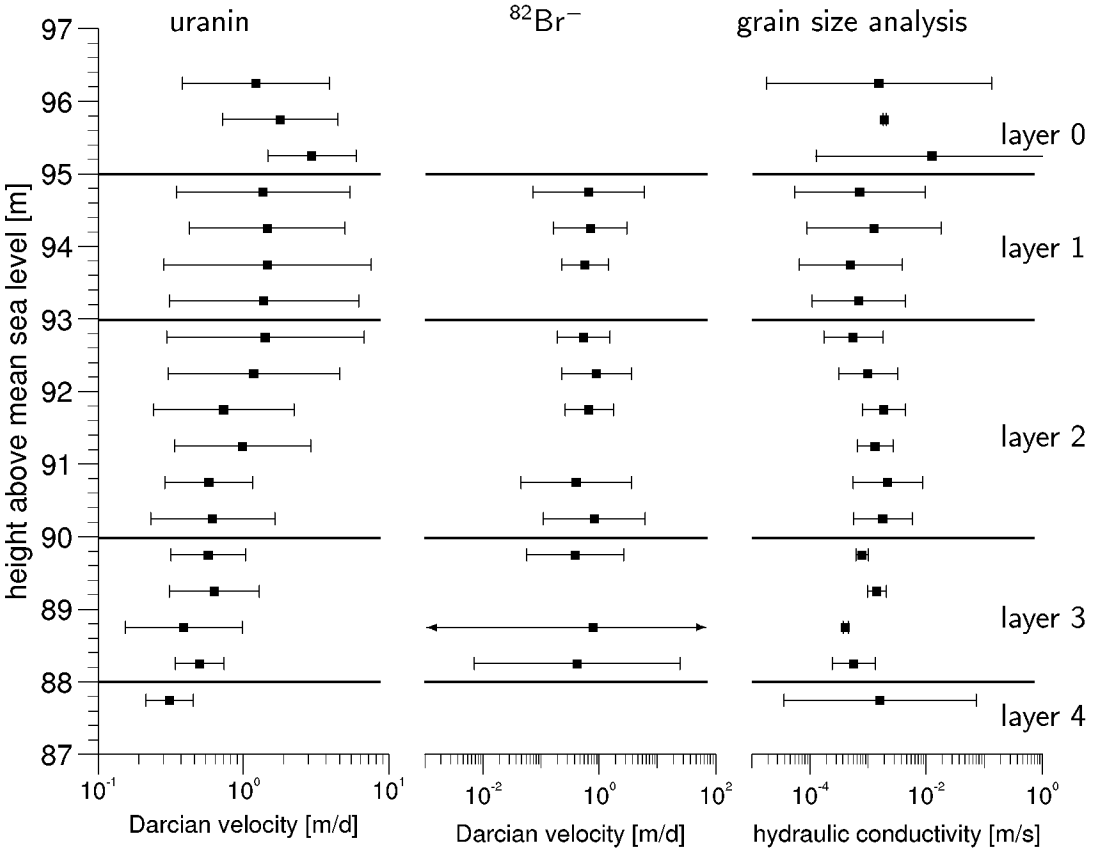

Figure 4.10: Distribution with depth of the Darcy velocities measured applying the groundwater flow velocimeter and $^{82}Br^-$ point dilution method, and hydraulic conductivities derived from grain size analysis, Krauthausen test site. The quads denote the geometric mean, the error bars show the standard deviation.

$^{82}Br^-$ point dilution method show a clear trend towards higher geometric means, from layer 3 to layer 1, whereas the hydraulic conductivities show a similar value in layer 3 and layer 1, which differs from the somewhat lower value at layer 2. However, hydraulic conductivity shows an overall upward trend when including layers 1 to 4. Likewise, the measurements of Darcy velocities with the groundwater flow velocimeter show this upward trend from layer 4 to layer 0, which coincides with the average linear velocity derived from tracer experiments (*Englert*, 1998).

Measurements of Darcy velocities with $^{82}Br^-$ show a decrease in the variance with the height above mean sea level for layer 3 to layer 1, whereas the hydraulic conductivities and the Darcy velocities measured with the groundwater flow velocimeter show an increase. This discrepancy could be due to the small number of Darcy velocity measurements with $^{82}Br^-$ in layer 1.

Chapter 5

Evaluation of Darcy Velocity Statistics

5.1 Measured Darcy Velocities

As shown in Chapter 4, magnitudes of Darcy velocities were measured on Krauthausen test site using the groundwater flow velocimeter. In the following, the focus is on the univariate statistical and geostatistical evaluation of these measurements for both all measurements and the reference layer defined in Subsection 4.1.3. According to the Darcy Equation 2.1, the Darcy velocity depends on hydraulic conductivity and gradient. As shown in Chapter 4, the hydraulic conductivity shows spatial variability and the hydraulic gradient shows spatial and time variability. Thus, the following evaluation of the heterogeneity of the Darcy velocity includes both time and space dependencies.

Both the overall measurements as well as the measurements within the reference layer show a skewness to the right side, which can be seen in histograms (Fig. 5.1 and B.2). This indicates a log-normal distribution of the Darcy velocity magnitudes. The histograms of the log-transformed values appear to be more or less symmetrical (Fig. B.1 and B.3).

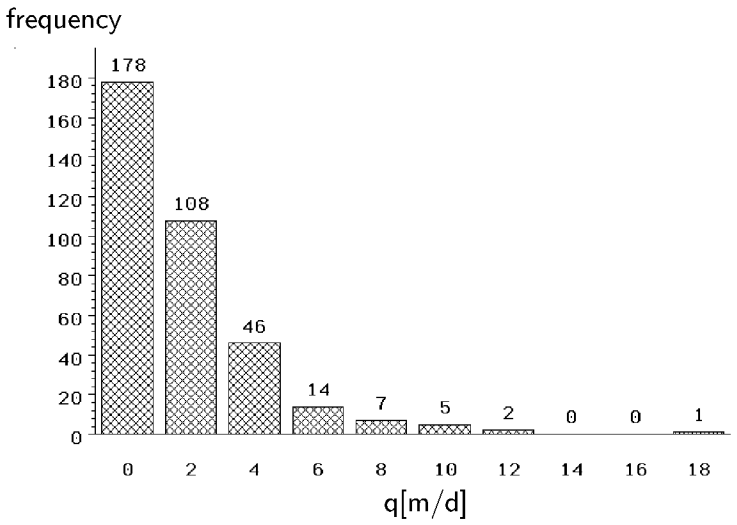

Figure 5.1: Histogram of all measured Darcy velocity magnitudes, obtained with the groundwater flow velocimeter at Krauthausen test site.

Statistical evaluation of all measured Darcy velocity magnitudes showed no clear preference for normal or log-normal distribution at a 0.0001 confidence level. The statistical test parameter W, however, is clearly higher for the log-normal distribution. For the measurements in the reference layer, the assumption of a log-normal distribution is more probable by two orders of magnitude than the assumption of a normal distribution. This suggests a better description of the measured velocities by log-normal than by normal distribution (Tab. 5.1).

Table 5.1: Statistical Parameters of the In Situ Measured Darcy Velocity Magnitudes (Test Site Krauthausen), Obtained with the Groundwater Flow Velocimeter

	all data		reference layer	
statistical parameter	q [m/d]	$\ln(q)$ [ln(m/d)]	q [m/d]	$\ln(q)$ [ln(m/d)]
number of observations	361	361	91	91
mean	1.88	0.01	1.13	-0.34
geom. mean	1.01		0.71	
variance	5.39	1.31	1.27	0.98
W test statistic	0.72	0.96	0.78	0.95
probability: $< W$	< 0.0001	< 0.0001	< 0.0001	< 0.0115

The statistical parameters of the Darcy velocities, both overall and for the reference layer, are given in Table 5.1. The discrepancy between reference layer and overall measurements in geometric mean and variance reflect the presence of layering of the aquifer at Krauthausen test site, shown in Subsection 4.2.1.

Using variogram analysis, the spatial heterogeneity of the measured Darcy velocities with groundwater flow velocimeter can be evaluated. Figure 5.2 shows a variogram of all measurements in the horizontal direction. Due to the lack of data, a separate study of different directions was not successful. Within this variogram calculation, the horizontal directions are assumed to be isotropic. A weighted fit to the semivariances, using an exponential model, shows a range of 2.46 ± 1.8 m and a sill of 1.15 ± 0.11 $(\mathrm{m/d})^2$.

In the vertical direction, the variogram (Fig. 5.3) shows a continuous increase of the semivariances, including plateaus at the semivariances of 0.26, 0.60 and 0.82. This shows, on the one hand, the trend of the Darcy velocity magnitudes within the aquifer, shown in Subsection 4.2.1, and, on the other hand, the layering of the aquifer. The fit of an exponential model to the semivariances including lag distances between 0.25 m and 1.00 m showed a range of 0.19 ± 0.03 m and a sill value of 0.33 ± 0.01 $(\mathrm{m/d})^2$. The fitted model describes the overall heterogeneity of the Darcy velocity magnitudes for distances below 1 m in the vertical direction.

The small sill value in the vertical direction, compared with the sill value in the horizontal direction, shows that the variability in the horizontal direction is higher than the variability in the vertical direction by factor 3. This could be due to the existence of layer spanning zonation of the aquifer at Krauthausen test site or due to the time dependence of the Darcy velocities. At this point, it should be kept in mind that the measurements at one well took approximately one day and consequently all wells are measured on different days.

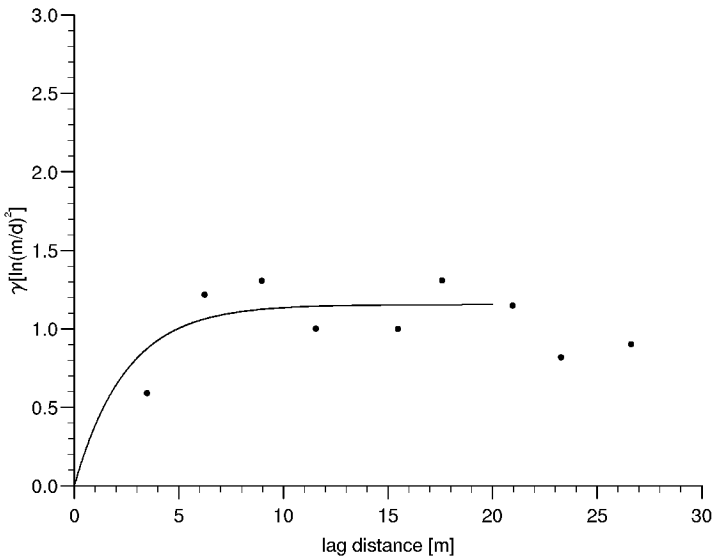

Figure 5.2: Horizontal variogram of $\ln|q|$ for all measurements and exponential fit.

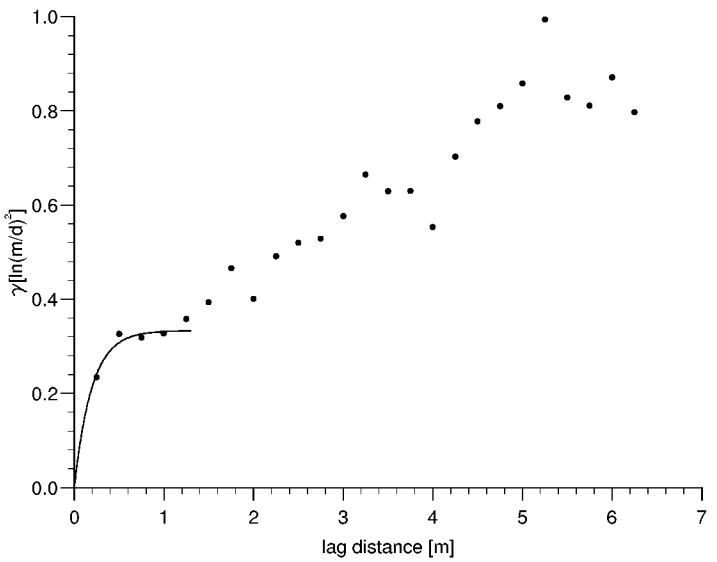

Figure 5.3: Vertical variogram of $\ln|q|$ for all measurements and exponential fit.

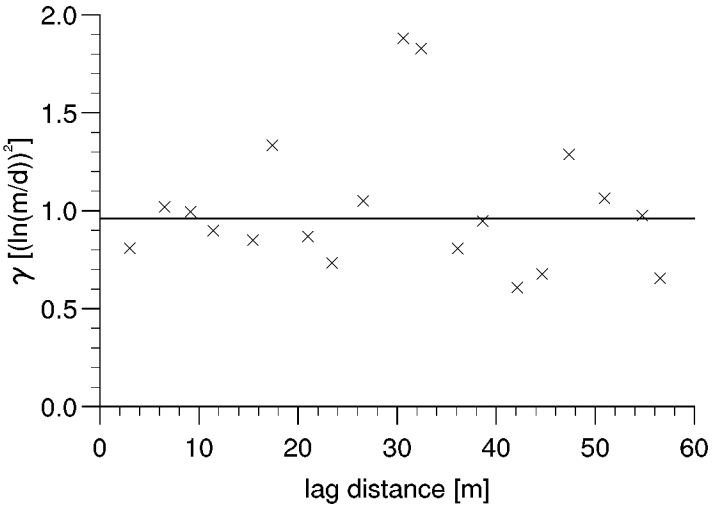

Figure 5.4: Horizontal variogram of $\ln|q|$ inside the reference layer, with the horizontal line indicating the variance.

The variogram in the horizontal direction, for the measurements of Darcy velocity magnitudes with the groundwater flow velocimeter in the reference layer, shows no clear autocorrelative behaviour (Fig. 5.4). This is is probably due to the lack of data, but could also be an effect of the zonation of the aquifer or the time dependency of the Darcy velocities.

The variogram in the vertical direction, including the measurements inside the reference layer, showed no clear autocorrelative behaviour (Fig. B.4). However, the values of the semivariances are smaller than the variance in the reference layer and the semivariances in the variogram in the horizontal direction. This again suggests either the zonation of the aquifer, or the time dependency of the Darcy velocities, or both.

A variogram analysis of Darcy velocity magnitudes, using $^{82}Br^-$ dilution was taken for the reference layer (*Vereecken et al.*, 2000). An exponential fit showed a range of 4.19 ± 2.16 m and a sill of 2.10 ± 0.18 $(\mathrm{m/d})^2$. The range is similar to the range obtained for the groundwater flow velocimeter measurements.

Univariate statistical analysis of the Darcy velocities measured by $^{82}Br^-$ dilution showed for all data $\mu_g|q| = 0.42$ m/d and $\sigma^2(\ln|q|) = 1.86$ $(\mathrm{m/d})^2$ and for the reference layer $\mu_g|q| = 0.41$ m/d and $\sigma^2(\ln|q|) = 2.01$. Statistical tests suggest better description by log-normal than by normal distribution (Tab. B.1). In comparison with the measurements with the groundwater flow velocimeter, these measurements show for both all data and the reference layer smaller values in the geometric mean and higher values in the variance and correlation length. Flow direction measurement allows vector decomposition of the measured Darcy velocities in q_y and q_x. A variance of $q_y = 3.96$ and of $q_x = 3.20$ was calculated.

Variorgam analysis, as it is used here, focuses on the evaluation of spatial variability. Due to the additional variability of the Darcy velocity in time, the evaluated correlation lengths, especially in the horizontal direction, are foreshortened.

5.2 Numerical Modelled Darcy Velocities

The groundwater flow velocity fields were calculated with the computer program TRACE. This is part of the software package TRACE/PARTRACE (*Neuendorf*, 1996; *Seidemann*, 1996) used in the forward modelling of groundwater flow and transport. It solves the three dimensional mixed form of the Richards equation (Eq. 2.3) for variably saturated porous media. The advantages of the software are time dependent modelling, the combined treatment of saturated and unsaturated zones, the implementation of heterogeneous hydraulic conductivity fields and the possibility of parallel computing. Numerical calculations were performed on a CRAY-T3E parallel computer using 32 processors for the runs of TRACE.

5.2.1 Description of the numerical cases

In stochastic theories, only uniform gradient flow fields can be used to estimate the heterogeneity of Darcy velocities. However, on Krauthausen test site spatial variations in the hydraulic gradient were found. Two numerical cases are calculated in order to analyse the effect of the variations in the hydraulic gradient on Darcy velocity statistics. The two numerical cases differ only in the boundary conditions. Case 1, denoted as the **simplified case**, refers to a hydraulic head situation with the assumption of a stationary constant mean hydraulic gradient for the entire study area. Case 2, denoted as the **triangulated case**, refers to a hydraulic head situation with the assumption of a stationary but spatially varying hydraulic gradient.

Both cases are calculated within the same three dimensional flow domain on a grid with 622296 nodes. The physical dimension of the grid is 170 m in length (y-direction), 70 m in width (x-direction) and 10 m in height (z-direction). The grid size in x- and y-direction is 2 m, where the grid size in z-direction is 5 cm. The grid size is $< 1/4$ of the autocorrelation length of the hydraulic conductivity. This is considered to reproduce the heterogeneity of hydraulic conductivities, stated by a variance and a autocorrelation length (*Bellin et al.*, 1992). The predefinitions of the two cases for the numerical modelling, including hydraulic conductivity field and boundary conditions, are discussed below.

Hydraulic Conductivity Field for Modelling

A Kraichnan generator (*Kraichnan*, 1970), implemented in the TRACE program, was used to generate a three dimensional, heterogeneous hydraulic conductivity field. In both cases the same realization is used. Input parameters (Tab. B.2 and B.3) for the stochastic simulation are the statistic parameters of hydraulic conductivity, derived from grain size analysis of Krauthausen test site samples from the depth 90 to 92 m above sea level (Subsection 4.1.3). The stochastically simulated hydraulic conductivity field is visualized in a horizontal cross section (Fig. 5.5) and a longitudinal cross section (Fig. 5.6).

The accuracy of the stochastically simulated hydraulic conductivity field was evaluated by comparing the statistical parameters derived from the generated field with the input statistics (Tab. B.2 and B.3).

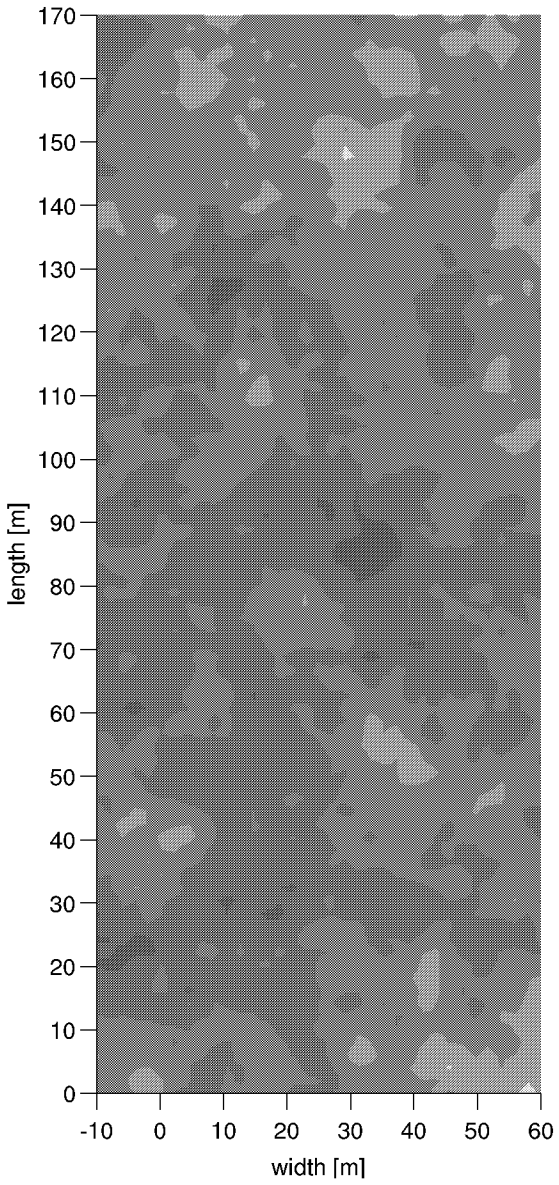

Figure 5.5: Horizontal section of the stochasticly generated hydraulic conductivity field, correlation length 11.8 m in both horizontal directions.

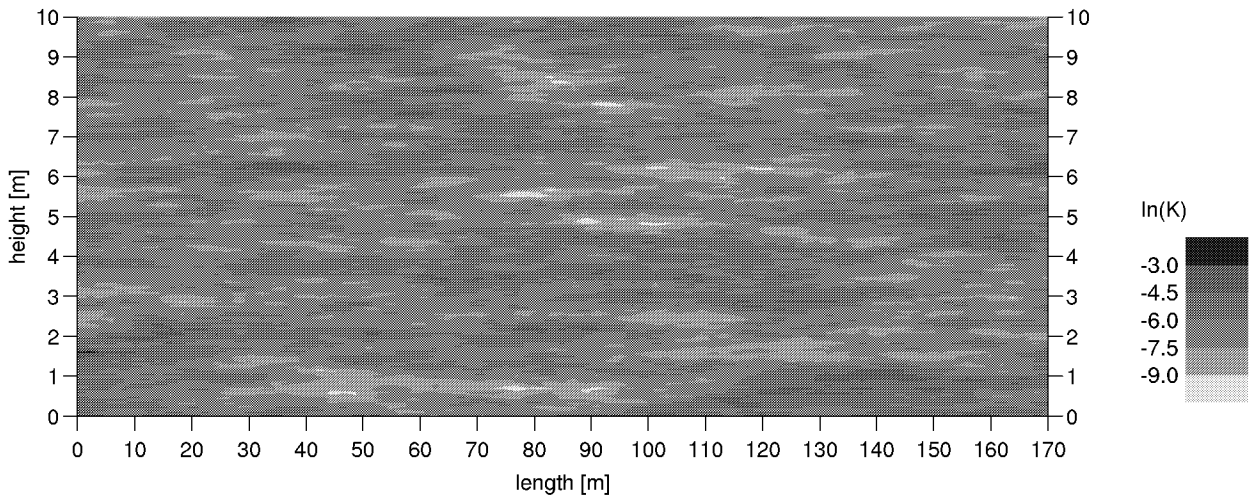

Figure 5.6: Longitudinal section of the stochasticly generated hydraulic conductivity field, correlation length in horizontal direction 11.8 m, in the vertical direction 0.2 m. Aspect ratio 1:7.

The mean and variance for logarithm of hydraulic conductivity are reproduced by the Kraichnan generator within an error of below 3% compared to the input. The statistical test of log-normal distribution of the hydraulic conductivities showed an acceptable result within a confidence interval of 15%.

The correlation lengths are reproduced quite well within an error of below 6% for all directions compared to the input. The sill is very close to the variance of the hydraulic conductivity in all directions. This shows that the statistical structure of the hydraulic conductivity is reproduced in all directions.

Boundary Conditions for Modelling

For both cases, the boundaries at the top and at the bottom of the flow domain are predefined by no flux Cauchy boundary conditions. Therefore, it is supposed that the infiltration at the top of the aquifer and the fairly impermeable bottom of the aquifer has no critical effect on the heterogeneous flow field inside the flow domain.

Whereas the front, back, left and right boundary of the modelling area are predefined as Dirichlet boundary conditions for the triangulated case, for the simplified case only front and back boundaries are defined as Dirichlet boundaries. The left and right boundaries of the simplified case are defined as no flux Cauchy boundary conditions. These predefinitions for the boundary conditions coincide with the assumption that the flow field should be parallel to the length of a modelling area in the simplified case. Consequently, the flux through the left and right boundaries has to be zero. In contrast, the flux through left and right boundaries in the triangulated case is not known and has to be calculated with respect to the Dirichlet boundary conditions. This is clarified by Figures B.5 and 5.7. The Dirichlet boundary conditions for both cases are derived from piezometric head measurements at the Krauthausen test site (Fig. B.5 a), Fig. 5.7 a) and Subsection 4.2.1).

Compared to the input of the Cauchy no-flux definition, for the bottom and top boundaries the computed flux balances are ≤ 0.11 m^3 for both cases. This is only 0.3% of the complete flux through the flow domain and is due to numerical errors.

Compared to the input of the Cauchy no-flux definition, for the left and right boundaries of the simplified case, the computed flux balances are ≤ 0.12 m^3. This is only 0.4% of the complete flux through the flow domain and is due to numerical errors. As expected, the modelled flux balances through Dirichlet boundaries differ in the simplified and the triangulated case. Approximately 100% of the discharge of the flow domain in the simplified case passes through the rear, whereas in the triangulated case about 75% pass through the back and about 25% through the left and right boundaries.

5.2.2 Calculated Darcy velocities

Computation of the two cases required ten minutes respectively, using 32 processors of a CRAY-T3E parallel computer. In order to eliminate the effects of boundary conditions on the flow field the five outermost grid nodes, at all boundaries of the computed flow domain, are excluded (*Naff et al.*, 1998).

Measurements with the groundwater flow velocimeter contain only information about the magnitude of the Darcy velocity. Therefore in a first step only Darcy velocity magni-

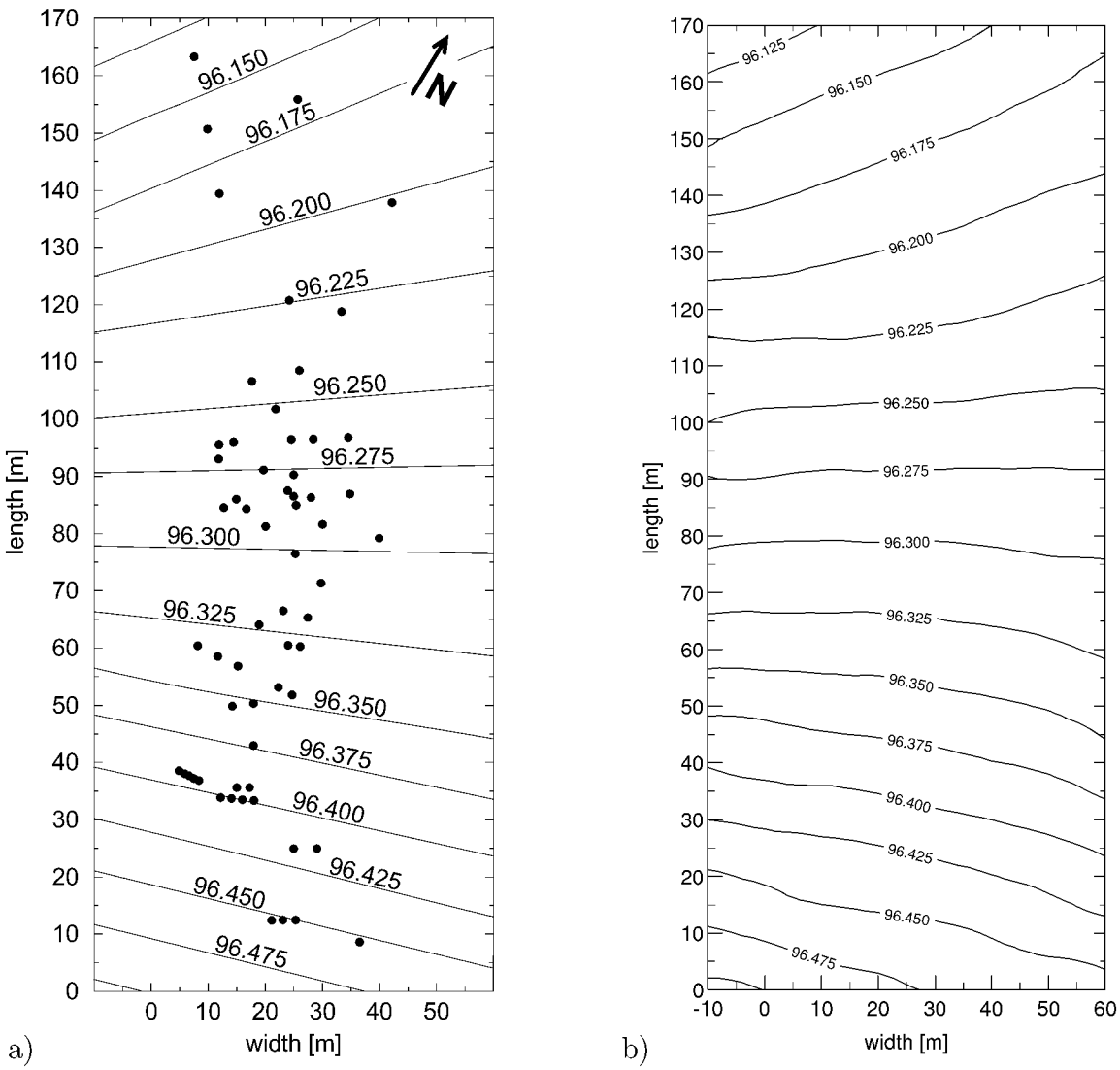

Figure 5.7: Total head situation of 3.8.2001 in metres above mean sea level, Krauthausen test site: • measured groundwater observation well
a) measured and triangulated
b) modelled on the base of boundary conditions derived from a)

tudes will be used in the following comparison. The main focus will be the comparability of direct measurements at certain positions at Krauthausen test site (the triangulated case) and modelled data calculated for the simplified case. Since stochastic theories requires an uniform mean hydraulic gradient in a second step comparison of the Darcy velocity component statistic will be used to test the validity of the application of stochastic theories to cases with a non uniform gradient.

The computed magnitudes of Darcy velocities are visualized in a longitudinal section

and in a horizontal section for both the simplified and for the triangulated case. In the sections through the Darcy velocity flow domains there are only small differences between the simplified and the triangulated case. Therefore, only the simplified case is depicted (Fig. 5.8 and 5.9).

The heterogeneity of the Darcy velocity is analyzed in detail by means of statistic and geostatistic methods. Due to excluded grid nodes close to the boundaries of the flow domain, the number of observations amount to 288876. Statistical evaluation of the velocity magnitude for both cases (Tab. 5.2) showed no clear preference for normal or log-normal distribution at a 0.01 confidence level. The statistical test parameter D, however, is two orders of magnitude smaller for the assumption of log-normal distribution, suggesting a better description of the magnitudes of the Darcy velocities by log-normal distribution than by normal distribution. This can also be seen for the y-component of the Darcy velocities (Tab. B.4). In contrast, the stochastic theories for groundwater flow predict a normal distribution for the y-component of the Darcy velocities.

Table 5.2: Statistical Parameters of the Modelled Magnitude of Darcy Velocity Fields, Based on a Single Realisation of the Hydraulic Conductivity Field

statistical parameter	simplified		triangulated	
	$\|q\|$ [m/d]	$\ln(\|q\|)$ [ln(m/d)]	$\|q\|$ [m/d]	$\ln(\|q\|)$ [ln(m/d)]
number of observations	288876	288876	288876	288876
mean	0.47	-1.11	0.49	-1.08
geom. mean [m/d]	0.33		0.34	
variance	0.22	0.73	0.25	0.74
D test statistic	0.17	$0.44 \cdot 10^{-2}$	0.18	$0.28 \cdot 10^{-2}$
probability: $> D$	< 0.01	< 0.01	< 0.01	< 0.01

The geometric mean of the magnitude of the Darcy velocities amounts to approximately 0.33 m/d, both for the simplified and the triangulated case. As expected, the value for the geometric mean from modelling is close to the one computed analytically using Darcy's law (Eq. 2.1) (0.32 m/d), taking into account the geometric mean of hydraulic conductivities ($1.88 \cdot 10^{-3}$ m/s) and the simplified hydraulic gradient (0.002). Equally, the variances (approximately 0.73) of log-transformed Darcy velocity magnitudes are similar for both the simplified and triangulated case (Tab. 5.2). Thus, modelled statistics of local Darcy velocity magnitudes are not strongly affected by small variations of the total head field.

As expected, since the input hydraulic conductivity field shows autocorrelative structure in all directions, so does the field of modelled magnitudes of the Darcy velocity (Tab. 5.3). The correlation length of the modelled magnitudes of the Darcy velocity are similar, both for the simplified and the triangulated case, in all directions. This shows that the geostatistical parameters of the modelled magnitudes of the Darcy velocity are little affected by the variation of the total head situation. For both cases, the correlation lengths of log-transformed Darcy velocities are approximately 1/2 times higher than the log-transformed hydraulic conductivity correlation lengths for x- and y-direction, but similar for the z-direction. One needs to keep in mind that typically the covariance of

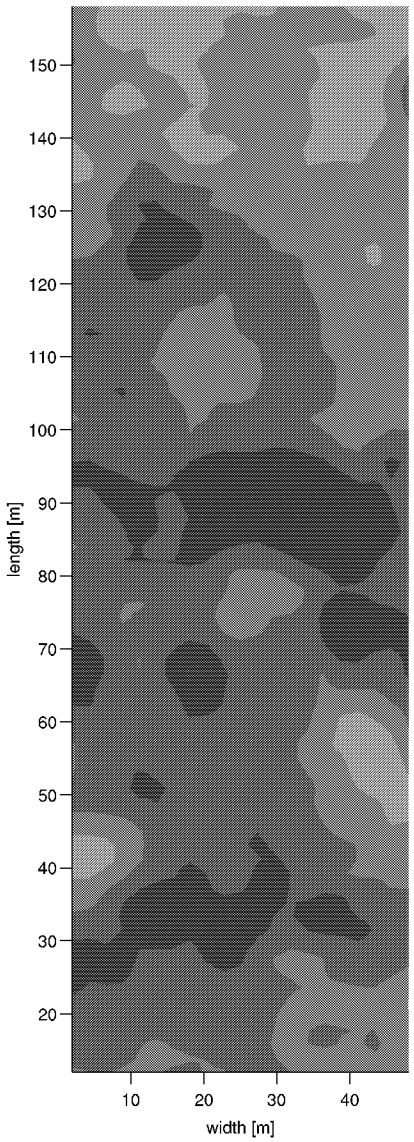

Figure 5.8: Horizontal section of the modelled Darcy velocity field taking into account the simplified total head situation of August 3, 2001, Krauthausen test side.

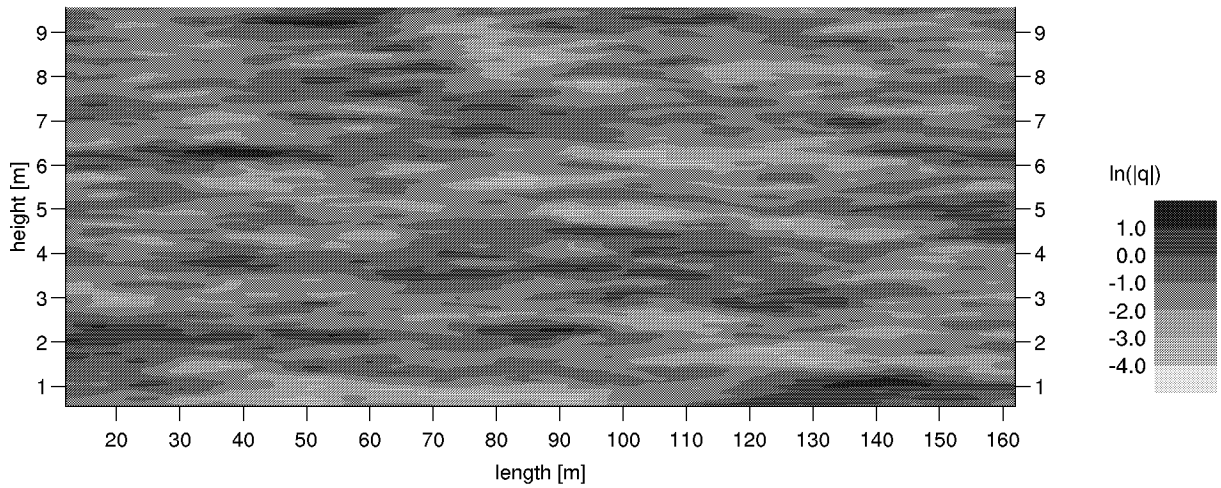

Figure 5.9: Longitudinal section of the modelled Darcy velocity field in consideration of the simplified total head situation of August 3, 2001, Krauthausen test side. Aspect ratio 1:7.

the x- and z- components of Darcy velocities show so called hole effects. This means that the covariance and the correlogram is characterized by the presence of holes (the function declines to values below zero and rise again), this reflects a tendency for high values surrounded by low values and vice versa (*Chilès and Delfiner*, 1999). These effects can be observed in Figures 5.11 to 5.12, B.10 and B.12. The hole effects are not considered in Table 5.3 for comparison purposes.

Table 5.3: Geostatistics of the Modelled Magnitude of Darcy Velocity Fields, Based on a Single Realisation of a Hydraulic Conductivity Field

geostatistical parameter	x-direction	y-direction	z-direction
	simplified total head situation		
correlation length [m]	19.18	15.93	0.23
std. error [m]	1.60	0.61	$1.09 \cdot 10^{-2}$
sill	0.88	0.77	0.77
std. error	$4.15 \cdot 10^{-2}$	$1.02 \cdot 10^{-2}$	$8.32 \cdot 10^{-3}$
	triangulated total head situation		
correlation length [m]	21.2	16.25	0.23
std. error [m]	1.75	0.62	$1.09 \cdot 10^{-2}$
sill	0.96	0.78	0.77
std. error	$4.71 \cdot 10^{-2}$	$1.04 \cdot 10^{-2}$	$8.33 \cdot 10^{-3}$

The geostatistical parameters are applied to an weighted exponential model without nugget using the log-transformed Darcy velocities. See also Table 5.2.

The statistical parameters of the y-component and the magnitude of Darcy velocities are alike (Tab. B.4). This is due to the fact that the mean of x- and z-component statistics is close to zero and 90% of the x- and z- Darcy velocity components are below 0.05 m/d.

The extent of the mean for the x- and z-component expresses the overall tendency for the flow direction, where negative values show left or down movement, positive values show right or up movement. The mean of the z-component of the Darcy velocities both for the simplified and the triangulated case is close to zero (Tab. B.5). The small divergences from zero are due to numerical errors described in the Subsection 5.2.1. In the simplified case, the x-component of Darcy velocities is close to zero as well. The x-component of the triangulated case is approximately -0.01 m/d. This is due to the fact that the water balance on the left side of the flow domain is -5.3 m^3, as compared to the one on the right side of only -3.8 m^3 (Subsection 5.2.1).

As expected, the variance of the modelled z-component of the Darcy velocities is similar for the simplified, as well as for the triangulated, total head situation. This is due to the same top and bottom boundaries (no flux boundaries) for both situations. The variance of the modelled x-component of the Darcy velocity is one order of magnitude larger in the triangulated case than in the simplified one. This shows the influence of spatial variations of the hydraulic gradient in the triangulated case on Darcy velocities.

5.3 Estimated Darcy Velocity Statistics

For the stochastic estimation of the Darcy velocity field, data from Krauthausen test site was used. As before in the modelling, statistical and geostatistical parameters of the hydraulic conductivities are derived from the reference layer 90 m to 92 m above sea level. The mean gradient is derived from piezometric head measurements at Krauthausen test site. The input parameters are given in Tab. 5.4.

Table 5.4: Statistical Parameters of Hydraulic Conductivity and Mean Hydraulic Gradient, as Used as Input Parameters for the Stochastic Estimation of Darcy Velocity Statistics

statistical parameter	Gaussian model	exponential model
J	0.002	
K_g	162.86 m/d	
$\mu(\vec{q}) = K_g \cdot J$	0.33 m/d	
σ_y^2	1.0	
λ_v	0.15 m	0.2 m
λ_h	13.5 m	11.8 m
$e = \frac{\lambda_v}{\lambda_h}$	0.011	0.017

The formulas given in Section 2.4 are used for the stochastic estimations. In Table 5.5, the estimated means and variances for the Darcy velocity components are presented using different methods of approximation and results from numerical modelling. The estimation of the mean Darcy velocity is identical for all approximating approaches in 2D. In 3D, 1st order estimation of the mean is equal for Gaussian and exponential model, but higher than the 2D estimation of the mean by factor 1.5. In 3D, the 2nd order estimations of the mean are higher than the 1st order estimations both for Gaussian and exponential model. Only little differences between Gaussian and exponential model can be detected for the 2D 1st and 2nd order as well as for the 3D 1st order estimations of variance. In 2D, the variances are quite similar for 1st and 2nd order estimation for both the exponential and Gaussian model. In 3D, estimated variances differ between the 1st and 2nd order for the y-component of the Darcy velocity for both the exponential and Gaussian model. For the exponential model, the variances for the x- and z-component of the Darcy velocity are higher for the 2nd order than for the 1st order approximation by factor 3. For the Gaussian model 2nd order estimation of the variances of x- and z-component of the Darcy velocity are not calculated, due to the absence of correction factors (Section 2.4).

In the following, the difference between stochastically estimated and numerically calculated statistical ensemble parameters of the Darcy velocity is analysed for 3D exponential model. To do so, the statistical stability of the Monte Carlo analysis needs to be tested. For this purpose, 10 realizations of the K-field, shown in Subsection 5.2.1, were generated using the Kraichnan generator. The variances of $\ln(K)$ derived from these fields are shown in Figure B.9. The variances of the separate realizations vary around the ensemble variance of the 10 realizations within a relative deviation of $< 4\%$. The

Table 5.5: Estimated Variances of the xyz- Components of the Darcy Velocities, Using Stochastic Theories

dimension	geostat. model for K	approach	variance q_x	q_y	q_z	mean $\|q\|$ [m/d]
2D	exponential	1st order	0.014	0.041	-	0.32
		2nd order	0.019	0.044	-	0.32
	Gaussian	1st order	0.014	0.041	-	0.32
		2nd order	0.016	0.041	-	0.32
3D	exponential	1st order	0.0002	0.104	0.0007	0.48
		2nd order	0.0005	0.250	0.002	0.56
		modelling	0.0029	0.266	0.0011	0.51
	Gaussian	1st order	0.0001	0.105	0.0005	0.48
		2nd order	n.c.	0.352	n.c.	0.52

n.c.: not calculated

jackknife method (*Wonnacott and Wonnacott*, 1985) is used to estimate the error of the variances at a 95% confidence interval. This resulted in a variance of $\ln(K)$ of 0.98 $\pm$ 0.01, indicating sufficient accuracy of the ensemble variance from 10 realizations.

In order to verify the accuracy of the required heterogeneity of the K-field, the ex ante given covariance function and the stochastically simulated ensemble covariances of $\ln(K)$ are presented in Figures B.6, B.7 and B.8. The ensemble covariances in y- and z-direction show small fluctuations around the ex ante given covariance function for covariances < 0.1. The simulated ensemble covariances in y- and z-direction otherwise fit excellently with the ex ante given covariance functions. In the x-direction, the ensemble covariances fit excellently until the lag distance reaches 40 m. For greater lag distances, the simulated ensemble covariances remain constant at a small covariance of 0.05, while the ex ante given covariance tends to zero.

The 10 realizations of the K-field are used for the numerical modelling of the flow velocity fields. The input parameters for these modellings are the same as those for the simplified case described in Section 5.2.1. In Figure B.9, the variances of $\ln(q_y)$ for single realizations are presented in comparison with the ensemble variance of 10 realizations. The variances of single realizations deviate from the ensemble variance by up to 9%. The jackknife method at a 95% confidence interval resulted in a variance of 0.76 $\pm$ 0.02 for the log-transformed y-component of the Darcy velocity. This indicates sufficient statistical stability for the ensemble variance of 10 realizations. The ensemble statistics of the modelled Darcy velocity magnitudes are given in Tab. 5.6.

The ensemble mean of the modelled Darcy velocities fit excellently with the mean Darcy velocity estimated by stochastic theories.

The ensemble covariances from modelling, as well as the 1st order and 2nd order estimated covariances, are shown for the y-direction in Figures 5.10 to 5.12. In order to compute the 1st order approximated covariances, the Equations 2.65 to 2.67 are used. Second order approximations of the covariances are computed by scaling the 1st order approximated covariances by the 1st to 2nd order correction factors given for the variances.

Table 5.6: Ensemble Parameters of Darcy Velocity Magnitudes Obtained by Modelling, Based on 10 Realisations of Hydraulic Conductivity Field

ensemble parameter	$\|q\|$[m/d]	$\ln\|q\|$[ln(m/d)]
N	2888760	
μ	0.51	-1.03
$\mu_g(\|q\|)$	0.36	
$\sigma^2(\|q\|)$	0.27	0.76
D test statistic	0.17	0.0028
probability: $> D$	0.01	0.01

The 1st order estimated variance of the y-component of the Darcy velocity is well below the one calculated by numerical modelling. In contrast, the 2nd order estimated variance of the y-component of the Darcy velocity (Tab. 5.5) is in good agreement with the ensemble variance from numerical modelling. Applying 1st order approximation, the estimated covariances for the y-component of the Darcy velocity clearly differ from the numerically calculated ensemble covariances. The covariances estimated by 2nd order approximation fit excellently.

First order as well as second order approximation of the velocity variance of the x-component are one order of magnitude below the ensemble variance of the numerically modelled x-component. First and second order approximated covariances are clearly below the modelled covariances until a lag distance of 25 m is reached. For greater lag distances, the estimated covariances are higher than the numerically calculated one.

The 1st order approximation for the variance of the z-component of the Darcy velocity is below the numerically calculated ensemble variance. The 2nd order approximation is above the ensemble variance of numerical modelling. For the z-component, the numerically calculated ensemble covariances occur in between the 1st order and 2nd order

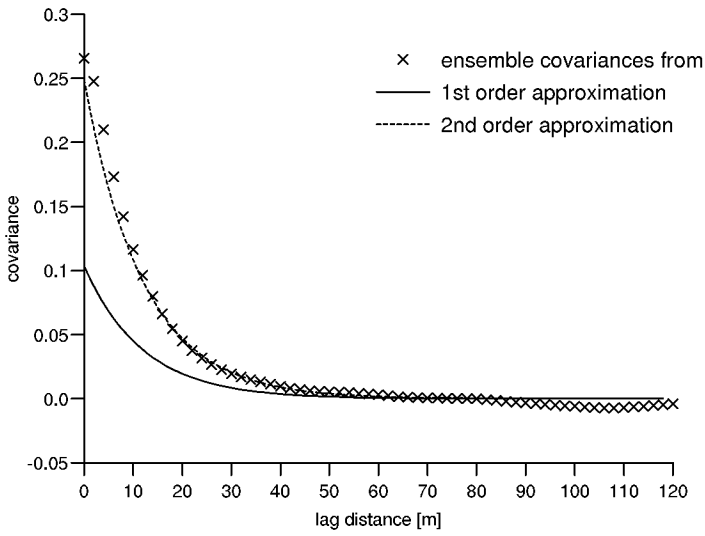

Figure 5.10: Covariance in y-direction of the y-component of the Darcy velocity.

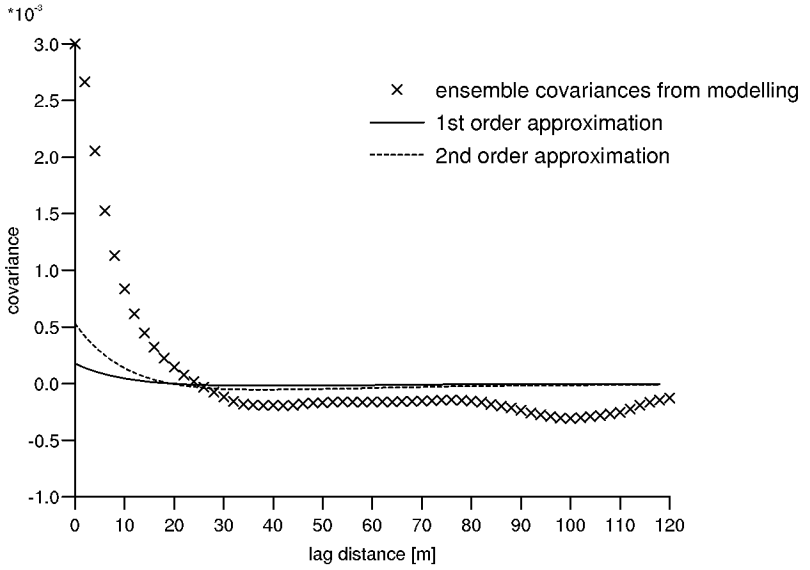

Figure 5.11: Covariance in y-direction of the x-component of the Darcy velocity.

estimated covariances.

However, the correlograms of the Darcy velocity in the y-direction, estimated using 1st order approximation and numerical calculation, fit quite well for the x- and z-component and fit excellently for the y-component (Fig. B.10 to B.12).

Finally, the evaluated statistical parameters from measured Darcy velocity magnitudes are compared with those from stochastical estimation and numerical simulation. At this point, it should be kept in mind that the α-factor is estimated only vaguely, although it influences the mean and the variance of the Darcy velocities. For comparison purposes, independent from the α-factor, the so called relative standard deviation $(\frac{\sigma(|q|)}{\mu(|q|)})$ is used. The means, standard deviations and relative standard deviations of the several approaches are presented in Table 5.7.

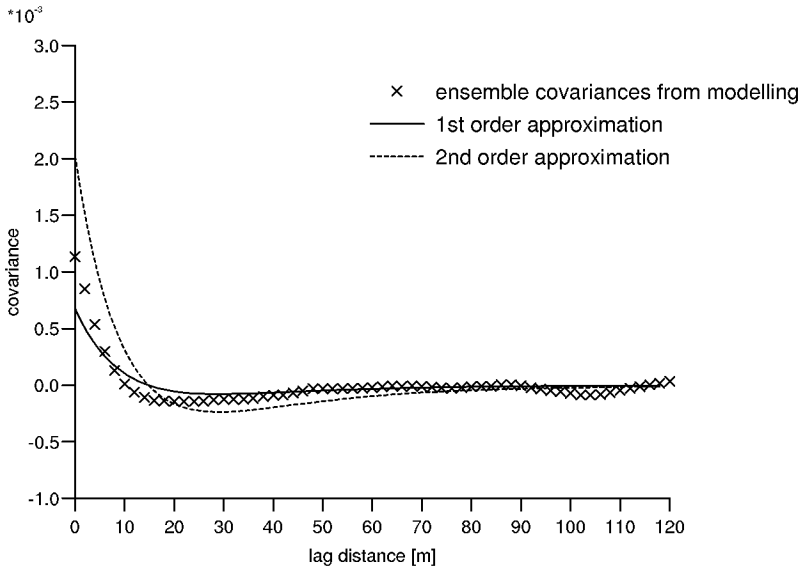

Figure 5.12: Covariance in y-direction of the z-component of the Darcy velocity.

Table 5.7: Estimated Darcy Velocity Statistics for the Reference Layer (Test Site Krauthausen)

	method modelling	stochastic theory		field measurement	
parameter	of 10 realisations	1st ord.	2nd ord.	$^{82}Br^-$	gwfv*
$\mu(\|q\|)$	0.52	0.48	0.56	1.2	1.1
$\sigma(\|q\|)$	0.52	0.32	0.50	2.3	1.1
$\frac{\sigma(\|q\|)}{\mu(\|q\|)}$	1.00	0.67	0.89	2.0	1.0

$*$ groundwater flow velocimeter

The means and standard deviations estimated from field measurements are well above the predictions from modelling and stochastic theories. This is probably due to the α-factor. The relative standard deviation is higher for the measurements with $^{82}Br^-$ than for modelling by factor 2, 2nd order stochastic estimation and measurements with the groundwater flow velocimeter. This could be due to the small number of measurements. However, the relative standard deviation is similar for modelling, 2nd order stochastic estimation and measurements with the groundwater flow velocimeter.

The autocorrelation lengths of the measured Darcy velocities in the horizontal direction are smaller than those from modelling and stochastic theories by factor 7. This could be due to the time variability of the Darcy velocities.

Chapter 6

Conclusions

A groundwater flow velocimeter using the point dilution technique has been developed in order to measure groundwater flow velocities. The resolution of the groundwater flow velocimeter in the vertical direction is 25 cm. The in situ dilution measurement of the tracer uranin was carried out by laser-induced fluorimetry. Calibration of the groundwater flow velocimeter shows a relative error of 50% for flow velocities ranging between 0.2 m/d and 1.1 m/d and a relative error of 10% for flow velocities ranging between 1.1 m/d and 14.7 m/d. This shows that the groundwater flow velocity inside a borehole can be measured with sufficient accuracy. The accuracy of determination of the Darcy velocity inside the aquifer from the measurements inside the borehole is strongly dependent on the accuracy of the α-factor, correcting the convergence of streamlines towards the borehole. The estimation of the α-factor is difficult due to a general lack of knowledge of the state of the well design.

On Krauthausen test site 361 groundwater flow velocity measurements were carried out with the groundwater flow velocimeter. Measurements showed a high variability in the magnitude of the Darcy velocity, ranging between 0.1 m/d and 17.8 m/d. The geometric mean of the magnitude of the Darcy velocities was 1.0 m/d within a variance of the log-transformed values of 1.3. Applying an exponential variogram model, a correlation length of 2.5 ± 1.8 m was found in the horizontal direction and 0.2 ± 0.03 m in the vertical direction. The experimental variogram in the vertical direction also indicates a trend of the Darcy velocity with depth and the layering of the Krauthausen aquifer.

A direct comparison of the measured Darcy velocities applying the groundwater flow velocimeter with hydraulic conductivities (*Döring*, 1997; *Englert et al.*, 2000a; *Vereecken et al.*, 2000), as well as with measured Darcy velocities applying $^{82}Br^-$ (*Drost*, 1996; *Englert et al.*, 2000b; *Vereecken et al.*, 2000), showed high discrepancies. This can be explained by a time dependence of the Darcy velocity, which is demonstrated in repetition measurements. This indicates that, beside the variability in space, there is variability in time of the local Darcy velocity, which coincides with time resolved measurements of flow velocities with the colloidal borescope (*Kearl and Case*, 1992; *Schöttler*, 1997).

Using the groundwater flow velocimeter, the vertical determination of the Darcy velocities with a measurement window of 0.5 m showed a general increase of geometric mean and variance with the position above mean sea level. This is in agreement with the measurements of hydraulic conductivity and the average linear velocity derived from tracer experiments (*Döring*, 1997; *Englert*, 1998; *Vereecken et al.*, 2000). Additionally,

the layering of the Krauthausen aquifer based on field studies, grain size analysis and measurements of hydraulic conductivities can be recovered by the Darcy velocity measurements.

The horizontal correlation length, derived from measurements with the groundwater flow velocimeter, is smaller than that evaluated from Darcy velocity measurements with $^{82}Br^-$ by factor 2 and smaller than that based on hydraulic conductivity measurements by factor 3. This can be attributed to the time dependency of the groundwater flow velocities. In the vertical direction, the autocorrelation lengths of the Darcy velocities, measured with the groundwater flow velocimeter and the hydraulic conductivities in the reference layer (90 m to 92 m above mean sea level), are similar. Like the hydraulic conductivities and the Darcy velocity measurements with $^{82}Br^-$, the Darcy velocity measurements with the groundwater flow velocimeter are better described by log-normal then normal distribution.

Special attention was given to the reference layer at Krauthausen test site due to a better measurement density. The geometric mean of the magnitude of the Darcy velocity, obtained from 91 measurements with the groundwater flow velocimeter, was 0.71 m/d with a variance of the log-transformed values equal to 0.98. Experimental variograms in the horizontal as well as in the vertical direction showed no clear autocorrelative structure. The lack of spatial structure may be explained by too small a sample size or an additional time dependent variability of the Darcy flow velocities.

Comparison of the geometric mean of Darcy velocity measurements with the groundwater flow velocimeter and with the one obtained from the Darcy velocity measurements applying $^{82}Br^-$, shows a discrepancy of factor 2. Applying Darcy's law to the geometric mean of hydraulic conductivities and the mean hydraulic gradient, a mean Darcy velocity of 0.33 m/d can be calculated, which is smaller than the measured Darcy velocities using the groundwater flow velocimeter by factor 2. The variance of the log-transformed Darcy velocity measurements with the groundwater flow velocimeter is smaller than the one with $^{82}Br^-$ by factor 2. The discrepancies show the uncertainties ascribed to differing sampling times and locations, differing volumes of averaging and the uncertainty due to estimating the α-factor.

In order to compute three dimensional heterogeneous Darcy velocity fields with input data from Krauthausen test site the TRACE routine (*Seidemann*, 1996; *Neuendorf*, 1996) was executed on a CRAY-T3E parallel computer. Two cases of groundwater models, differing in the boundary conditions derived from isoline plots of the groundwater levels, were calculated. Case 1 is based on a mean gradient for the entire flow domain, whereas case 2 is based on a triangulated isoline plot of the groundwater levels from Krauthausen test site. Comparison of the results of the two modelled cases show that there is little difference. Only the variance of the x-component of the Darcy velocity differs by one order of magnitude.

A Monte Carlo analysis on three dimensional calculations using ten realizations of the heterogeneous K field were performed. It was shown that ensemble parameters derived from the results of the Monte Carlo analysis are statistically stabile.

In order to stochastically estimate the effective hydraulic conductivity, the formulas of *Dagan* (1989) were used for the 1st order and the formulas of *Deng and Cushman* (1995) and *Hsu and Neuman* (1997) were used for 2nd order approximation. The estimation of the variance and covariance were calculated for 1st order approximation using

formulas given in *Russo* (1995) and *Hsu and Neuman* (1997). Formulas from *Deng and Cushman* (1995) and figures in *Hsu and Neuman* (1997) were used to determine 2nd order correction factors for the variance.

A comparison of stochastically estimated and numerically modelled Darcy velocity statistics were performed using input data from the reference layer at the Krauthausen test site. In the following the focus is on the Darcy velocity components with y denoting the longitudinal, x denoting the transversal horizontal and z denoting the transversal vertical direction.

The first order estimated variance of the y-component of Darcy velocity is well below the one calculated by numerical modelling. In contrast, the second order estimated variance of the y-component of the Darcy velocity is in agreement with the corresponding ensemble variance from numerical modelling. The first order as well as second order approximation of the velocity variance of the x-component are one order of magnitude below the corresponding ensemble variance of the numerically modelled x-component. The 1st order approximation for the variance of the z-component of the Darcy velocity is below the numerically calculated ensemble variance. The 2nd order approximation is above the ensemble variance from numerical modelling.

Applying the 1st order approximation, the estimated covariances for x-, y- and z-component of the Darcy velocity differ clearly from numerically calculated ensemble covariances. The covariances estimated by 2nd order approximation fit excellently with the numerically calculated ensemble covariances only for the y-component of the Darcy velocity. For the x-component, 2nd order approximated covariances are clearly below the modelled covariances until a lag distance of 25 m. For greater lag distances the estimated covariances are higher than the numerically calculated one. For the z-component, the numerically calculated ensemble covariances are in between 1st order and 2nd order estimated covariances. However, the correlograms of the Darcy velocity in the y-direction, estimated using 1st order approximation and numerical calculation, fit quite well for the x- and z-component and fit excellently for the y-component.

In the following the focus will be on the Darcy velocity magnitude. Thus estimation of Darcy velocity statistics, both from numerical modelling and from stochastic theories, show smaller mean by factor 2 (2), smaller variances by factor 4 (20) and longer correlation length in the horizontal direction by factor 7 (4) than directly measured Darcy velocities using the groundwater flow velocimeter (point dilution measurements with $^{82}Br^{-}$). The autocorrelation length of Darcy velocity magnitudes in the vertical direction are similar for numerical modelling and direct measurement with the groundwater flow velocimeter. The high discrepancies in mean, variance and horizontal autocorrelation length are due to the limited knowledge of the α-factor and the time variability of Darcy velocities. The relative standard deviation is used to exclude the effects on mean and variance caused by the α-factor . A comparison shows that the relative standard deviation is similar for modelling, 2nd order approximation and direct measurements with the groundwater flow velocimeter, but higher for the direct measurements with $^{82}Br^{-}$ by factor 2.

The nonconformity in predicting the variances of Darcy velocity x- and z-component both, from numerical modelling and from stochastic theories poses problems in predicting the macrodispersion, being dependent on these variances.

The stated temporal variability of Darcy velocity can cause a contraction of the

autocorrelation length and can affect the variance by tending towards higher values. This rises the question on the consequences of temporal variability of Darcy velocity on dispersion and mixing processes in the course of transport in heterogeneous porous media.

Future work needs to analyse the time dependent variability of the local Darcy velocity and as its impact on transport in porous media by implementing temporal variable boundary conditions in numerical models and stochastic theories. Recommended is also a prove of the accuracy when predicting the heterogeneity of the Darcy velocity and consequently transport processes beyond the specific situation of the Krauthausen aquifer.

Bibliography

Akin, H., and H. Siemes, *Praktische Geostatistik - Eine Einführung für den Bergbau und die Geowissenschaften*, 1st ed., Springer-Verlag, Berlin, 1988.

Alden, A. S., and C. L. Munster, Field test of the in situ permeable groundwater flow sensor, *GWMR*, pp. 81–88, 1997.

Bachmat, Y., S. Mandel, and M. Bugayevski, A single well tracer technique for evaluating aquifer parameters, i. theoretical work, *J. of Hydrol.*, *99*, 143–163, 1988.

Ballard, S., The in situ permeable flow sensors: A groundwater flow velocity meter, *Ground Water*, *34*(2), 1996.

Barczewski, B., Development of a laser-fluorometer for sensitive local concentration measurements in flows, in *21st IAHR Congress*, IAHR, Melbourne, Australia, 1985.

Barczewski, B., and P. Marshall, Development and application of a lightfibre fluorometer for tracer tests, in *Tracer Hydrogeology*, edited by W. Hötzl, pp. 33–39, 1992.

Bear, J., *dynamics of fluids in porous media*, 1st ed., american elsvier publishing company, inc., New York and London and Amsterdam, 1972.

Bellin, A., P. Salandin, and A. Rinaldo, Simulation of dispesion in heterogeneous porous formations: Statistics first-order theories convergence of computations, *Water Resour. Res.*, *28*(9), 2211–2227, 1992.

Beyer, W., Bestimmung der Wasserdurchlässigkeit von Kiesen und Sanden aus der Kornverteilung, *Wasserwirtschaft-Wassertechnik (WWT)*, *14*, 165–168, 1964.

Bialas, Z., and A. S. Kleczkowski, Über den praktischen Gebrauch von einigen empirischen Formeln zur Berechnung des Durchlässigkeitskoeffizienten K, *Archivum Hydrotechniki, Warschau*, 1970.

Bidaux, P., and C. F. Tsang, Fluid flow patterns around a well bore or an underground drift with complex skin effects, *Water Resour. Res.*, *27*(11), 2993–3008, 1991.

Boggs, M. J., S. C. Young, L. M. Beard, L. W. Gelhar, K. R. Rehfeld, and E. E. Adams, Field study of dispersion in a heterogeneous aquifer. 1. overview and site description, *Water Resour. Res.*, *28*(12), 3281–3291, 1992.

Buckingham, E., *Studies on the Movement of Soil Moisture*, vol. 38 of *Bureau of Soils Bull.*, U.S. Departement of Agriculture, Washington, D.C., 1907.

Busch, K.-F., L. Luckner, and K. Tiemer, *Geohydraulik*, vol. 3 of *Lehrbuch der Hydrogeologie*, 3rd ed., Gebrüder Bornträger, Berlin and Stuttgart, 1993.

Carslaw, H. S., and J. C. Jaeger, *Conduction of Heat in Soils*, Oxford University Press, New York, 1959.

Chandra, U., W. Drost, H. Moser, W. Stichler, and H. Kussmaul, Application of single borehole techniques: A study of groundwater flow in the vicinity of a water works drawing bank filtrate on the Lower Rhine, in *Nuclear techniques in groundwater pollution research*, Panel Proceeding Series, pp. 267–282, International Atomic Energy Agency, Vienna, Austria, 1980.

Chilès, J. P., and P. Delfiner, *Geostatistics, Modeling Spatial Uncertainty*, Wiley Series in Probability and Statistics, 1st ed., John Wiley and Sons, inc., New York, 1999.

Dagan, G., Solute transport in heterogeneous formations, *J. Fluid Mech.*, *145*, 151–177, 1986.

Dagan, G., *Flow and Transport in Porous Formations*, 1st ed., Springer-Verlag, Heidelberg and Berlin, 1989.

Darcy, H., *Les Fontaines Publiques de la Ville Dijon*, V. Dalmont, Paris, 1856.

Delleur, J. W., *The Handbook of Groundwater Engineering*, 1st ed., CRC Press and Springer, Boca Raton and Heidelberg, 1999.

Deng, F. W., and J. H. Cushman, On higher-order corrections to the flow velocity covariance, *Water Resour. Res.*, *31*(7), 1659–1672, 1995.

Deutsch, C. V., and A. G. Journel, *GSLIB, Geostatistical Software Library and User's Guide*, Applied Geostatistic Series, 2nd ed., Oxford University Press, New York, Oxford, 1998.

Di Federico, V., and S. P. Neuman, Transport in multiscale log conductivity fields with truncated power variograms, *Water Resour. Res.*, *34*(5), 963–973, 1998.

Döring, U., Transport der reaktiven Stoffe Eosin, Uranin und Lithium in einem heterogenen Grundwasserleiter, Ph.D. thesis, Christian Albrechts Universität Kiel, 1997.

Drost, W., Messung von Filtergeschwindigkeiten auf dem Testfeld Krauthausen, Ergebnisbericht.

Drost, W., and F. Neumaier, Application of single borhole methods in groundwater research, in *Isotope techniques in groundwater hydrology*, vol. 2, pp. 241–254, Vienna, 1974.

Drost, W., D. Klotz, A. Koch, H. Moser, F. Neumaier, and W. Rauert, Point dilution methods of investigating ground water flow by means of radioisotopes, *Water Resour. Res.*, *4*(1), 125–146, 1968.

Earlougher, R. C., *Advances in Well Test Analysis*, Society of Petroleum Engineers of AIME, Dallas, 1977.

Englert, A., Räumliche Variabilität der Hydraulischen Durchlässigkeit eines Quartären Aquifers (Testfeld Krauthausen), Master's thesis, RWTH Aachen, 1998.

Englert, A., U. Hashagen, U. Jaekel, O. Nitzsche, H. Schwarze, and H. Vereecken, Transport von gelösten Stoffen im Grundwasser, Untersuchungen am Testfeld Krauthausen, *Grundwasser*, *5*(3), 115–124, 2000a.

Englert, A., U. Hashagen, and H. Vereecken, Auswertung lokaler Fließgeschwindigkeitsmessungen bezüglich stochastischer Theorien, Untersuchungen am Testfeld Krauthausen, in *HydroGeoEvent 2000, Wasser-Gesteins-Wechselwirkungen*, edited by M. Herbert, M. Isenbeck-Schröter, and C. Scholz, vol. 12, p. 138, FH-DGG, DGG, Heidelberg, 2000b.

Englert, A., J. Höltkemeier, and H. Vereecken, A single well probe with laser induced fluorometry measuring local darcian velocities, in *New Approaches Characterising Groundwater Flow*, edited by K. P. Seiler and S. Wohnlich, vol. 2, pp. 705–708, IAH, Swets, Zeitlinger Lisse, Munich, 2001.

Gelhar, L. W., *Stochastic Subsurface Hydrogeology*, Prentice Hall, Englewood Cliffs, New Jersery, 1993.

Gelhar, L. W., and C. L. Axness, Three dimensional stochastic analysis of macrodispersion in aquifers, *Water Resour. Res.*, *19*(1), 1983.

Guilbault, G. G., *Practical Fluorescence*, 1st ed., Marcel Dekker INC, New York, 1973.

Hall, S. H., S. P. Luttrell, and W. E. Cronin, A method for estimating effective porosity and groundwater velocity, *Ground Water*, *29*(2), 171–174, 1991.

Hsu, K. C., and S. P. Neuman, Second-order expressions for velocity moments in two- and three-dimensional statistically anisotropic media, *Water Resour. Res.*, *33*(4), 625–637, 1997.

Hsu, K. C., D. Zhang, and S. P. Neuman, Higher-order effects on flow and transport in randomly heterogeneous porous media, *Water Resour. Res.*, *32*(3), 571–582, 1996.

Journel, A. G., and C. J. Huijbregts, *Mining Geostatistics*, 4th ed., Academic Press, London, 1989.

Kearl, P. M., Observations of particle movement in monitoring well using the colloidal borescope, *J. of Hydrology*, *1-4*(200), 323–344, 1997.

Kearl, P. M., and C. M. Case, Direct field measurement of groundwater velocities, *Tech. rep.*, American Institute of Hydrology, 1992.

Kerfoot, B., and V. A. Massard, Monitoring well screen influences on direct flowmeter measurements, *GWMR*, pp. 74–77, 1985.

Klostermann, J., *Das Quartär der Niederrheinischen Bucht*, 1st ed., Geologisches Landesamt Nordrhein-Westfalen, Krefeld, 1992.

Klotz, D., Berechnung der Filtergeschwindigkeit einer Grundwasserströmung aus Tracerverdünnungsversuchen in einem Filterpegel, *Tech. rep.*, GSF, 1977, GSF-Bericht R 149.

Klotz, D., Berechnete Durchlässigkeiten handelsüblicher Brunnenfilterrohre und Kunststoff-Kiesbelagfilter, *Tech. rep.*, GSF, 1990, GSF-Bericht Nr. 35.

Kraichnan, R. H., Diffusion by a random velocity field, *The Physics of Fluids*, *13*(1), 22–31, 1970.

Lamertz, F., Messung räumlicher Variabilität hydraulischer Parameter unter Anwendung von Pumpversuchen, Master's thesis, RWTH Aachen, 2001.

Langguth, H. R., and R. Voigt, *Hydrogeologische Methoden*, 1st ed., Springer Verlag, Berlin, 1980.

Leap, D. I., and P. G. Kaplan, A single-well tracing method for estimating regional advective velocity in a confined aquifer: Theroy and preliminary laboratory verification, *Water Resour. Res.*, *24*(7), 993–998, 1988.

Leblanc, D. R., S. P. Garabedian, K. M. Hess, L. W. Gelhar, R. D. Quadri, K. G. Stollenwerk, and W. W. Wood, Large scale natural gradient tracer test in sand and gravel, Cape Cod, Massachusetts - 1. experimental design and observed tracer moment, *Water Resour. Res.*, *27*(5), 895–910, 1991.

Mackay, D. M., D. L. Freyberg, P. V. Roberts, and J. A. Cherry, A natural gradient experiment on solute transport in a sand aquifer. - 1. approach and overview of plume movement, *Water Resour. Res.*, *22*(13), 2017–2029, 1986.

Matheron, G., *Les variables régionalisées et leur estimation. Une application de la théorie des fonctions aléatoires aux Sciences de la Nature*, Masson, Paris, 1965.

Milne-Thompson, L. M., *Theoretical Hydrodynamics*, The Mc Millian Company, Inc., New York, 1968.

Molz, F., R. Morin, A. Hess, J. Melville, and O. Goven, The impeller meter for measuring permeability variations: evaluation and comparison with tests, *Water Resour. Res.*, *25*(7), 1677–1686, 1989.

Momii, K., K. Jinno, and F. Hirano, Laboratory studies on a new laser doppler velocimeter system for horizontal groundwater velocity measurements in a borehole, *Water Resour. Res.*, *29*(2), 283–291, 1993.

Mualem, Y., Extension of the similarity hypothesis used for modeling the soil water characteristic, *Water Resour. Res.*, *13*, 773–780, 1977.

Naff, R. L., D. F. Haley, and E. A. Sudicky, High-resolution monte carlo simulation of flow and conservative transport in heterogeneous porous media; 1. methodology and flow results, *Water Resour. Res.*, *34*(4), 663–677, 1998.

Neuendorf, O., Numerische 3-D Simulation des Stofftransportes in einem heterogenen Aquifer, Ph.D. thesis, RWTH Aachen, 1996.

Novakowski, K. S., A composite analytic model for analysis of pumping tests affected by well bore storage and finite thickness skin, *Water Resour. Res.*, *25*(9), 1937–1946, 1989.

Ogilvi, N. A., An electrolytical method of determining the filtration velocity of underground waters, *Bull. Sci-Tech. Inf.*, *4*(16), 1958, Gosgeoltekhisdat, Moscow (in Russian).

Paillet, F., R. Crowder, and A. Hess, High-resolution flowmeter logging applications with the heat-pulse flowmeter, *JEEG*, *1*(1), 1–11, 1996.

Prüfert, J., Krauthausen test site, notice in writing on the geology of Krauthausen test site, geological survey NRW, 1999.

Richards, L. A., Capillary conduction of liquids through porous mediums, *Physics*, *1*, 1931.

Russo, D., On the velocity covariance and transport modeling in heterogeneous anisotropic porous formations: 1. saturated flow, *Water Resour. Res.*, *31*(1), 129–137, 1995.

Sano, O., Viscous flow past a cylindric hole bored inside a porous media, *J. Jpn. Soc. Fluid Mech.*, *2*, 252–259, 1983, (in Japanese).

Schafmeister, M. T., *Geostatistik für die hydrogeologische Praxis*, 1st ed., Springer-Verlag, Berlin, Heidelberg, 1999.

Schöttler, M., Meßbarkeit der Grundwasserbewegung durch Visualisierung der Strömung in Bohrbrunnen, Ph.D. thesis, Universität Köln, 1997, published by Shaker Verlag, Aachen 1997.

Schöttler, M., Informationen zum GFV-Messsystem, *Tech. rep.*, Phrealog, 2001.

Schulmann, S., *Fluorescence and Phosphorescence Spectroscopy*, 1st ed., Pergamon, Oxford, 1977.

Schulze, M., Bedeutung des gelösten organischen Kohlenstoffs für das Schicksal hydrophober organischer Verbindungen in ungesättigten Bodenzonen, Ph.D. thesis, TU Dresden, 1998.

Schwarze, H., U. Jaekel, and H. Vereecken, Estimation of macrodispersion by different approximation methods for flow and transport in randomly heterogeneous media, *Transport in Porous Media*, *43*, 265–287, 2001.

Schwedt, G., *Fluorimetrische Analyse*, 1st ed., Verlag Chemie, Basel, 1981.

Seidemann, R., Parallelisierung eines Finite Elemente Programms zur Modellierung des Transports von Stoffen durch heterogene poröse Medien, Ph.D. thesis, Rheinische Friedrich-Wilhelms Universität Bonn, 1996.

Seiler, K. P., Durchlässigkeit, Porosität und Kornverteilung quartärer Kies-Sand-Ablagerungen des bayerischen Alpenvorlandes, *Tech. Rep. 114(8)*, gwf, 1973, 353-358.

Shapiro, S. S., and M. B. Wilk, An analysis of variance test for normality (complete sampels), *Biometrica*, *52*, 591–611, 1965.

Teutsch, G., and H. Kobus, The enviromental research field site Horkheimer Insel: Research program, instrumentation and first results, *J. Hydraulic Res.*, *28*(4), 491–501, 1990.

van Genuchten, M. T., A closed - form equation for predicting the hydraulic conductivity of unsaturated soils, *Soil Sci. Soc. Am. J.*, *19*(1), 161–180, 1980.

Vereecken, H., U. Döring, H. Hardelauf, U. Jaekel, U. Hashagen, O. Neuendorf, H. Schwarze, and R. Seidemann, Analysis of solute transport in heterogeneous aquifer: The Krauthausen field experiment, *J. Contam. Hydrol.*, *45*, 329–358, 2000.

Verruijt, A., *Theory of Groundwater Flow*, 2nd ed., The Macmillan Press LTD, Hong Kong, 1982.

Walter, R., *Geologie von Mitteleuropa*, E. Schweizerbartsche Verlagsbuchhandlung (Nägele und Obermiller), Stuttgart, 1992.

Wonnacott, R. J., and T. H. Wonnacott, *Introductary Statistics*, 4th ed., John Wiley and Sons, Inc., Singapore, 1985.

Yeh, G.-T., On the computation of Darcian velocity and mass balance in the finite element modeling of groundwater flow, *Water Resour. Res.*, *17*(5), 1529–1534, 1981.

Appendix A

Darcy Velocity Measurements at Krauthausen Test Site

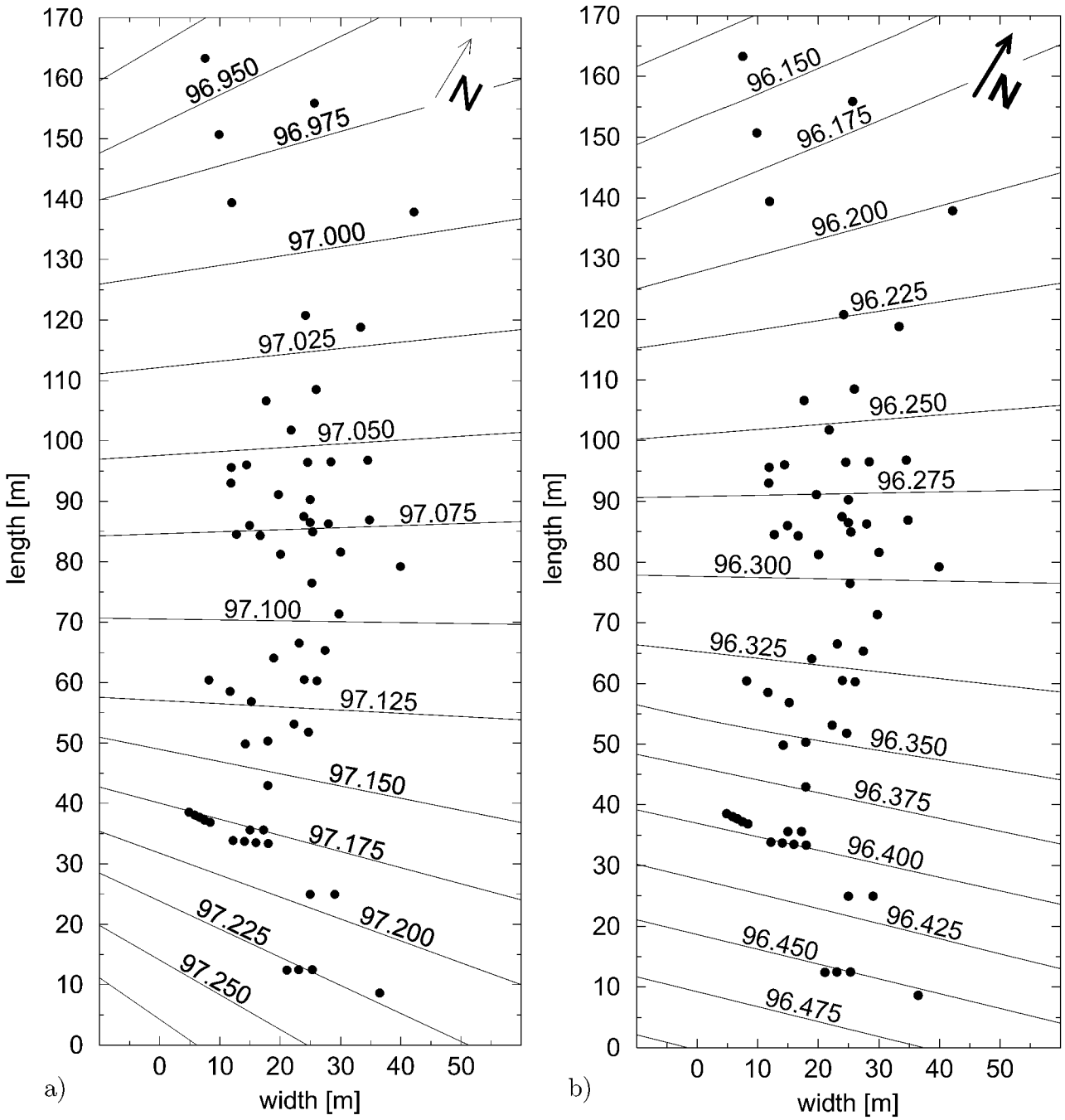

Figure A.1: Contour maps of the water table in m above mean sea level: a) May 17, 2001, b) August 3, 2001

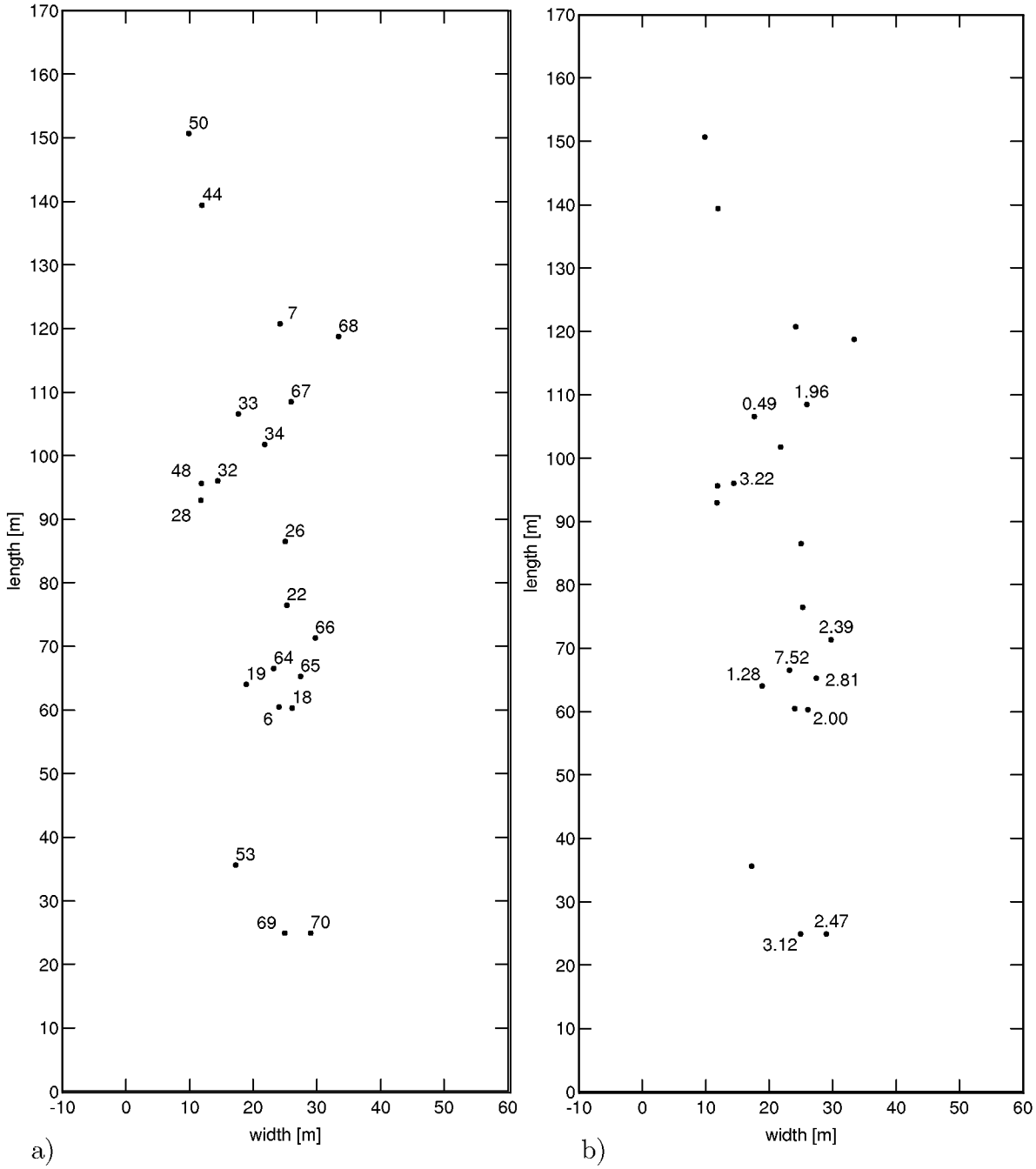

Figure A.2: Measurements of the Darcy velocities with the groundwater flow velocimeter (layer 0): a) number of the well studied, b) geometric mean of Darcy velocities measured at the well.

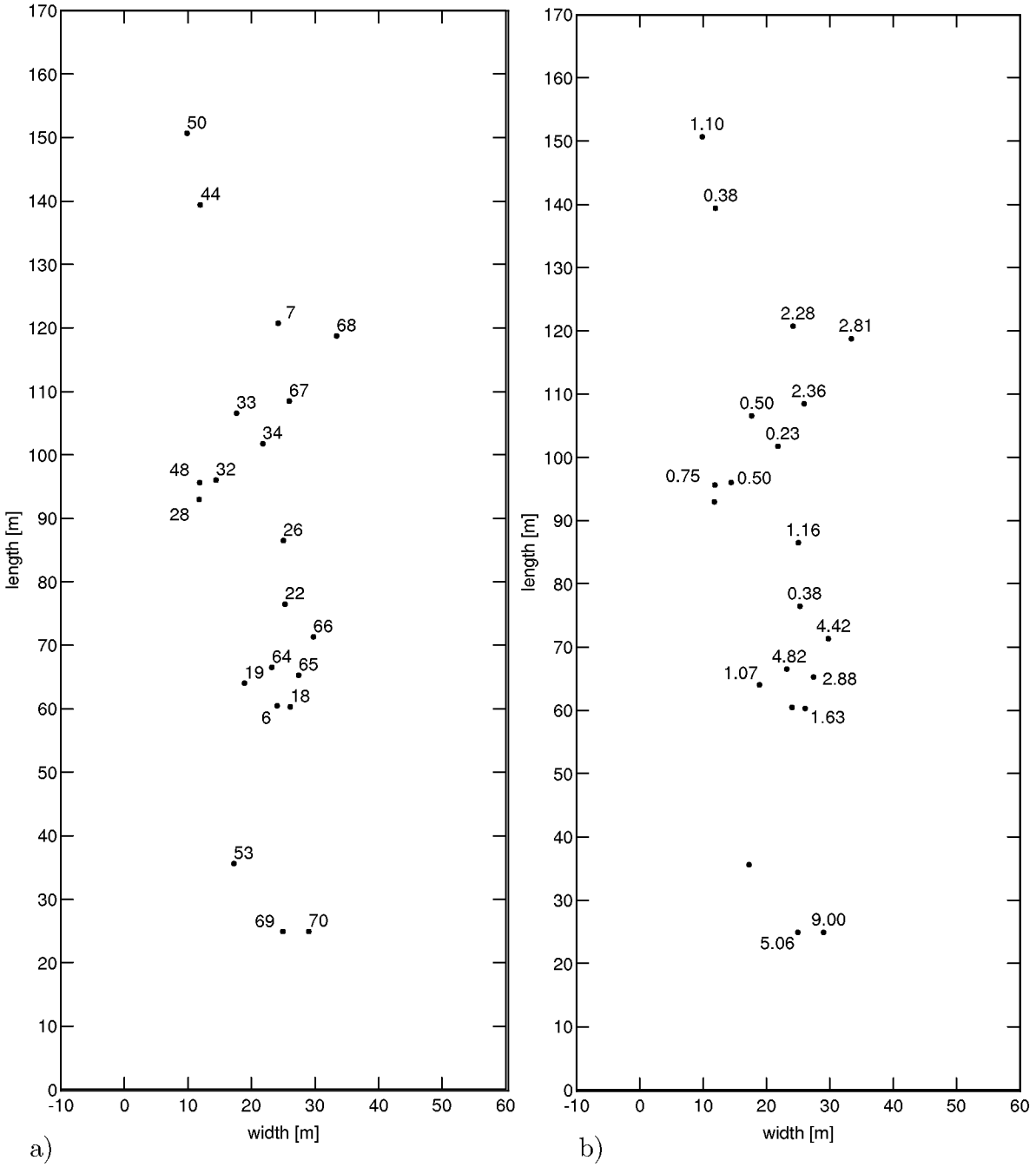

Figure A.3: Measurements of the Darcy velocities with the groundwater flow velocimeter (layer 1): a) number of the well studied, b) geometric mean of Darcy velocities measured at the well.

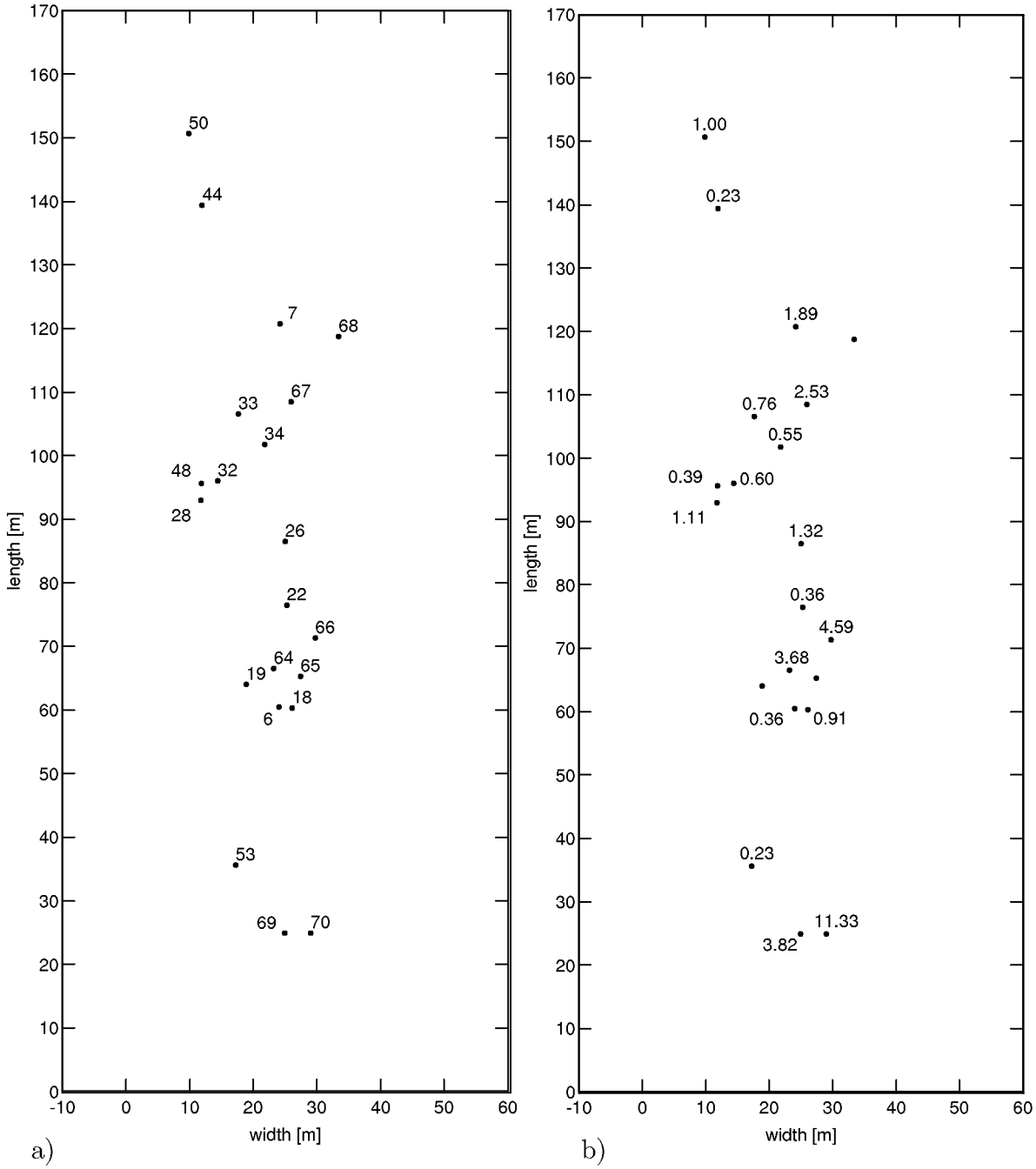

Figure A.4: Measurements of the Darcy velocities with the groundwater flow velocimeter (layer 2): a) number of the well studied, b) geometric mean of Darcy velocities measured at the well.

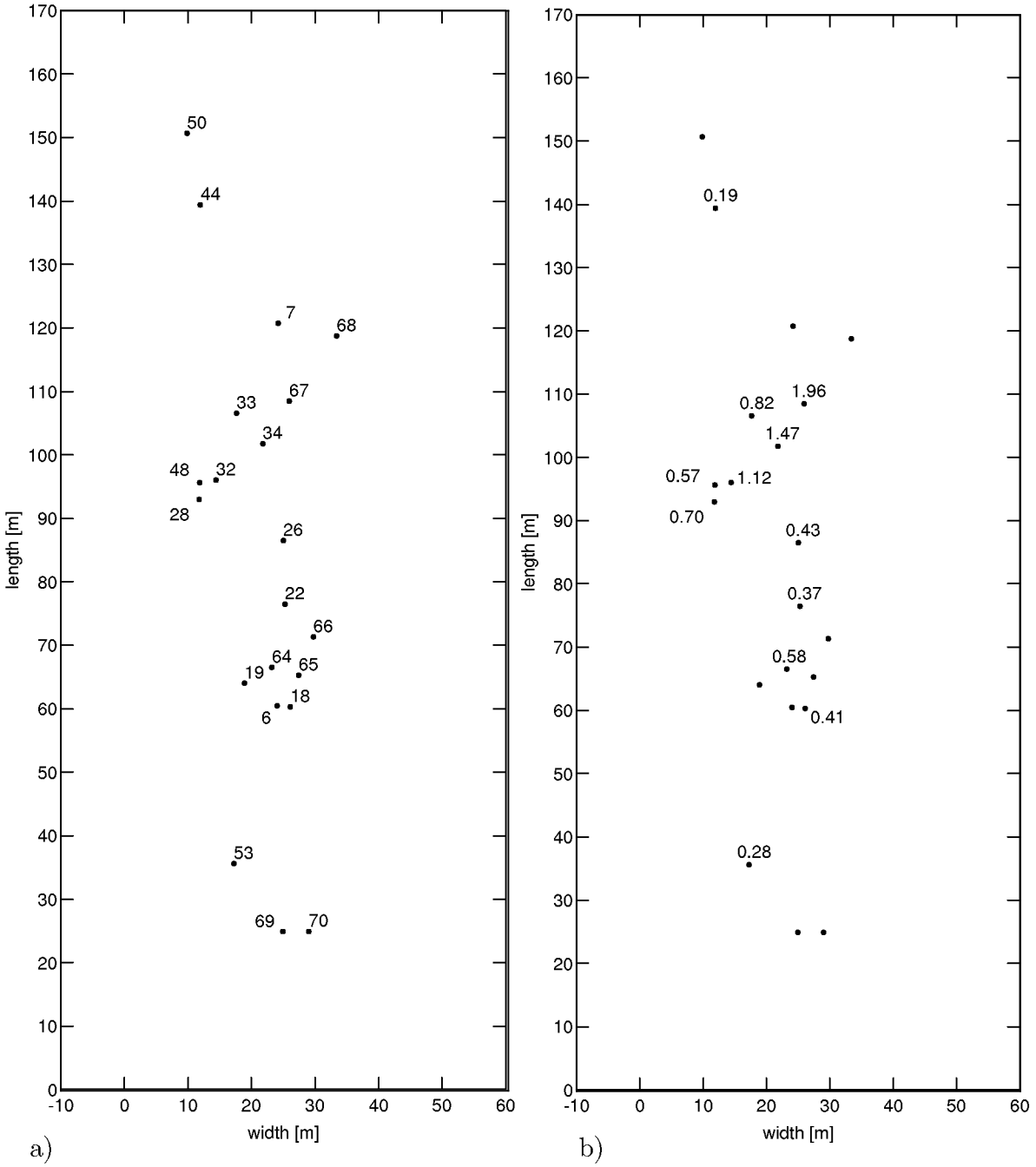

Figure A.5: Measurements of the Darcy velocities with the groundwater flow velocimeter (layer 3): a) number of the well studied, b) geometric mean of Darcy velocities measured at the well.

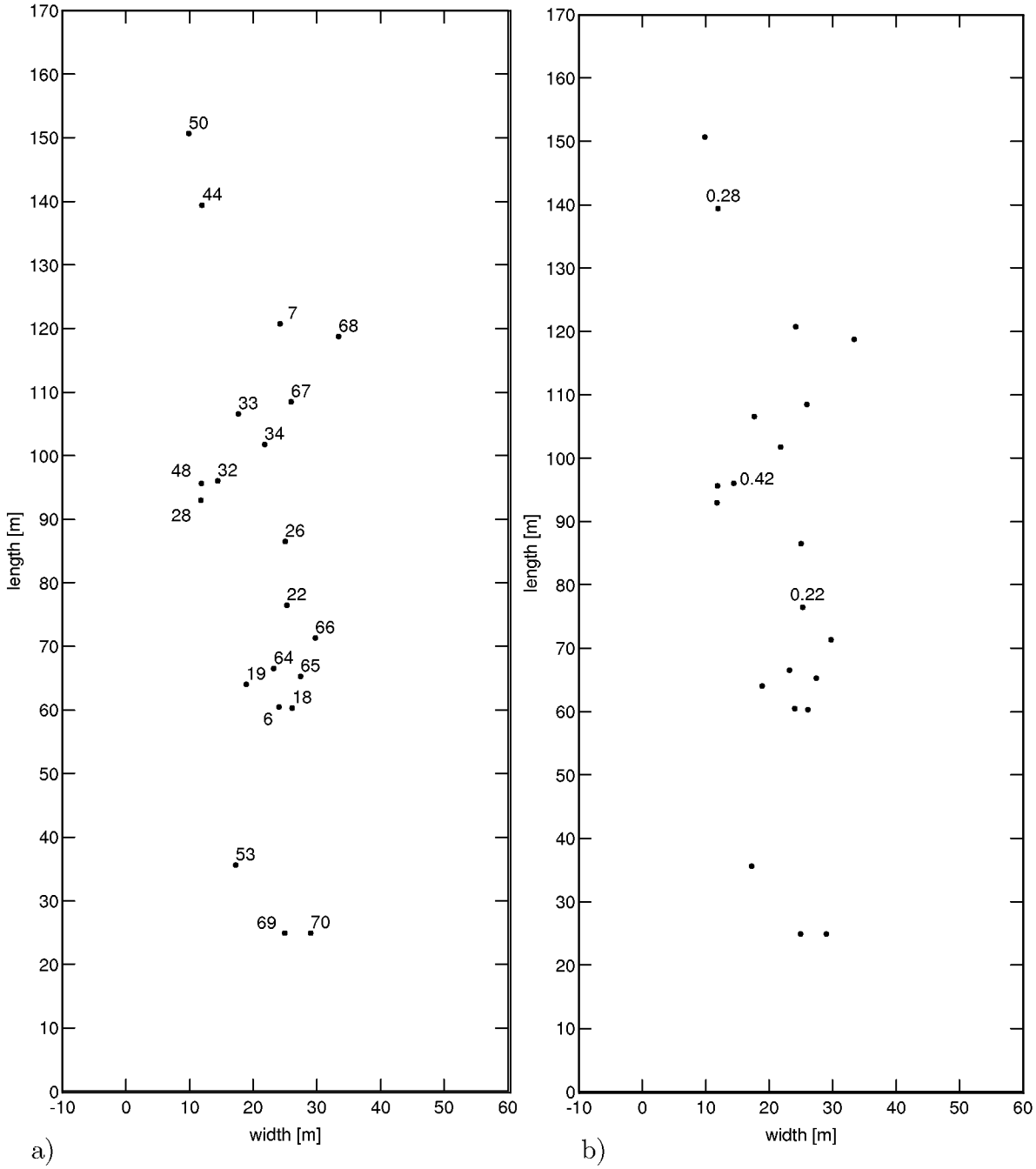

Figure A.6: Measurements of the Darcy velocities with the groundwater flow velocimeter (layer 4): a) number of the well studied, b) geometric mean of Darcy velocities measured at the well.

Table A.1: Ion Balance of Krauthausen Test Site Groundwater

	cations		
		[mg/l]	[meq/l]
sodium	Na^+	28.10	1.23
potassium	K^+	3.30	0.08
magnesium	Mg^{2+}	21.90	1.80
calcium	Ca^{2+}	135.00	6.74
total iron	$\sum Fe$	0.10	<0.01
total manganese	$\sum Mn$	n. d.[1]	-
ammonium	NH_4^+	0.27	0.01
$\sum$ cations		188.67	9.86
	anions		
bicarbonate	HCO_3^-	201.00	3.30
chloride	Cl^-	75.80	2.14
nitrate	NO_3^-	96.80	1.56
sulphate	SO_4^{2-}	139.00	2.90
phosphate	PO_3^{4-}	n. d.	-
$\sum$ anions		512.60	9.90

29.07.1995, observation well number 1, [1]not detectable

Table A.2: Statistics of Hydraulic Conductivities derived from Grain Size Analysis

	effective grain		geom. mean	variance	auto-correlation length [m]		nugget	
method	diameter	N	K [m/s]	$\ln(K)$	vert.	hor.	ver.	hor.
Seiler (1973)	10	335	$1.42 \cdot 10^{-3}$	1.77	0.7	6.7	0.3	0
Seiler (1973)	25	333	$1.41 \cdot 10^{-3}$	1.93	0.4	-	0.3	-
Beyer (1964)	10	348	$5.51 \cdot 10^{-4}$	2.08	1.5	-	0.3	-
Bialas et al. (1970)	20	348	$1.10 \cdot 10^{-3}$	2.20	5.2	-	0.1	-

autocorrelation lengths and nuggets refer to an exponential model; measurements were taken between 87.35 m - 97.00 m above mean sea level (test site Krauthausen)

Table A.3: Geostatistics of K Derived from Grain Size Analysis

model	error model	range [m]	error range [m]	sill	error sill
Gaussian hor.	0.18	13.5	4.1	0.99	0.13
Gaussian ver.	0.11	0.15	0.03	0.56	0.03
exponential hor.	0.17	11.8	7.1	1.02	0.17
exponential ver.	0.10	0.20	0.05	0.60	0.03

reference layer is located at 90.4 m to 92.2 m asl (test site Krauthausen)

Table A.4: In Situ Measurements of Darcy Velocities with the Groundwater Flow Velocimeter at Test Site Krauthausen

	position above mean sea level		numbers of observations		geometric mean [m/d]		variance of $\ln(\|q\|)$	
well	from	to [m]	all	layer*	all	layer*	all	layer*
6	91.44	92.19	4	2	0.36	0.16	2.27	0.66
7	91.24	93.99	12	3	2.01	1.82	0.10	0.20
18	89.53	95.28	24	7	1.11	0.69	0.70	1.16
19	94.32	95.07	4	-	1.12	-	0.04	-
22	87.85	94.85	28	7	0.36	0.48	0.46	0.88
26	89.44	93.44	15	6	1.12	1.46	0.60	0.73
28	89.20	90.95	8	4	0.88	1.11	0.08	0.02
32	87.39	95.14	31	7	0.70	0.47	0.70	0.77
33	89.32	95.07	24	7	0.65	0.84	0.21	0.16
34	89.36	94.61	21	7	0.48	0.94	0.81	0.05
44	87.73	94.98	30	7	0.25	0.21	0.15	0.10
48	89.18	94.93	24	7	0.52	0.32	0.41	0.25
50	90.40	94.65	18	6	1.04	0.78	0.12	0.14
53	89.31	91.81	11	7	0.24	0.23	0.05	0.00
64	88.91	95.16	26	7	2.88	3.00	0.94	0.23
65	94.29	95.04	4	-	2.87	-	0.05	-
66	92.13	95.13	13	-	4.26	-	0.05	-
67	89.27	95.02	24	7	2.37	2.11	0.14	0.11
68	93.14	94.89	8	-	2.81	-	0.15	-
69	92.32	96.07	16	-	4.13	-	0.18	-
70	92.36	96.10	16	-	6.27	-	1.05	-

layer*= reference layer

Table A.5: In Situ Measurements of the Darcy Velocities with the Groundwater Flow Velocimeter, Arranged by Layer

	layer 0			layer 1			layer 2			layer 3			layer 4		
well	N	μ_g (q)	σ^2 $(\ln q)$	N	μ_g (q)	σ^2 $(\ln q)$	N	μ_g (q)	σ^2 $(\ln q)$	N	μ_g (q)	σ^2 $(\ln q)$	N	μ_g (q)	σ^2 $(\ln q)$
6	-	-	-	-	-	-	4	0.36	2.27	-	-	-	-	-	-
7	-	-	-	4	2.28	0.09	8	1.89	0.10	-	-	-	-	-	-
18	2	2.00	0.07	8	1.63	0.42	12	0.91	0.80	2	0.41	0.05	-	-	-
19	1	1.28	-	3	1.07	0.04	-	-	-	-	-	-	-	-	-
22	-	-	-	8	0.38	0.51	11	0.36	0.77	8	0.37	0.10	1	0.22	-
26	-	-	-	2	1.16	2.14	11	1.32	0.41	2	0.43	0.01	-	-	-
28	-	-	-	-	-	-	4	1.11	0.02	4	0.70	0.03	-	-	-
32	1	3.22	-	8	0.50	0.87	12	0.60	0.60	8	1.12	0.23	2	0.42	1.00
33	1	0.49	-	8	0.50	0.18	12	0.76	0.13	3	0.82	0.47	-	-	-
34	-	-	-	7	0.23	0.33	11	0.55	0.61	3	1.47	0.14	-	-	-
44	-	-	-	8	0.38	0.04	12	0.23	0.09	8	0.19	0.14	2	0.28	0.19
48	-	-	-	8	0.75	0.44	12	0.39	0.37	4	0.57	0.10	-	-	-
50	-	-	-	7	1.10	0.07	11	1.00	0.15	-	-	-	-	-	-
53	-	-	-	-	-	-	8	0.23	0.00	3	0.28	0.19	-	-	-
64	1	7.52	-	8	4.82	0.17	12	3.68	0.26	5	0.58	0.75	-	-	
65	1	2.81	-	3	2.88	0.08	-	-	-	-	-	-	-	-	-
66	1	2.39	-	8	4.42	0.03	4	4.59	0.03		-	-	-	-	-
67	1	1.96	-	8	2.36	0.09	12	2.53	0.19	3	1.96	0.20	-	-	-
68	-	-	-	8	2.81	0.15	-	-	-	-	-	-	-	-	-
69	5	3.12	0.23	8	5.06	0.10	3	3.82	0.16	-	-	-	-	-	-
70	5	2.47	2.10	8	9.00	0.13	3	11.33	0.01	-	-	-	-	-	-

Table A.6: Repeated In Situ Measurements with the Groundwater Flow Velocimeter

well	depth, above mean sea level [m]	first measurement [m/d]	second measurement [m/d]	relative deviation [%]
32	90.39	0.64	0.63	2
32	90.64	0.38	0.26	32
32	90.89	0.39	0.17	56
32	91.14	0.44	2.69	84
32	91.39	0.32	0.52	39
32	91.64	0.25	0.33	24
22	91.35	0.48	0.72	34

Table A.7: In Situ Measurements of the Darcy Velocities with $^{82}Br^-$ Dilution

well	position above mean sea level		numbers of observations		geometric mean [m/d]		variance of ln($\|q\|$)	
number	from	to [m]	all	layer*	all	layer*	all	layer*
14	89.79	90.79	2	2	0.06	0.06	6.42	6.42
15	89.79	90.79	2	2	0.43	0.43	0.33	0.33
16	89.79	90.79	2	2	0.18	0.18	0.01	0.01
18	89.80	90.80	2	2	0.65	0.65	0.20	0.20
22	88.30	94.80	11	3	1.75	1.85	0.67	0.62
23	89.80	90.80	2	2	0.16	0.16	0.09	0.09
26	89.79	90.79	2	2	0.11	0.11	0.02	0.02
27	89.79	90.79	2	2	5.27	5.27	0.00	0.00
28	89.80	90.80	2	2	2.25	2.25	3.98	3.98
29	89.79	90.79	2	2	0.22	0.22	0.22	0.22
31	89.79	90.79	2	2	0.29	0.29	1.06	1.06
32	88.29	94.79	11	3	0.64	0.50	1.47	0.04
34	89.80	90.80	2	2	0.07	0.07	7.49	7.49
41	89.80	90.80	2	2	1.32	1.32	0.00	0.00
44	89.80	90.80	2	2	0.31	0.31	1.46	1.46
47	89.79	90.79	2	2	1.01	1.01	0.25	0.25
48	89.79	90.79	2	2	1.25	1.25	0.79	0.79
50	89.50	90.79	2	2	0.15	0.15	0.38	0.38
51	90.79	90.79	1	1	0.08	0.08	-	-
52	89.79	90.79	2	2	0.33	0.33	0.41	0.41
53	89.79	94.79	9	3	0.24	0.29	0.11	0.01
54	89.78	94.78	6	2	0.30	0.19	0.26	0.64
55	90.79	90.79	1	1	6.40	6.40	-	-
57	90.80	90.80	1	1	0.47	0.47	-	-
58	90.79	90.80	1	1	0.06	0.06	-	-
59	90.79	90.79	1	1	0.26	0.26	-	-
60	89.79	90.79	2	2	0.38	0.38	0.07	0.07
61	89.79	90.79	2	2	0.2	0.2	-	-
62	89.79	90.79	2	2	1.46	1.46	9.27	9.27

layer*= reference layer

Table A.8: Estimation of Statistical Parameters of Measured Hydraulic Conductivities and Darcy Velocities in the Reference Layer, Based on Different Sampling Densities

	K [m/s]		$\|q\|$ [m/d]	
parameter	3 wells	31 wells	3 wells	29 wells
N	45	173	9	56
μ_g	$8.2 \cdot 10^{-4}$	$1.9 \cdot 10^{-3}$	0.7	0.4
$\sigma^2_{(ln)}$	0.9	1.0	0.8	2.0

Table A.9: Number, Geometric Mean and Variance of the In Situ Measured Darcy Velocities and Hydraulic Conductivities, Arranged by Layer

	K [m/s]			q [m/d] / uranin			q [m/d] / $^{82}Br^-$		
layer	N	$\mu_g(K)$	$\sigma^2(\ln K)$	N	$\mu_g(q)$	$\sigma^2(\ln q)$	N	$\mu_g(q)$	$\sigma^2(\ln q)$
0	43	$2.80 \cdot 10^{-3}$	2.98	19	2.43	0.78	0	-	-
1	42	$7.32 \cdot 10^{-4}$	2.16	122	1.42	1.40	11	0.64	1.24
2	193	$1.69 \cdot 10^{-3}$	1.07	162	0.88	1.22	43	0.48	1.84
3	44	$7.20 \cdot 10^{-4}$	0.56	53	0.55	0.63	28	0.41	2.21
4	13	$1.62 \cdot 10^{-3}$	3.81	5	0.31	0.37	0	-	-

Appendix B

Evaluation of Darcy Velocity Statistics

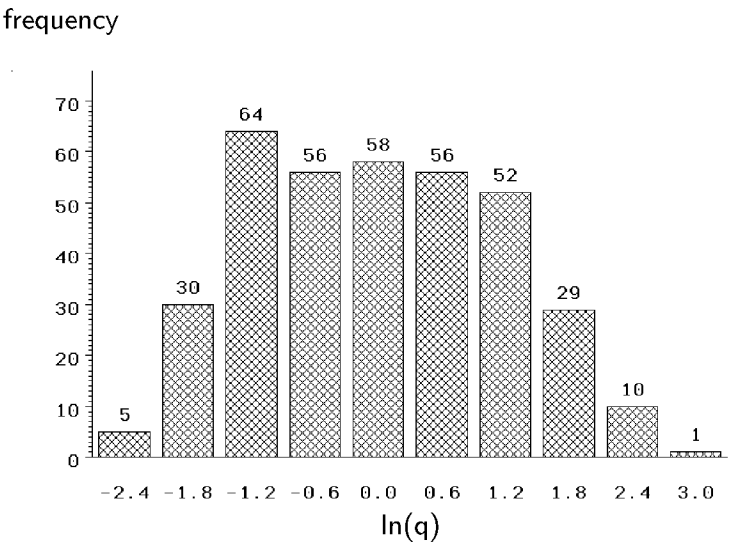

Figure B.1: Histogram of all measured log-transformed Darcy velocity magnitudes, obtained with the groundwater flow velocimeter at Krauthausen test site.

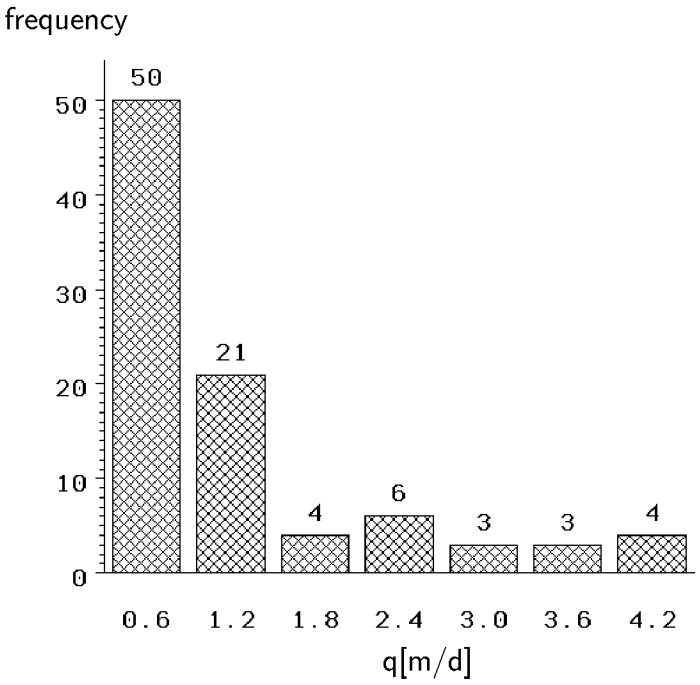

Figure B.2: Histogram of measured Darcy velocity magnitudes within the reference layer.

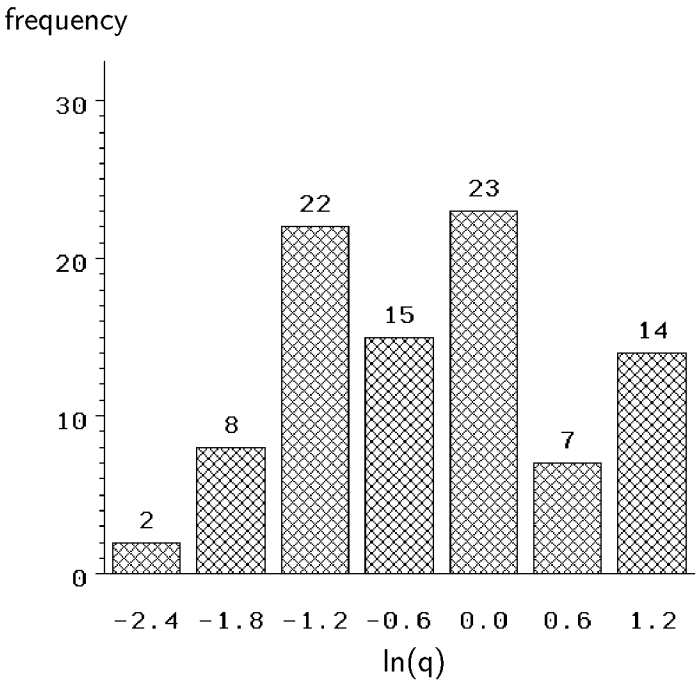

Figure B.3: Histogram of measured Darcy velocity magnitudes within the reference layer, log-transformed.

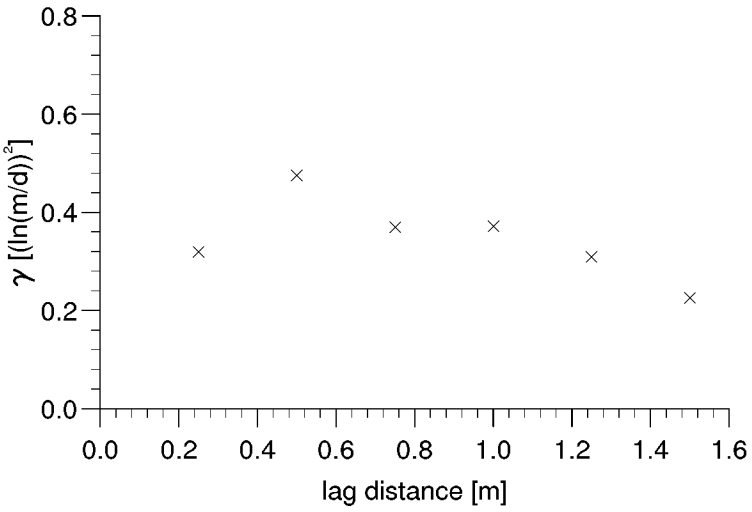

Figure B.4: Vertical variogram of $\ln|q|$ inside the reference layer.

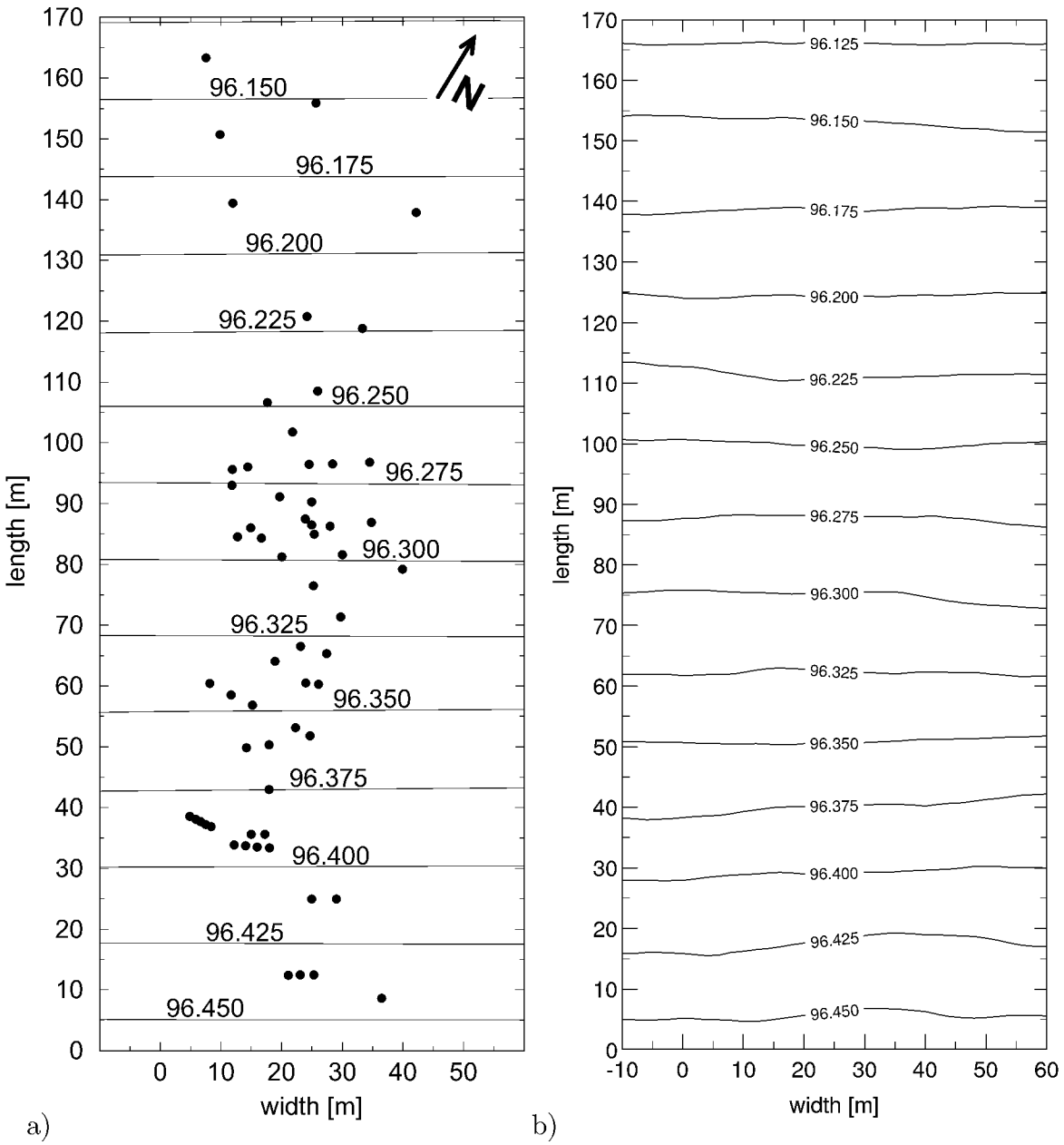

Figure B.5: Simplified total head situation of August 3, 2001 in metres above mean sea level, Krauthausen test site: • measured groundwater observation well
a) measured and linear interpolated, perpendicular to the mean flow direction
b) modelled on the base of boundary conditions derived from a)

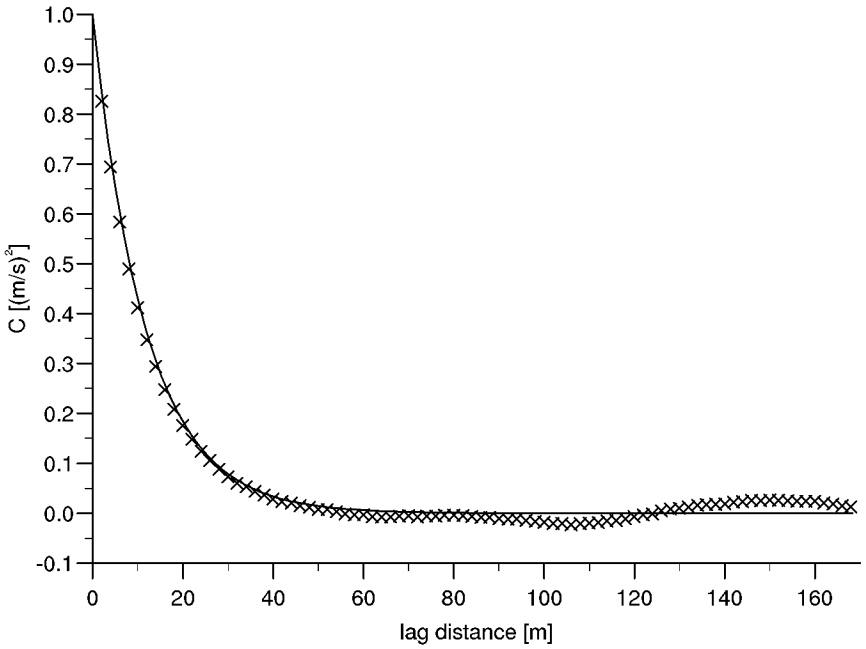

Figure B.6: Simulated ensemble covariances of $\ln(K)$ in y-direction and ex ante given covariance function.

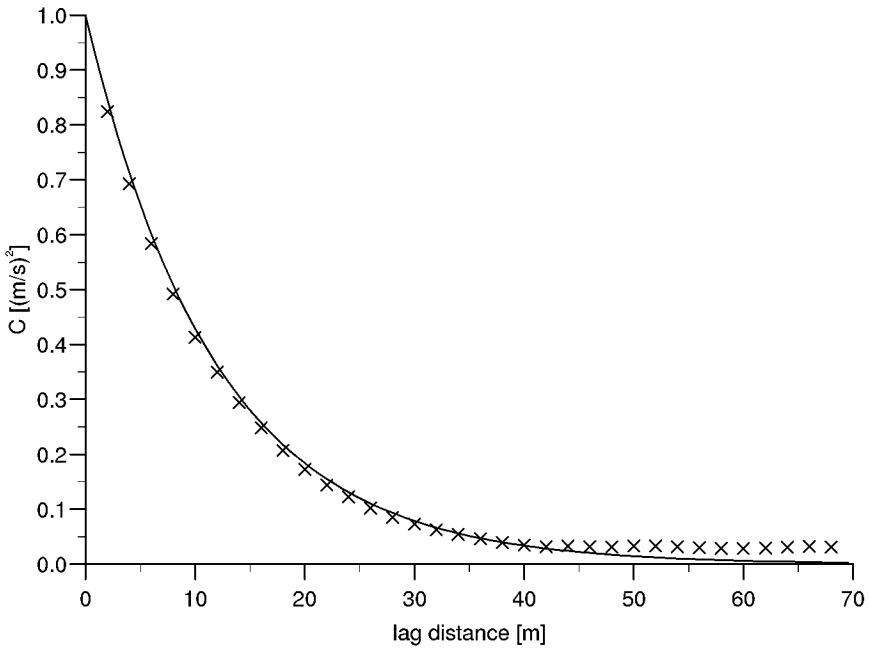

Figure B.7: Simulated ensemble covariances of $\ln(K)$ in x-direction and ex ante given covariance function.

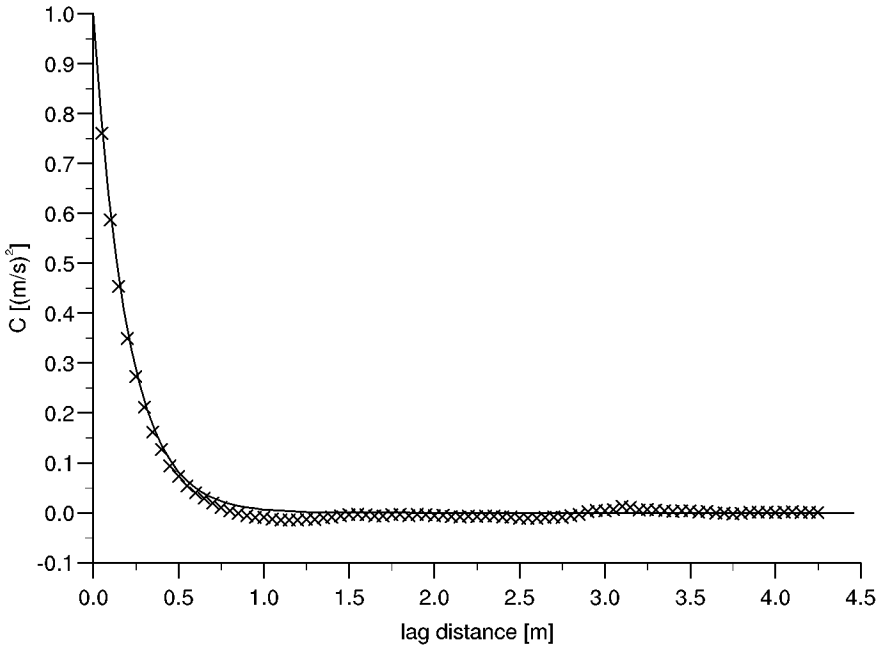

Figure B.8: Simulated ensemble covariances of $\ln(K)$ in z-direction and ex ante given covariance function.

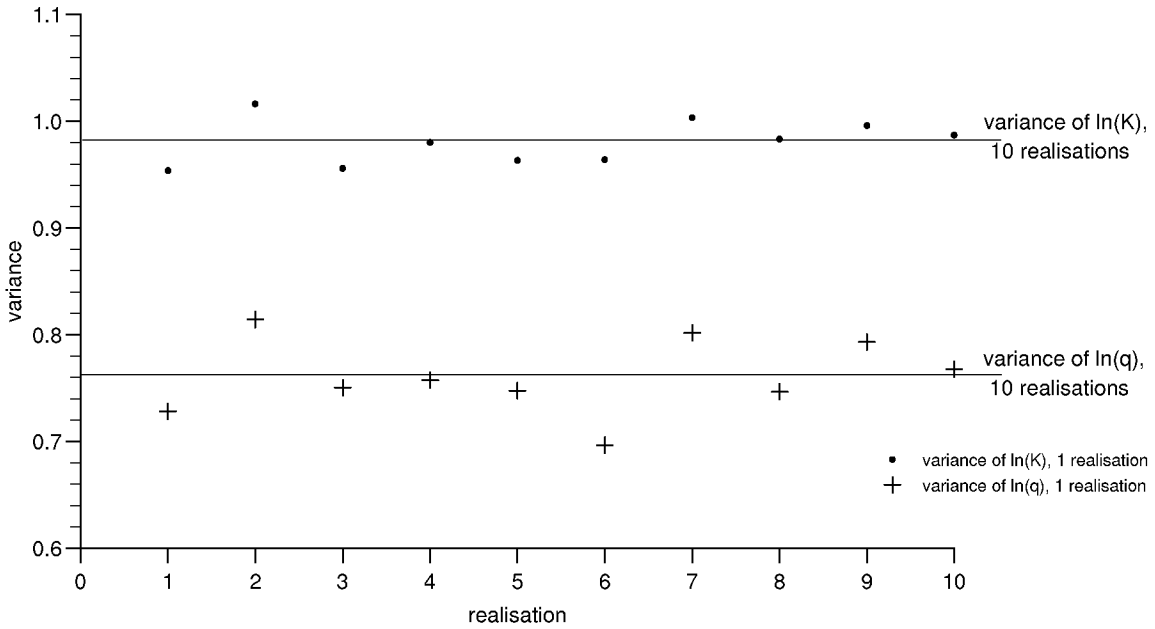

Figure B.9: Comparison of ensemble variance and variances of single realizations.

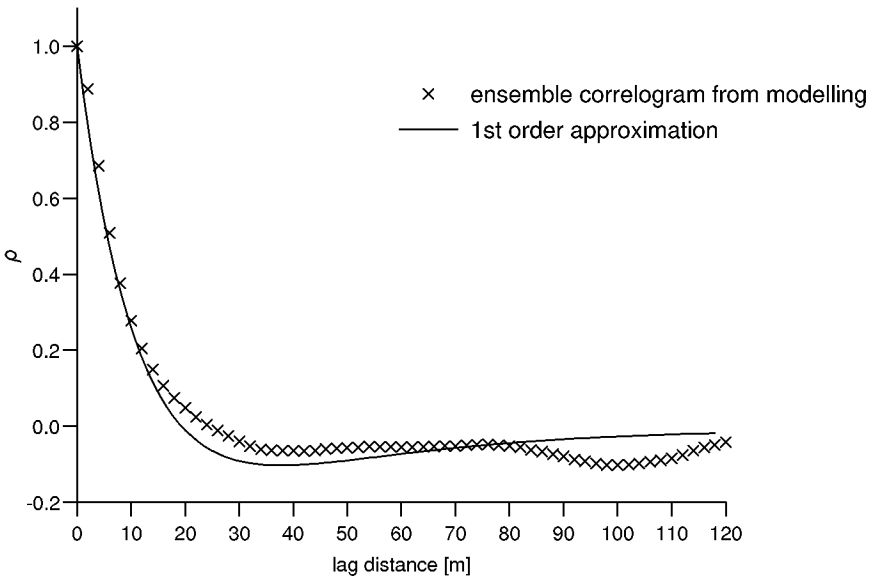

Figure B.10: Correlogram of x-component of the Darcy velocity in y-direction, modelled and stochastically estimated.

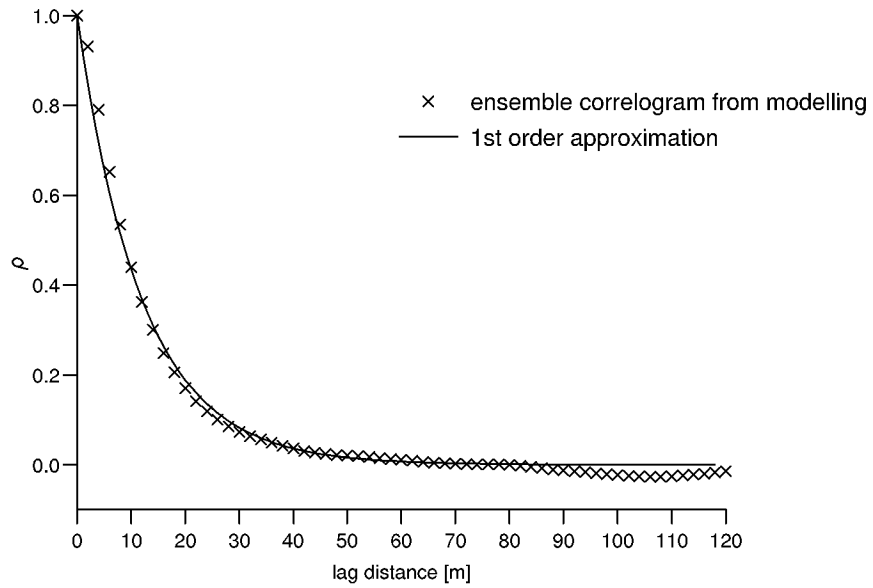

Figure B.11: Correlogram of y-component of the Darcy velocity in y-direction, modelled and stochastically estimated.

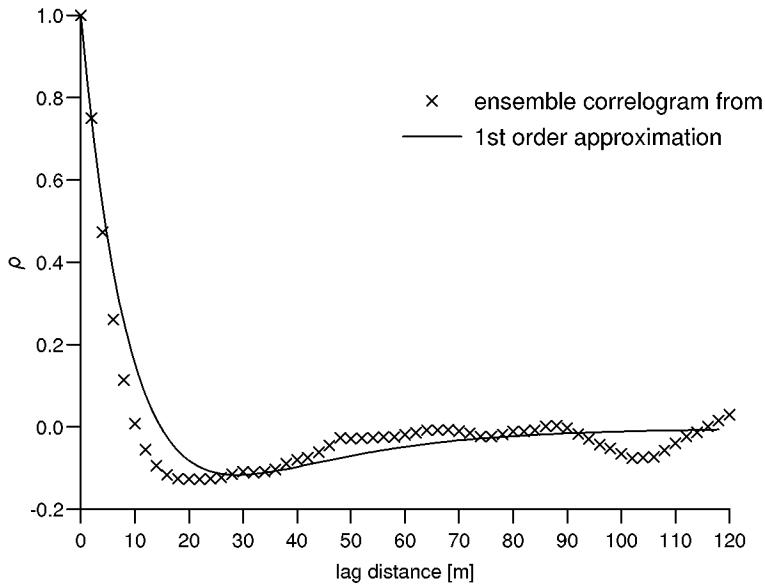

Figure B.12: Correlogram of z-component of the Darcy velocity in y-direction, modelled and stochastically estimated.

Table B.1: Statistics of the In Situ Measured Darcy Velocity Magnitudes, using $^{82}Br^-$

	all data		reference layer	
statistical parameter	q [m/d]	$\ln(q)$ [ln(m/d)]	q [m/d]	$\ln(q)$ [ln(m/d)]
number of observations	82	82	56	56
mean	1.21	-0.75	1.18	-0.89
geom. mean	0.47		0.41	
variance	4.65	1.86	5.48	2.01
W test statistic	0.56	0.97	0.51	0.95
probability: $< W$	< 0.0001	< 0.1367	< 0.0001	< 0.0690

Table B.2: Hydraulic Conductivity Field Statistics for Modelling

	$\ln(K)$[ln(m/s)]	
statistical parameter	simulated	input
number of observations	595000	173
mean	-6.34	-6.27
geom. mean [m/s]	$1.76 \cdot 10^{-3}$	$1.88 \cdot 10^{-3}$
variance	0.97	1.00
test statistic	$D = 0.82 \cdot 10^{-3}$	$W = 0.99$
probability: $> D$, $< W$ resp.	< 0.15	< 0.89

The hydraulic conductivity field (simulated) is computed with a Kraichnan generator taking into account $\ln(K)$ statistics from Krauthausen test site (input).

Table B.3: Geostatistics of the Hydraulic Conductivity Field for Modelling

geostatistical	x-direction		y-direction		z-direction	
parameter	simulated	input	simulated	input	simulated	input
correlation length [m]	11.94	11.8	11.09	11.8	0.19	0.20
std. error [m]	0.14	7.10	0.14	7.10	$2.18 \cdot 10^{-3}$	0.05
sill	1.00	1.02	0.96	1.02	0.99	0.60
std. error	$4.02 \cdot 10^{-3}$	0.17	$3.26 \cdot 10^{-3}$	0.17	$2.30 \cdot 10^{-3}$	0.03

The geostatistical parameters are applied to a weighted exponential model without nuggets using log-transformed K values. See also Table B.2.

Table B.4: Statistics of the Modelled y-Component of Darcy Velocity Fields, Based on a Single Realisation of a Hydraulic Conductivity Field

statistical parameter	simplified		triangulated	
	q_y [m/d]	$\ln(q_y)$ [ln(m/d)]	q_y [m/d]	$\ln(q_y)$ [ln(m/d)]
number of observations	288876	288876	288876	288876
mean	0.47	-1.12	0.48	-1.11
geom. mean	0.34		0.33	
variance	0.22	0.75	0.24	0.77
D test statistic	0.17	$0.51 \cdot 10^{-2}$	0.18	$0.56 \cdot 10^{-2}$
probability: $> D$	< 0.01	< 0.01	< 0.01	< 0.01

Table B.5: Statistics of the Modelled x- and z-Component of Darcy Velocity Fields, Based on a Single Realisation of a Hydraulic Conductivity Field

statistical parameter	simplified q_x [m/d]	triangulated q_x [m/d]	simplified q_z [m/d]	triangulated q_z [m/d]
number of observations	288876	288876	288876	288876
mean	$-2.35 \cdot 10^{-3}$	$-9.66 \cdot 10^{-3}$	$1.66 \cdot 10^{-3}$	$2.61 \cdot 10^{-3}$
variance	$1.56 \cdot 10^{-3}$	$2.02 \cdot 10^{-2}$	$0.96 \cdot 10^{-3}$	$1.07 \cdot 10^{-3}$
D test statistic	0.18	0.15	0.019	0.028
probability: $> D$	< 0.01	< 0.01	< 0.01	< 0.01

Forschungszentrum Jülich
in der Helmholtz-Gemeinschaft

Jül-4084
August 2003
ISSN 0944-2952